EINZELMOLEKÜL-KRAFTSPEKTROSKOPIE AN MOLEKULAREN MASCHINEN UND REZEPTOR-LIGAND-SYSTEMEN

Dissertation an der Fakultät für Physik
der Ludwig-Maximilians-Universität
München

vorgelegt von

Gregor Neuert
aus Breitscheid im Westerwald

München, 31. August 2005

1. Gutachter:	Prof. Dr. Hermann E. Gaub
2. Gutachter:	Prof. Dr. Roland R. Netz
Tag der mündlichen Prüfung:	06. Dezember 2005

1. Zusammenfassung

Biologische molekulare Maschinen erfüllen in der Natur zentrale Aufgaben und erstrecken sich über alle Bereiche des Lebens. Ihren Aufbau und ihre Funktionsweise im Detail zu untersuchen und zu verstehen, ist ein großes Feld der aktuellen Forschung.

Inspiriert durch die biologischen molekularen Maschinen wurde in den letzten Jahren versucht, künstliche molekulare Maschinen aufzubauen. Einer dieser Ansätze verwendet ein photoaktives Polymer, das durch das Bestrahlen mit Licht unterschiedlicher Wellenlänge kontrahiert oder relaxiert werden kann. Wird dieses photoaktive Polymer an ein Kraftspektroskop gekoppelt und über Totale Interne Reflexion (TIR) angeregt, so lässt sich damit eine künstliche molekulare Maschine realisieren, die aus einem einzelnen Polymer besteht. Bestandteil dieses photoaktiven Polymers sind Azobenzoleinheiten, die reversibel zwischen der cis- und der trans-Konformation geschaltet werden können. Dadurch wird das Polymer (Azobenzolpolypeptid) kontrahiert oder relaxiert und kann Arbeit an der Cantileverspitze des Kraftspektroskops verrichten.

Ein Ziel dieser Arbeit war es, ein detailliertes Verständnis dieser künstlichen molekularen Maschine zu erlangen. Dazu wurde zuerst das Schalten der Azobenzoleinheiten im Polymer bei niedriger Kraft demonstriert. Anschließend wurde eine externe Kraft angelegt und beobachtet, dass sich das Schaltverhalten erst bei sehr hohen Kräften verändert.

Das zweite Ziel war die Entwicklung eines theoretischen Modells, zur Beschreibung der Kraft-Abstandskurve des Azobenzolpolypeptid über den gesamten Kraftbereich. Dazu wurden ab-initio quantenmechanische Rechnungen für das Azobenzol durchgeführt und mit dem Modell der „Frei-Rotierenden-Kette“ kombiniert. Dieses Modell hat den Vorteil, dass es mit der Segmentlänge und der Anzahl der Monomere als Fittparameter auskommt. Es ist nun

möglich die Kraft-Abstandskurven des Azobenzolpolypeptid direkt durch die Anzahl der Azobenzoleinheiten in der trans- und in der cis-Konformation über den ganzen Kraftbereich (0 bis 1000pN) zu beschreiben. Das Schaltverhalten des Polymers wird damit durch das Verhältnis der Anteile im cis- bzw. trans-Zustand ausgedrückt.

Ein weiterer Schwerpunkt dieser Arbeit war die Untersuchung eines Rezeptor-Ligand-Systems. Am Beispiel des anti-Digoxigenin Antikörpers gegen Digoxigenin wurden Experimente über einen großen Bereich von Kraftladungsraten durchgeführt. Dadurch zeigte sich, dass die bisherige Analysemethode nur grobe Einblicke in die Energielandschaft der Rezeptor-Ligand-Wechselwirkung zulässt. Es konnte beispielsweise eine natürliche Dissoziationsrate von $k_{off}=0.015s^{-1}$ aus den kraftspektroskopischen Experimenten bestimmt werden, die mit Messungen an Fv-Fragmenten am Ensemble gut übereinstimmen ($k_{off}=0.023s^{-1}$).

Aussagen bezüglich der Energielandschaft gestalteten sich schwieriger. Zuerst wurde das Maximum der Krafthistogramme als Funktion der Maxima der Ladungsratenhistogramme in einem Diagramm dargestellt. Dieses Diagramm wurde nach der Methode von Evans ausgewertet. Daraus ergab sich für den niedrigen Ladungsratenbereich die obige Dissoziationsrate von $k_{off}=0.015s^{-1}$ und eine Potentialweite von $\Delta x=1.15nm$. Für den hohen Ladungsratenbereich ergab sich eine Dissoziationsrate von $k_{off}=4.56s^{-1}$ und eine Potentialweite von $\Delta x=0.35nm$. Mit diesen Werten wurde nun versucht, die einzelnen Krafthistogramme für alle Ladungsraten zu fitten. Es hatte sich gezeigt, dass es bei niedrigen und bei hohen Ladungsraten eine Übereinstimmung zwischen dem gemessenen Krafthistogramm und der berechneten Wahrscheinlichkeitsverteilung gab. Allerdings konnte bei sehr hohen Ladungsraten und in dem Übergansbereich zwischen den beiden Bereichen keine Übereinstimmung erzielt werden. Daher sind Aussagen über die Energielandschaft nur beschränkt möglich. Um eine vollständige Auswertung der experimentellen Daten zu

erreichen, werden weitere Entwicklungen bezüglich des theoretischen Modells nötig sein. Ein Ansatz besteht darin, ein mögliches Potential anzunehmen und darauf die Theorie von Kramers anwenden. Das Ergebnis wäre dann eine kraftabhängige Dissoziationskonstante k_{off} für ein spezielles Potential.

Des Weiteren wurde in dieser Arbeit ein Mehrkanal-Oberflächen-Plasmonen-Resonanz (SPR)-Spektrometer aufgebaut und charakterisiert.

2. Einführung

In der belebten Welt spielen molekulare Maschinen eine zentrale Rolle [1]. Ihre Funktionen umfassen beispielsweise die Umwandlung von Energie [2, 3], das Übersetzen der genetischen Information in funktionelle Bausteine [4, 5], die Fortbewegung von Zellen [6], die Zellteilung [7], den intrazellulärer Transport [8] sowie die Muskelkontraktion [9-11].

Energieumwandlung kann, um ein Bespiel zu nennen, durch eine rotierende F0, F1-ATPase erfolgen [2, 3]. Dieses Enzym realisiert die Umwandlung, indem es Adenosintriphosphat (ATP) zu Adenosindiphosphat (ADP) und inorganischem Phosphor (P_i) hydrolisiert. Die dabei freigesetzte chemische Energie wird zum Aufbau eines Protonengradienten über eine Zellmembran genutzt: Diese molekulare Maschine pumpt folglich Protonen durch die Membran von außen nach innen. Die Rotation dieser Maschine kann u. a. auch mit Einzelmolekülmethoden nachgewiesen werden. Hierzu wird ein Fluoreszenz markiertes Aktinfilament mit Hilfe einer Rezeptor-Ligand-Bindung an die F0,F1-ATPase gekoppelt [2].

Neben rotierenden Maschinen verfügt die Natur über so genannte lineare Maschinen [13]. Eine dieser linearen Maschinen ist das Myosin V, das Organelle entlang von Aktinfilamenten unidirektional und prozessiv transportiert [10, 11]. Um dies zu realisieren, wird die zu transportierende Last durch eine Rezeptor-Ligand-Wechselwirkung an eine entsprechende Bindungsstelle des Myosin V gebunden, welches sich auf einem Aktinfilament fortbewegen kann [14]. Dieser Bewegung liegt eine weitere Rezeptor-Ligand-Bindung zugrunde, welche durch Konformationsänderungen im Molekül moduliert werden kann und dadurch für die relative Bewegung verantwortlich ist.

Inspiriert durch die biologischen molekularen Maschinen, wurde in den letzten Jahren vermehrt versucht, künstliche molekulare Maschinen experimentell zu realisieren[15, 16].

Einer dieser Ansätze verwendet ein photoaktives Polymer, das durch Licht bestimmter Wellenlängen zwischen zwei Konformationen umgeschaltet werden kann und dadurch eine Längenänderung erfährt. Dieses Polymer wurde kovalent zwischen einem Piezostellglied und einer Blattfeder eingespannt [17]. An der Blattfeder wird mechanische Arbeit verrichtet, wenn die extern eingekoppelte optische Energie das photoaktive Polymer umschaltet und das Polymer daraufhin kontrahiert [18].

Betrachtet man die obigen Beispiele unter dem Gesichtspunkt unterschiedlicher Kraftregime, so lässt sich folgende Unterteilung machen. Das eine Kraftregime beschreibt den Bereich, in dem die Maschine arbeiten kann, das ist z.B. das Rotieren der ATPase [2, 12], die lineare unidirektionale Bewegung des Myosins [10] oder das Umschalten der Untereinheiten des photoaktiven Polymers [17, 18].
Das zweite Kraftregime beschreibt den Bereich, in dem der Aktuator angekoppelt wird, um z.B. die Arbeit der Maschine abzugreifen. Im Falle der ATPase ist das die Biotin-Streptavidin-Bindung [2, 12, 19, 20]. Bei Myosin V ist es die Bindung des Myosins an das Aktinfilament in Abwesenheit von ATP [21]. Für die künstliche Polymer-Maschine ist es die kovalente Bindung des Polymers an die Blattfeder und an die Glasunterlage [22].

Beide Kraftregime wurden im Rahmen dieser Dissertation jeweils an einem repräsentativen Beispiel untersucht. Das erste Kraftregime wurde an einer künstlichen molekularen Maschine untersucht und modelliert. Hierbei handelt es sich um ein mit Licht schaltbares Azobenzol-Polymer, das zwischen der Blattfeder und einer Glasunterlage kovalent verankert ist und an der Blattfeder Arbeit verrichten kann. Das zweite Kraftregime wird in dem untersuchten künstlichen System durch kovalente Bindungen repräsentiert. Alternativ dazu können jedoch auch Rezeptor-Ligand-Interaktionen benutzt werden, um die Ankopplung an den Aktuator zu realisieren. In natürlichen Systemen erfolgt die Ankopplung an den Aktuator sehr häufig über

eine Rezeptor-Ligand-Interaktion. Daher wurde als Beispiel für das zweite Kraftregime eine Rezeptor-Ligand Interaktion, nämlich die Bindung von Digoxigenin an einen anti-Digoxigenin Antikörper, untersucht.
Zur Charakterisierung beider Kraftregime wurde ein Kraftmikroskop [23, 24] benutzt. Parallel zu diesen Einzelmolekülmessungen wurde an einer Methode gearbeitet, um Rezeptor-Ligand-Interaktionen im Ensemble zu messen.

3. Einzelmolekül-Kraftspektroskopie

Vor etwas mehr als 20 Jahren gelang es erstmals, einzelne Atome an einer Oberfläche mit Hilfe des Rasterkraftmikroskops abzubilden [25]. Zur Abbildung wird eine atomar scharfe Spitze an einer Blattfeder, dem so genannten Cantilever verwendet, welche eine Probenoberfläche abtastet, die in x,y,z -Richtung verschoben werden kann. Die Verschiebung der Probenoberfläche erfolgt durch piezoelektrische Kristalle mit einer Genauigkeit von einigen Angström. Die Auslenkung der Blattfeder wird mit einer Laseroptik detektiert und kann in eine Kraft umgerechnet werden. Diese Kraft repräsentiert die Wechselwirkung zwischen der Spitze und der Probenoberfläche dar und kann mit einer Genauigkeit von einigen wenigen Pikonewton gemessen werden. Wenn man Moleküle zwischen Spitze und Oberfläche bindet, kann die Kraft, die diese Moleküle zusammenhält, ermittelt werden. Aufgrund dieser Eigenschaften eignet sich das Kraftmikroskop ausgezeichnet, gezielt und kontrolliert Kräfte auszuüben (siehe Abbildung 1) [23, 24].

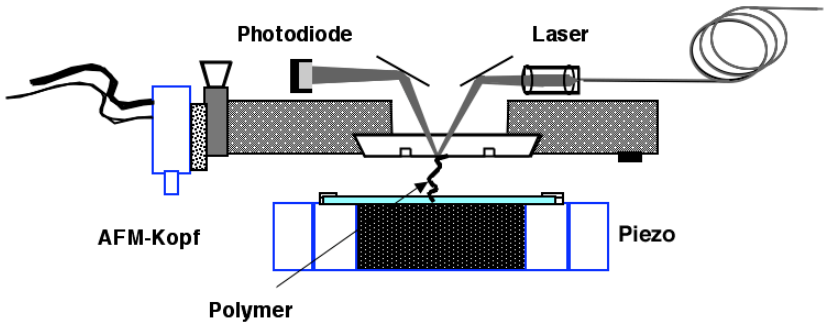

Abbildung 1: Experimenteller Aufbau eines opto-mechanischen Kraftspektroskops. Kraftspektrometer mit Laseroptik, Piezo-kontrollierter Glasunterlage, Cantilever für die Kraftmessung und Photodetektor (übernommen von [27].

Im Rahmen dieser Dissertation sollen unter anderem Moleküle untersucht werden, die photoaktiv sind. Aus diesem Grund wurde das verwendete Kraftmikroskop so erweitert, dass die Moleküle belichtet werden können. Über Total-Interne-Reflexion (TIR) kann Licht der Wellenlängen λ_1=365nm und λ_2=420nm in den Glasobjektträger eingekoppelt werden [17, 18].

4. Künstliche Molekulare Maschine

Das lichtschaltbare Polymer ist aus Azobenzolmonomeren aufgebaut, die durch ein Tripeptid (Lys – Gly – Gly) miteinander verbunden sind. Die Azobenzolmonomere können mit zwei unterschiedlichen Wellenlängen zwischen der cis- und trans-Konformation hin und her geschaltet werden (Abbildung 2). In der cis-Konformation besitzt ein Monomer eine Länge von 6.0Å, in der trans-Konformation ist es 9.1Å lang. Aufgrund dieser deutlichen, Licht-Induzieren Längenänderung eignet sich Azobenzol grundsätzlich für kraftspektroskopische Untersuchungen. Für eine verbesserte Detektion dieser Änderung im experimentellen Aufbau, wurden mehrere Azobenzolmonomere zu einem Polymer verbunden. Dadurch wird die Längenänderung eines einzelnen Monomers amplifiziert [17, 18] .

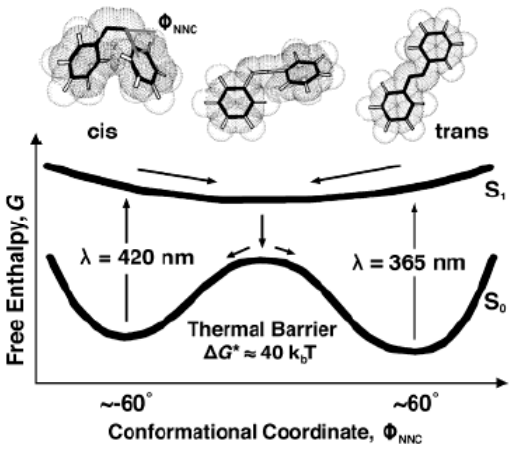

Abbildung 2:
Schematische Darstellung der Energielandschaft der reversiblen cis / trans Isomerisierung des Azobenzol. Die cis-Konformation kann durch Anregung mit Licht der Wellenlänge λ1=365nm erreicht werden und die trans-Konformation bei Licht der Wellenlänge λ2=420nm. Die beiden Konformationen sind stabil über die Dauer der Experimente, da cis- und die trans-Konformation durch eine thermische Energiebarriere von ca. $40k_BT$ getrennt sind [26] (übernommen von [18]).

Für die experimentelle Realisierung wurde das verwendete Azobenzolpolypeptid auf der einen Seite an einer Cantileverspitze und auf der anderen an einer Glasoberfläche kovalent verankert (Abbildung 3).

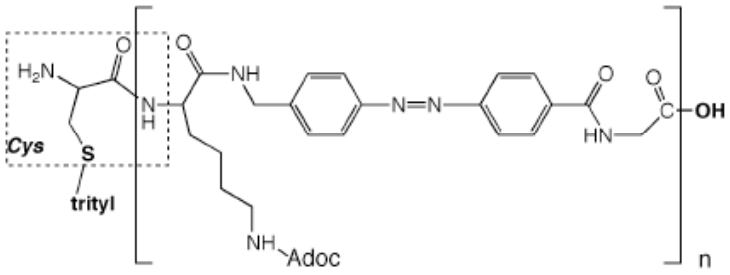

Abbildung 3: Molekulare Details des Azobenzolpolypeptides (übernommen von [18]).

Durch die kovalente Verankerung zwischen der Spitze und der Unterlage ist es möglich, das gleiche Polymer mehrmals zu dehnen und zu relaxieren.

In Abbildung 4 ist gezeigt, wie im Experiment durch die Einkopplung von Licht unterschiedlicher Wellenlänge das Polymer zwischen einem poly-trans und einem poly-cis Zustand reversibel geschaltet wird: λ_1=365nm schaltet vom trans- in den cis-Zustand und λ_2=420nm schaltet vom cis- in den trans-Zustand. Wird an das poly-trans Polymer eine

externe Kraft durch den Cantilever angelegt und das Polymer durch Licht in den poly-cis Zustand geschaltet, so kontrahiert das Polymer und verrichtet eine Arbeit gegen die extern angelegte Kraft (Abbildung 4b, II->III). Das Azobenzolpolypeptid kann auch in einem Kreiszyklus, bestehend aus Dehnen, Relaxieren und Belichten, betrieben werden. Dies führt dann zur Realisierung einer synthetischen Einzelmolekül-Maschine (siehe Abbildung 4) [17, 18]. In dieser Dissertation werden die Eigenschaften des lichtschaltbaren Azobenzolpolypeptid untersucht und dessen charakteristische Kraft–Dehnungsverhalten analysiert.

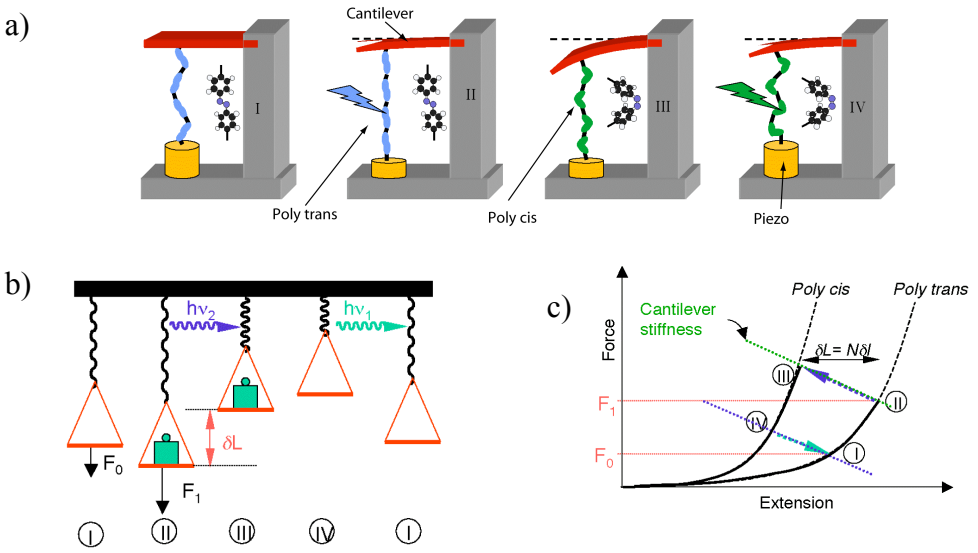

Abbildung 4: Experimentelle Realisierung der Einzelmolekülmaschine.
a) Experimenteller Ablauf einer Einzelmolekülmaschine in einem Kraftspektroskopie-Experiment; b) Illustration des Arbeitszyklus einer solchen Maschine. Die unterschiedlichen Federn stellen das Polymer im trans- und cis-Zustand dar. Das Gewicht beschreibt das Strecken des Polymers; c) Arbeitszyklus einer optisch angetriebenen Einzelmolekülmaschine in einem Kraft-Abstands-Diagramm (übernommen von [17, 27]).

5. Modellierung einer künstlichen Molekularen-Maschine

In dem vorangegangenen Kapitel wurde gezeigt, dass durch Licht das Azobenzolpolypeptid von einem poly-trans in einen poly-cis Zustand geschaltet werden kann, wodurch die Gesamtlänge des Polymers abnimmt (Abbildung 4c). Idealerweise sollte das Umschalten der

einzelnen Azobenzoleinheiten direkt in die Beschreibung der Kraftkurve eingehen. Dazu wurden von Prof. Dr. Roland R. Netz ab-initio quantenmechanische Rechnungen [28] zu Azobenzolmonomeren sowie zu Peptiden durchgeführt. Diese Rechnungen ergeben für verschiedene Konformationen des Azobenzols die jeweiligen Grundzustandsenergien. Im nächsten Schritt wurde je eine Konformation für den cis- und den trans-Zustand ausgewählt und das Azobenzolmonomer jeweils in dieser Konformation gestreckt. Das Ergebnis ist eine 1-dimensionale Energielandschaft in Zugrichtung. Diese ist sehr unterschiedlich für die cis- und für die trans-Konformation und lässt sich mit einer Funktion E(z) beschreiben. Leitet man diese Funktion nach z ab (dE(z) / dz), ergibt sich die Kraft-Abstandabhängigkeit in z-Richtung für die cis- und trans-Konformation (F(z)).

Diese Kraft-Abstandabhängigkeit beschreibt hauptsächlich den hohen Kraftbereich und spiegelt im wesentlichen das Elastizitätsverhalten des Polymerrückgrat ohne Fluktuationen (bei T=0K) wieder [29]. Da die Experimente aber bei T=300K durchgeführt werden, müssen die Fluktuationen des Polymer ebenfalls berücksichtigt werden. Kombiniert man das Modell der „Frei–Rotierenden–Kette“ mit den ab-initio Rechnungen, lässt sich damit die experimentelle Kraftkurve vollständig beschreiben (siehe Abbildung 5).

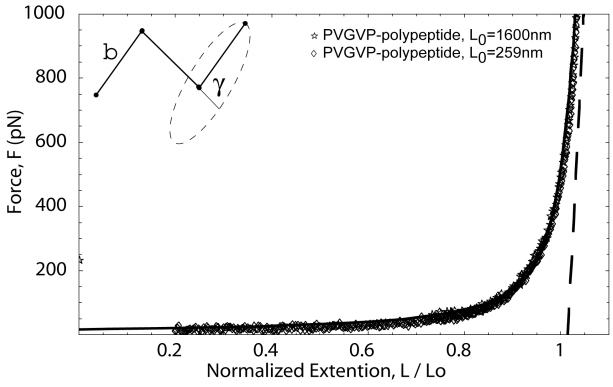

Abbildung 5:
Kombinierter Fit aus „Frei-Rotierender-Kette“ und ab-initio quantenmechanischen Rechnungen (durchgezogene Linie) für normalisierte Kraft-Abstandskurven von zwei ungeladenen, verschieden langen Polypeptidketten (übernommen von [30]).

6. Rezeptor-Ligand-Interaktion

Während in den Kapiteln 4 und 5 die Eigenschaften einer molekularen Maschine experimentell und theoretisch analysiert wurden, soll in diesem Kapitel eine Möglichkeit der Ankopplung einer molekularen Maschine an einen Aktuator untersucht werden. Exemplarisch wurde die Wechselwirkung eines anti-Digoxigenin Antikörpers mit seinem Antigen Digoxigenin mit dem Kraftmikroskop im Detail charakterisiert.

Grundlage für diese Art der Untersuchung sind die Überlegungen von Bell, die beschreiben, dass durch eine extern angelegte Kraft die Potentiallandschaft einer nicht-kovalenten Bindung verschoben wird [31]. Diese Veränderung ist direkt proportional zur extern angelegten Kraft. Prof. Dr. E. Evans hat aufgrund dieser Erkenntnisse einen direkten Zusammenhang zwischen der Abrisskraft und der angelegten Kraft pro Zeit (Kraftladungsrate) hergestellt [32].

Er konnte zeigen, wie mit zunehmender Kraftladungsrate die Abrisskraft ansteigt [20]. Die experimentellen Daten können mit zwei unterschiedlichen Methoden ausgewertet werden: In der ersten Methode wird die maximale Abrisskraft über den Logarithmus der Kraftladungsrate aufgetragen. Daraus lässt sich die natürliche Dissoziationsrate k_{off} und der Abstand vom Potentialminimum zum Übergangszustand Δx bestimmen [33]. Ändert sich die Kraftladungsrate über einen großen Bereich, kommt es zu einer nichtlinearen Abhängigkeit der Kraft von der Ladungsrate. Bisher wurde diese Abhängigkeit als ein Doppelpotential interpretiert [15].

Wie oben beschrieben, stellen die einzelnen Punkte in dem Kraft-Ladungsratendiagramm Maximalwerte dar. Diese Maximalwerte wurden aus Kraft- und Ladungsratenhistogrammen gewonnen. Bei der zweiten Methode werden die Krafthistogramme direkt analysiert [34]. Die Krafthistogramme stellen die Abrisskräfte vieler einzelner Abrisse dar. Es konnte gezeigt werden, dass ein einzelnes Krafthistogramm durch eine Wahrscheinlichkeitsdichte p(F) beschrieben werden kann [20, 34] . Diese Funktion ist nicht nur abhängig von der Kraft, sondern auch von der natürlichen Dissoziationskonstante k_{off}, der Potentialweite Δx und der Kraftladungsrate dF/dt. Wird diese Funktion an das gemessene Krafthistogramm mit der dazugehörigen Ladungsrate angefittet, dann lässt sich daraus k_{off} und Δx ablesen.
Beide Analysemethoden sollten zu dem gleichen Ergebnis führen.
Grundlage für die bisher beschriebene Analyse ist, dass es sich hier um sehr tiefe Potentiale handelt und die Potentialweite durch eine extern angelegte Kraft nicht verändert wird, d.h. dass $\Delta x(F=0) = \Delta x(F>0)$ angenommen wurde [31, 32]. Graphisch ist das in Abbildung 6a gezeigt.

Unter diesen Annahmen wurde versucht, die gemessenen Krafthistogramme für Ladungsraten zwischen 30pN/s und 63000pN/s auszuwerten. In dieser Arbeit wurde jedoch gezeigt, dass nur einige wenige Krafthistogramme mit den obigen Methoden ausgewertet werden konnten. Um in Zukunft eine vollständige Auswertung zu gewährleisten, muss die Theorie von Kramers angewendet werden, die die Form des Potentials berücksichtigt (siehe Abbildung 6b).

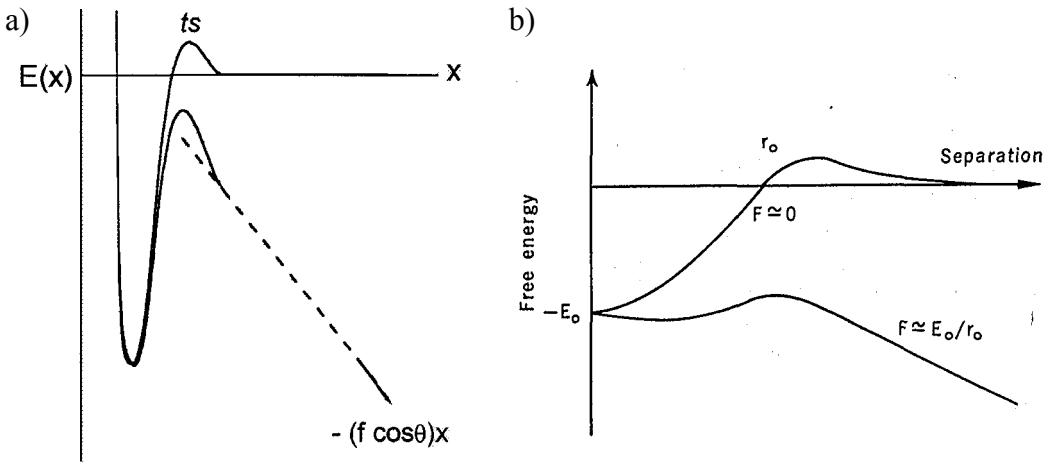

Abbildung 6: Hypothetische Energielandschaft einer Rezeptor-Ligand-Wechselwirkung.
a) Modell von Bell und Evans mit $\Delta x(F)=\Delta x(0)=\Delta x$ und ohne Berücksichtigung der Form des Potentials (übernommen von [35]).
b) Potential für das Modell von Kramers unter Berücksichtigung der Form der Potentiallandschaft mit $\Delta x(F)\neq\Delta x(0)$ (übernommen von [31] .

7. Komplementäre Methode zur Beschreibung einer Rezeptor – Ligand Interaktion

Neben der Einzelmolekülkraftspektroskopie gibt es verschiedene experimentelle Methoden, die es erlauben, Experimente am Ensemble durchzuführen. Eine weit verbreitete Methode um Rezeptor-Ligand-Systeme zu untersuchen, ist die Oberflächen-Plasmon-Resonanz (SPR)-Spektroskopie [36]. Mit dieser Methode ist es möglich, die Assoziationskonstante k_{on} und die Dissoziationskonstante k_{off} eines Rezeptor-Ligand-Systems zu messen.
Im Rahmen dieser Dissertation wurde ein Mehrkanal-SPR-Gerät aufgebaut und charakterisiert. Dieses Gerät hat zum einen den Vorteil, dass bis zu 6 Kanäle parallel gemessen werden können und so z.B. differenzielle Messungen möglich werden. Weiterhin ist dieses Gerät ideal dafür geeignet, mit anderen Techniken kombiniert zu werden.

8. Literatur

1. Schliwa, M. (2002). Molecular Motors, 1 Edition (Wiley - VCH).
2. Noji, H., Yasuda, R., Yoshida, M., and Kinosita, K. (1997). Direct observation of the rotation of F-1-ATPase. Nature *386*, 299-302.
3. Yoshida, M., Muneyuki, E., and Hisabori, T. (2001). ATP synthase - A marvellous rotary engine of the cell. Nature Reviews Molecular Cell Biology *2*, 669-677.
4. Allemand, J.F., Bensimon, D., and Croquette, V. (2003). Stretching DNA and RNA to probe their interactions with proteins. Current Opinion in Structural Biology *13*, 266-274.
5. Shaevitz, J.W., Abbondanzieri, E.A., Landick, R., and Block, S.M. (2003). Backtracking by single RNA polymerase molecules observed at near-base-pair resolution. Nature *426*, 684-687.
6. Ridley, A.J., Schwartz, M.A., Burridge, K., Firtel, R.A., Ginsberg, M.H., Borisy, G., Parsons, J.T., and Horwitz, A.R. (2003). Cell migration: Integrating signals from front to back. Science *302*, 1704-1709.
7. Ben-Yehuda, S., Rudner, D.Z., and Losick, R. (2003). RacA, a bacterial protein that anchors chromosomes to the cell poles. Science *299*, 532-536.
8. Holthuis, J.C.M., and Levine, T.P. (2005). Lipid traffic: Floppy drives and a superhighway. Nature Reviews Molecular Cell Biology *6*, 209-220.
9. Rief, M., Gautel, M., Oesterhelt, F., Fernandez, J.M., and Gaub, H.E. (1997). Reversible unfolding of individual titin immunoglobulin domains by AFM. Science *276*, 1109-1112.
10. Mehta, A.D., Rock, R.S., Rief, M., Spudich, J.A., Mooseker, M.S., and Cheney, R.E. (1999). Myosin-V is a processive actin-based motor. Nature *400*, 590-593.
11. Mehta, A.D., Rief, M., Spudich, J.A., Smith, D.A., and Simmons, R.M. (1999). Single-molecule biomechanics with optical methods. Science *283*, 1689-1695.
12. Itoh, H., Takahashi, A., Adachi, K., Noji, H., Yasuda, R., Yoshida, M., and Kinosita, K. (2004). Mechanically driven ATP synthesis by F-1-ATPase. Nature *427*, 465-468.
13. Vale, R.D., and Milligan, R.A. (2000). The way things move: Looking under the hood of molecular motor proteins. Science *288*, 88-95.
14. Clemen, A.E., Vilfan, M., Jaud, J., Zhang, J., Barmann, M., and Rief, M. (2005). Force-dependent stepping kinetics of Myosin-v. Biophys J *88*, 4402-4410.
15. Merkel, R., Nassoy, P., Leung, A., Ritchie, K., and Evans, E. (1999). Energy landscapes of receptor-ligand bonds explored with dynamic force spectroscopy. Nature *397*, 50-53.
16. Balzani, V., Credi, A., Raymo, F.M., and Stoddart, J.F. (2000). Artificial molecular machines. Angewandte Chemie-International Edition *39*, 3349-3391.
17. Hugel, T., Holland, N.B., Cattani, A., Moroder, L., Seitz, M., and Gaub, H.E. (2002). Single-molecule optomechanical cycle. Science *296*, 1103-1106.
18. Holland, N.B., Hugel, T., Neuert, G., Cattani-Scholz, A., Renner, C., Oesterhelt, D., Moroder, L., Seitz, M., and Gaub, H.E. (2003). Single molecule force spectroscopy of azobenzene polymers: Switching elasticity of single photochromic macromolecules. Macromolecules *36*, 2015-2023.
19. Moy, V.T., Florin, E.L., and Gaub, H.E. (1994). Adhesive Forces between Ligand and Receptor Measured by Afm. Colloids and Surfaces a-Physicochemical and Engineering Aspects *93*, 343-348.

20. Friedsam, C., Wehle, A.K., Kühner, F., and Gaub, H.E. (2003). Dynamic single-molecule force spectroscopy: bond rupture analysis with variable spacer length. Journal of Physics-Condensed Matter *15*, S1709-S1723.
21. Nishizaka, T., Miyata, H., Yoshikawa, H., Ishiwata, S., and Kinosita, K. (1995). Unbinding Force of a Single Motor Molecule of Muscle Measured Using Optical Tweezers. Nature *377*, 251-254.
22. Grandbois, M., Beyer, M., Rief, M., Clausen-Schaumann, H., and Gaub, H.E. (1999). How strong is a covalent bond? Science *283*, 1727-1730.
23. Hugel, T., and Seitz, M. (2001). The study of molecular interactions by AFM force spectroscopy. Macromolecular Rapid Communications *22*, 989-1016.
24. Clausen-Schaumann, H., Seitz, M., Krautbauer, R., and Gaub, H.E. (2000). Force spectroscopy with single bio-molecules. Current Opinion in Chemical Biology *4*, 524-530.
25. Binnig, G., Quate, C.F., and Gerber, C. (1986). Atomic force microscope. Phys. Rev. Lett. *56*, 930.
26. Monti, S., Orlandi, G., and Palmieri, P. (1982). Chem. Phys. *71*, 87.
27. Neuert, G., and Gaub, H.E. (2005). Molekulare Maschinen - Nano-Biotechnologie auf dem Weg zum Silizium-Kohlenstoff-Hybriden. In Materie in Raum und Zeit. (S. Hirzer Verlag).
28. Netz, R.R. (2001). Strongly stretched semiflexible extensible polyelectrolytes and DNA. Macromolecules *34*, 7522-7529.
29. Hugel, T., Rief, M., Seitz, M., Gaub, H.E., and Netz, R.R. (2005). Highly stretched single polymers: Atomic-force-microscope experiments versus ab-initio theory. Physical Review Letters *94*.
30. Neuert, G., Hugel, T., Netz, R.R., and Gaub, H.E. (2005). Elasticity of poly(azobenzene-peptides). submitted.
31. Bell, G.I. (1978). Models for the specific adhesion of cells to cells. Science *200*, 618-627.
32. Evans, E., and Ritchie, K. (1997). Dynamic strength of molecular adhesion bonds. Biophysical Journal *72*, 1541-1555.
33. Schwesinger, F., Ros, R., Strunz, T., Anselmetti, D., Guntherodt, H.J., Honegger, A., Jermutus, L., Tiefenauer, L., and Pluckthun, A. (2000). Unbinding forces of single antibody-antigen complexes correlate with their thermal dissociation rates. Proceedings of the National Academy of Sciences of the United States of America *97*, 9972-9977.
34. Kühner, F., Costa, L.T., Bisch, P.M., Thalhammer, S., Heckl, W.M., and Gaub, H.E. (2004). LexA-DNA bond strength by single molecule force spectroscopy. Biophysical Journal *87*, 2683-2690.
35. Evans, E. (2001). Probing the relation between force--lifetime--and chemistry in single molecular bonds. Annu Rev Biophys Biomol Struct *30*, 105-128.
36. McDonnell, J.M. (2001). Surface plasmon resonance: towards an understanding of the mechanisms of biological molecular recognition. Current Opinion in Chemical Biology *5*, 572-577.

9. Anhang

P1

“Molekulare Maschinen -
Nano-Biotechnologie auf dem Weg zu Silizium-Kohlenstoff-Hybriden“

G. Neuert und H. E. Gaub

Buchkapitel in Materie in Raum und Zeit, S. Hirzel Verlag, 2005

Molekulare Maschinen

Nano-Biotechnologie auf dem Weg zu Silizium-Kohlenstoff-Hybriden

Gregor Neuert und Hermann Eduard Gaub

Kohlenstoff, das für die Entwicklung des Lebens zentrale Element ermöglicht durch seine spezielle Chemie die Vielfalt und dynamische Anpassung an Neues, seine Verbindungen sind die Basis des Lebens. Silizium, das Nachbarelement hingegen ist das Synonym für technologischen Fortschritt, ein Symbol für Schnelligkeit, aber auch für Materialbeherrschung und für Miniaturisierung. Das Spannungsfeld, aber auch die Symbiose dieser beiden "Welten" sind die Triebfedern der Nano-Biotechnologie, einer sich sehr schnell entwickelnden neuen Forschungsrichtung. Die Biotechnologie, die es mit enormer Effizienz geschafft hat, die von Mutter Natur durch Jahrmillionen der Evolution optimierten molekularen Prozesse zu verstehen und nutzbar zu machen, trifft in einer rapide zunehmenden Anzahl von Berührungspunkten mit der aus der Siliziumtechnologie durch fortschreitende Miniaturisierung hervorgegangene Nanotechnologie zusammen. Beispielhaft soll diese Begegnung an den molekularen Maschinen, einem Schnittgebiet beider Felder, veranschaulicht werden (Abb. 1).

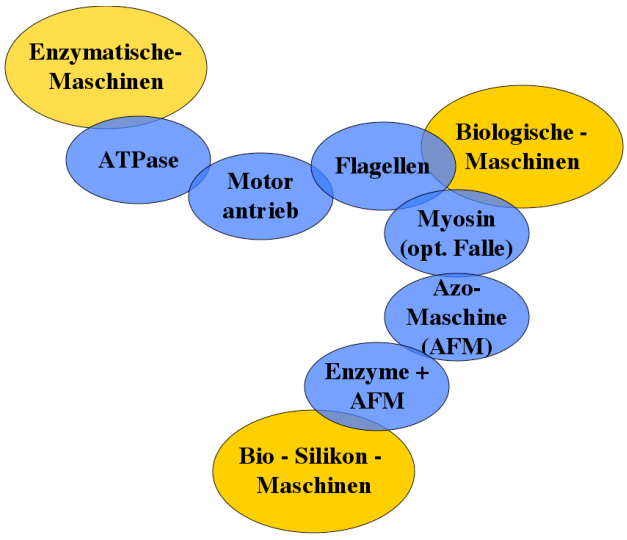

Abbildung 1: Verschmelzung von biologischen molekularen Maschinen mit der Nanotechnologie

Nanomechanische Funktionseinheiten

Mit der Entwicklung der Silizium-Technologie wurde es möglich, nicht nur elektronische, sondern auch mechanische Systeme zu miniaturisieren; eine Grundvoraussetzung für die Implementierung einer breit angelegten Nanotechnologie, die neben Informationsaustausch auch Materialtransport einschließt. Nanoelektromechanische Funktionseinheiten (NEMS für *NanoElectroMechanical Systems*) in der Größenordnung von einigen hundert Nanometern (Nanometer = nm = 10^{-9} Meter) können heute mit Standardtechnologien hergestellt werden. Ein Beispiel für solch ein nanoelektromechanisches System stellt die Kombination eines mechanischen Resonators mit einem elektronischen Antrieb dar, wie sie in Abb. 2 zu sehen ist [1]. In diesem Modellmotor wird der mechanisch frei schwingende Klöppel durch hochfrequente elektrische Felder angetrieben, was mittlerweile selbst bei Raumtemperatur realisiert werden kann. Obwohl diese in der Gruppe von Jörg Kotthaus an der LMU München entwickelte Struktur den kleinsten bisher bekannten Nanomotor darstellt, muss man sich vergegenwärtigen, dass er damit immer noch um ca. zwei Größenordungen massiver ausfällt als typische biologische Maschinen, die zudem gleich noch Regulation und Steuerung mit eingebaut haben. Es lohnt sich also sehr genau unter die Lupe zu nehmen, welche Konzepte Mutter Natur in ihrer Jahrmillionen währenden Evolution ausgewählt hat und wie sie in der Kohlenstoff-Welt umgesetzt wurden.

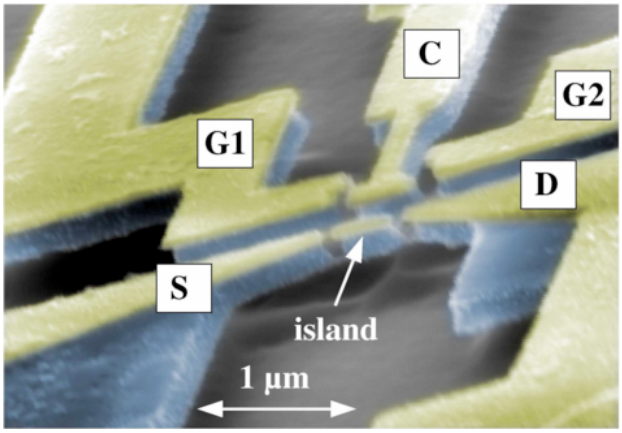

Abbildung 2: Resonante nanoelektromechanische Maschine (NEMS) (Abb. J. Kotthaus)

Ein weiterführendes Ziel könnte dann darin bestehen, die silikonbasierte Nanotechnologie mit den biologischen Maschinen auf molekularer Ebene zu verschmelzen, um gezielt von außen einzelne biologische Maschinen zu adressieren, zu manipulieren oder zu verbinden. Dieser Ansatz nutzt im idealen Fall die Halbleitertechnologie mit ihrem genauen und hochparallelen

„Top down“-Ansatz und verbindet diesen mit der Selbstorganisation („Bottum up“) der Natur, um hybride nanobiotechnologische Maschinen zu entwickeln.

Molekulare Maschinen in der Biologie

Molekulare Maschinen nehmen in der belebten Welt eine ganz zentrale Rolle ein. Sie sind meist aus vielen funktionell gekoppelten Protein-Untereinheiten aufgebaut, oft auch mit integrierten Nukleinsäurestrukturen, und übernehmen solche wichtigen Funktionen wie Wandlung von Energie, Übersetzung der genetischen Information in funktionelle Bausteine, Fortbewegung, Zellteilung, intrazellulären Transport und Muskelkontraktion, um nur einige wenige zu nennen.
Energieumwandlung wird z. B. durch die rotierende Fo, F1-ATPase (ATP-spaltendes Enzym mit den Einheiten Fo und F1) realisiert [2]. Ein anderes Beispiel einer rotierenden Maschine stellt der Flagellenmotor des Bakteriums dar [3].
Neben den rotierenden Maschinen sind auch lineare progressive Motoren in der Natur von entscheidender Bedeutung. Beispielsweise wird der Transport von Organellen (Abb. 3), mit linearem progressiven Motor, hier dem Myosin V, bewerkstelligt [4]. Auf diese Beispiele soll hier weiter eingegangen werden.

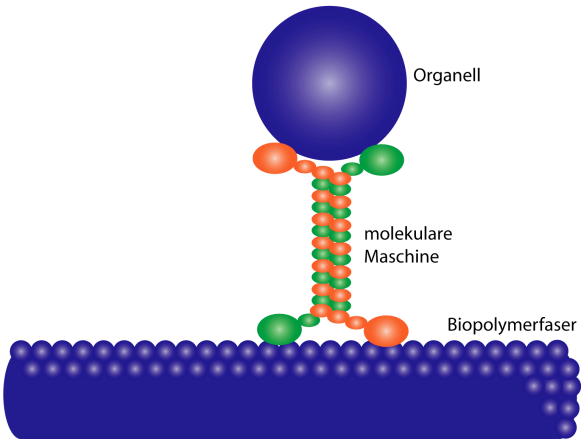

Abbildung 3: Transport von Organellen durch molekulare Maschinen entlang von Biopolymerfasern

Möglich geworden ist dieser detaillierte Einblick in die Funktionsweise dieser molekularen Maschinen durch die Entwicklung äußerst empfindlicher Techniken wie der optischen Falle [5] oder des Kraftmikroskop [6], die es erlauben, mit einzelnen Molekülen zu experimentieren.

F1-ATPase

ATP (Adenosintriphosphat), die zentrale und universelle chemische Energiewährung, muss jeder funktionellen Einheit in hinreichender Menge zur Verfügung stehen. Die ATP-Synthase, der hierfür zuständige Enzymkomplex, ist also eine der zentralen molekularen Maschinen, die schon in der Evolution an ganz vorderster Stelle gestanden haben muss. Um so mehr schockierte die Erkenntnis, die sich in den letzten zehn Jahren, hauptsächlich aufgrund der bahnbrechenden Experimente in den Gruppen von Wolfgang Junge und Kinosita durchgesetzt hat: Die Synthase besteht aus einer rotierenden molekularen Maschine, die zyklisch ADP (Adenosindiphosphat) und Pi (ionischen Phosphor) aufnimmt, um im nächsten Segment ein fertiges ATP wieder auszuspucken [2, 7, 8]. Über eine Art Kardanwelle ist diese Maschine an eine Turbine angeflanscht, die ihrerseits vom Protonengradienten über der Membran angetrieben wird (Abb. 4). Die vergleichsweise einfache chemische Reaktion wird also durch einen mechanisch gekoppelten Maschinenkomplex bewerkstelligt, der durch eine molekulare Turbine angetrieben wird.

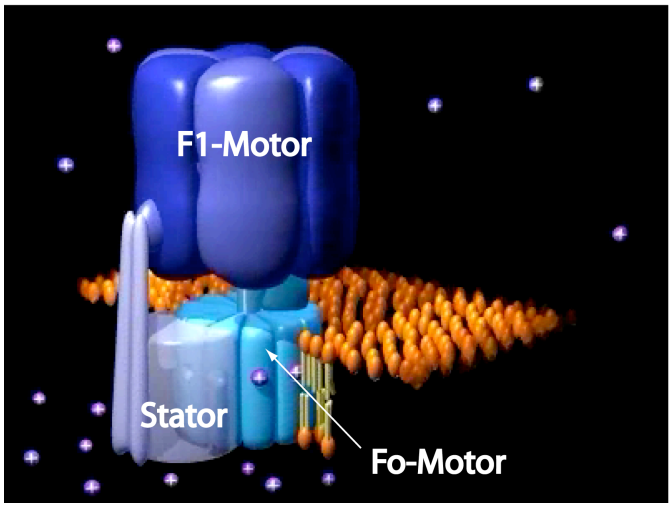

Abbildung 4: Aufbau und Funktion der Fo, F1-ATPase, bestehend aus Fo-Maschine, F1-Maschine und Stator (Abb. W. Junge).

Im Detail weiß man heute, dass die Fo, F1-ATPase sich in drei Untereinheiten aufteilt. Der erste Teil ist die F1-Maschine, die sich außerhalb der Membran befindet und ATP aus ADP und Pi synthetisiert. Der zweite Teil ist die Fo-Maschine, die in der Membran verankert ist und durch einen Protonengradienten über der Membran in Rotation versetzt wird. Der dritte

Teil der Fo, F1-ATPase ist der Stator, der beide Maschinen mechanisch miteinander verbindet [9].

Da es sich hier um eine rotierende Maschine handelt, also ein zyklischer Prozess zugrunde liegt, ist die Vermutung zulässig, dass diese in zwei Richtungen betrieben werden kann. In der einen Richtung wird durch einen Protonengradienten über der Membran von innen nach außen die Fo-Maschine zum Rotieren angetrieben. Ist ein Überschuss von ADP und Pi vorhanden, so binden beide Moleküle an eine Untereinheit der F1-Maschine, und unter Ausnutzung eines Protonengradienten über der Membran kommt es zur Rotation der Fo-Einheit der Maschine. Da hierbei ATP synthetisiert wird, spricht man von der ATP-Synthase [2, 7].

Genauso kann die Maschine auch in die andere Richtung rotieren. Dazu wird in der Umgebung der F1-Einheit ein Überschuss von ATP benötigt. Das ATP bindet an eine der Untereinheiten und durch Hydrolyse wird ATP zu ADP und Pi abgebaut. Die rotierende Fo-Maschine pumpt nun Protonen in die entgegengesetzte Richtung [2, 8].

Mithilfe von Einzelmolekülexperimenten lässt sich zeigen, dass bei einem ATP-Überschuss die F1-Maschine in 120°-Schritten rotiert und dass für jeden Schritt ein ATP-Molekül hydrolisiert wird [7]. Aus den gemessenen Drehmomenten kann man eine bemerkenswerte Effizienz von fast 100 Prozent für diese Maschine ableiten. Auch die Größe der gesamten ATP-Produktion eines Organismus, lässt die Bedeutung dieser molekularen Maschine noch einmal klarer werden: Wird die tägliche Energieaufnahme des Menschen mit etwa 3000 Kilokalorien angesetzt, und nehmen wir an, dass 70 Prozent davon als ATP am schließlichen Endverbraucher ankommt, dann können bei der pro ATP-Synthese benötigten Energie von 20 k_BT ca. 10^{28} ATP-Moleküle gebildet werden, die ca. 100 Kilogramm wiegen! Angesichts der nur wenige Nanometer großen Maschinen eine sehr bemerkenswerte Leistung, die allerdings auch zeigt, wie vielfach und damit auch wie wichtig dieser Prozess ist.

Solche Maschinen beflügeln natürlich die Phantasien, diese Funktionseinheiten in eine künstliche Umgebung einzubauen. Erste Versuche wurden beispielsweise mit einer isolierten F1-ATPase durchgeführt. Dazu wurde diese auf einem SiO_2/Ni-Substrat immobilisiert und so modifiziert, dass ein molekularer Draht mit der F1-ATPase verbunden ist. Wird durch Zugabe von ATP Energie gewonnen, führt dies zu einer rotierenden Bewegung der F1-ATPase und damit zur Rotation des molekularen Drahts [10]. Dies ist eines der möglichen Beispiele, wie eine biologische molekulare Maschine in eine artifizielle Umgebung eingebettet werden kann, um dort Arbeit zu verrichten.

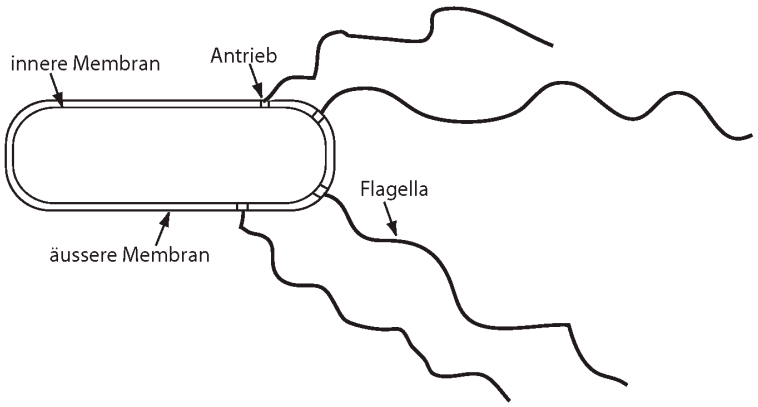

Abbildung 5: Schematische Darstellung eines Bakterium mit Flagella.

Flagellen

Ein weiteres Beispiel für eine rotierende Maschine stellt der Antrieb des Flagellums dar (Abb. 5) [3]. Flagellen sind lange, dünne, helikale Filamente, die über eine Maschine mit dem Bakterium verknüpft sind. Das Charakteristische an ihnen ist, dass sie um ein Vielfaches länger sind als das Bakterium selbst und weit in das externe Medium hineinragen.
Ähnlich wie bei der ATPase lässt sich der Flagellenantrieb in drei Untereinheiten aufteilen (Abb. 6). Der erste Teil ist eine rotierende Maschine, die sich in der Zellwand befindet und in beide Richtungen rotieren kann. Der zweite Teil ist eine flexible Verbindung zwischen der Maschine und dem Filament. Der dritte Teil ist das helikale lange Filament, das als Propeller dient. Das Drehmoment des Flagellums, das diese Maschine erzeugt, wird zwischen dem Stator, der fest mit der Zellwand verbunden ist, und dem Rotor am Flagellenfilament aufgebaut. Dabei wird die Maschine durch einen Protonengradienten vom Zelläußeren ins Zellinnere angetrieben.

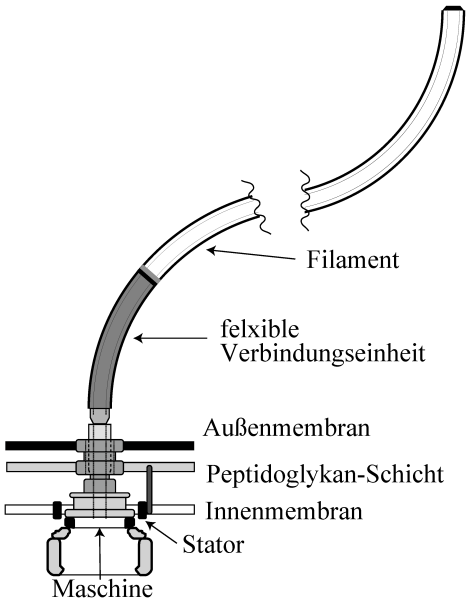

Abbildung 6: Detaillierter Aufbau des Antriebs des Flagellums, bestehend aus Maschine, Stator und flexible Verbindungseinheit.

Der Vergleich zwischen der ATPase und dem Flagellum zeigt eine stark angestiegene Komplexität im Aufbau des Flagellums. Diese Komplexität kann nur durch Selbstorganisation bewerkstelligt werden. Dazu werden durch den Kanal im Inneren des Flagellums nacheinander die einzelnen Bausteine (Proteine) geschickt, die sich dann am Ende in der entsprechenden Art und Weise miteinander verknüpfen. Diese hochkomplexen Flagellen sind in der Lage, Bakterien mit bis zu 35 Mikrometern/Sekunde anzutreiben.
Langfristig ist man an einem umfassenden Verständnis des Flagellenantriebs interessiert. Es stellt sich ferner die Frage, ob es möglich wäre, diesen Antrieb zu isolieren und in eine artifizielle Umgebung einzubauen, um dann Hybridsysteme anzutreiben. Darüber hinaus gewinnt auch die Vorstellung, einzelne Antriebskomponenten zu isolieren und diese gezielt zu manipulieren oder mit anderen nicht biologischen Komponenten zu verbinden, sehr an Faszination.

Myosin V

Neben den rotierenden Maschinen gibt es in der Natur auch eine große Zahl verschiedener linearer Motoren. Deren Bewegung vollzieht sich unidirektional und meist prozessiv entlang von Proteinpolymeren wie Aktinfilamenten oder Mikrotubuli (Abb. 3) [4, 11].
Myosin V, das hier eingehender diskutiert werden soll, ist ein Proteinkomplex, der zum einen eine globuläre Cargo-Bindungsstelle besitzt (Abb. 7), an der z. B. Vesikel oder Makromoleküle angebunden werden können, und zum anderen über globuläre Motordomänen

verfügt, die für das Fortbewegen verantwortlich sind. Beide Einheiten, die Lastenbindungsstelle und die Motordomäne, sind über eine strukturierte Polypeptidkette verbunden. Unter Hydrolyse von ATP bewegt sich Myosin V prozessiv entlang von Aktinfilamenten.

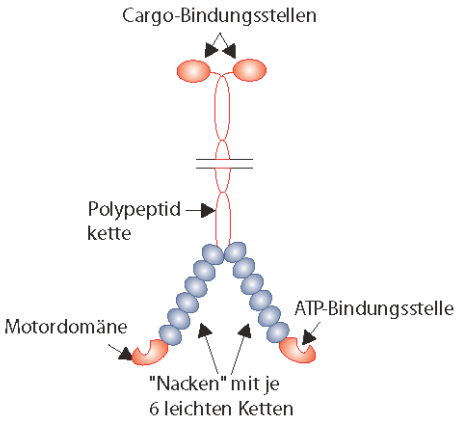

Abbildung 7: Molekulare Maschine Myosin V mit Cargo-Bindungsstelle, Polypeptidkette, Motordomäne und ATP-Bindungseinheit (Abb. M. Rief).

Das große Interessante an solchen linearen molekularen Motoren liegt zum einen darin begründet, dass auf deren Fehlfunktionen eine Reihe ernsthafter Krankheiten zurückgeführt werden konnte. Viel interessanter ist aber im Rahmen der hier diskutierten Hybridstrukturen die Möglichkeit, solche Motoren zum gerichteten Transport artifizieller Strukturen nutzen zu können. Eine mögliche Anwendung wurde jüngst demonstriert, indem einzelne molekulare Maschinen auf einer strukturierten Oberfläche immobilisiert wurden. Diese Motoren konnten unter ATP-Verbrauch einzelne Mikrotubuli durch einen vorstrukturierten Parcours transportieren und so verschiedene Lasten befördern, die an den Mikrotubuli befestigt waren [12].

Es wurde dargelegt, dass biologische molekulare Maschinen chemisch angetrieben werden. ATP und Protonengradienten stellen dabei die wichtigsten Energiequellen dar. Ein Vergleich zwischen den biologischen molekularen Maschinen und den artifiziellen nanoelektromechanischen Maschinen zeigt, dass die Art des Antriebs der biologischen molekularen Maschinen vergleichsweise langsam ist, da alle Prozesse diffusiv gebremst werden. Der große Vorteil biologischer Maschinen ist aber ihre bemerkenswerte Eigenschaft, sich selber zu organisieren und funktionierende Systeme aufzubauen.

Demgegenüber steht der große Vorteil der Siliziumtechnologie, eine parallele designgerichtete Technologie zu sein, die zudem schnell arbeitet. Eine Kombination beider

Technologien wäre also hochgradig komplementär! Leider leiden die meisten halbleitenden Materialien unter den sehr korrosiven Bedingungen in einer Zelle, was die Versschmelzung erschwert. Jedoch: Lösungsstrategien mit intelligenter Oberflächenchemie sind in der Entwicklung. Außerdem muss in der Siliziumtechnologie immer noch der „Top-down"-Ansatz beschritten werden, der aber in seiner Größe beschränkt ist. Auch hier können aber moderne Raster-Sonden-Techniken bereits die Brücke schließen.

Nanotechnologische Einzelmolekül-Werkzeuge

Möglich geworden sind diese detaillierten Einblicke in die Funktionsweisen molekularer Maschinen erst in den letzten Jahren durch die Entwicklung neuer, extrem empfindlicher Einzelmolekül-Techniken. Da die Entwicklung dieser Techniken direkt mit der Entwicklung künftiger Hybridsysteme einhergeht, soll hier näher auf die wichtigsten eingegangen werden.

Optische Falle

Bei einer optischen Falle handelt es sich um ein optisches Gradientenfeld, typischerweise realisiert durch einen stark fokussierten Laserstrahl. Auf Teilchen mit hohem relativem Brechungsindex wirkt eine Kraft zu hohen Feldstärken hin, die bei geeigneter Wahl der Feldgeometrie benutzt werden kann, um diese Teilchen zu manipulieren (Abb. 8a). Typischerweise können optische Fallen Kräfte zwischen 0,1 und 100 pN (Piconewton) ausüben und mit einer lateralen Genauigkeit im Nanometerbereich messen [5].

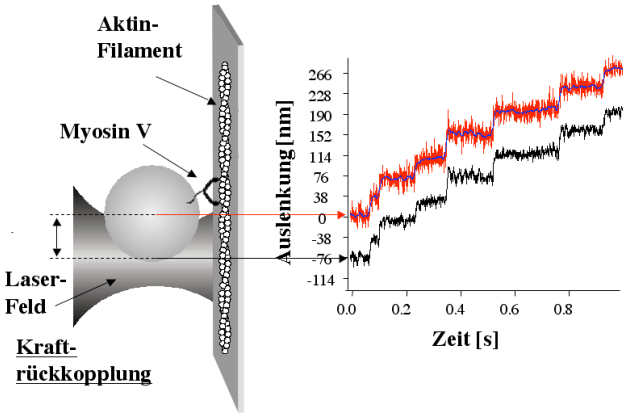

Abbildung 8: a) Aufbau einer optischen Falle, bestehend aus Laserstrahl mit eingefangener Kugel und positionierbarer geregelter Unterlage. Myosin V ist an die Kugel angebunden und bewegt sich entlang eines Aktin-Filaments. b) Auslenkung der Kugel durch die Bewegung der Myosin V-Maschine mit der Zeit (Abb. M. Rief).

Wird eine molekulare Maschine wie Myosin V an ein Latexkügelchen gebunden und dieses in Kontakt mit einem Aktinfilament gebracht, so fängt Myosin V an, sich entlang der Aktinfilamente unter Verbrauch von ATP zu bewegen. Diese Bewegung führt dazu, dass die Kugel aus dem Laserstrahl herausgezogen wird. Damit die Kraft nicht zu groß wird, regelt man die Probe nach, d. h. die Unterlage, auf der die Aktinfilamente liegen, wird so bewegt, dass die Kraft wieder sinkt. Diese laterale Veränderung, aufgetragen über die Zeit, resultiert in einer stufenförmigen Abhängigkeit (Abb. 8b). Die resultierenden Stufen repräsentieren das Bewegungsverhalten des Myosin V entlang der Aktinfilamente. Ebenso ist es möglich, die Länge und Zeit pro Schritt zu messen, um so Informationen über die Lauflänge und Geschwindigkeit der Maschine zu gewinnen [4, 11].

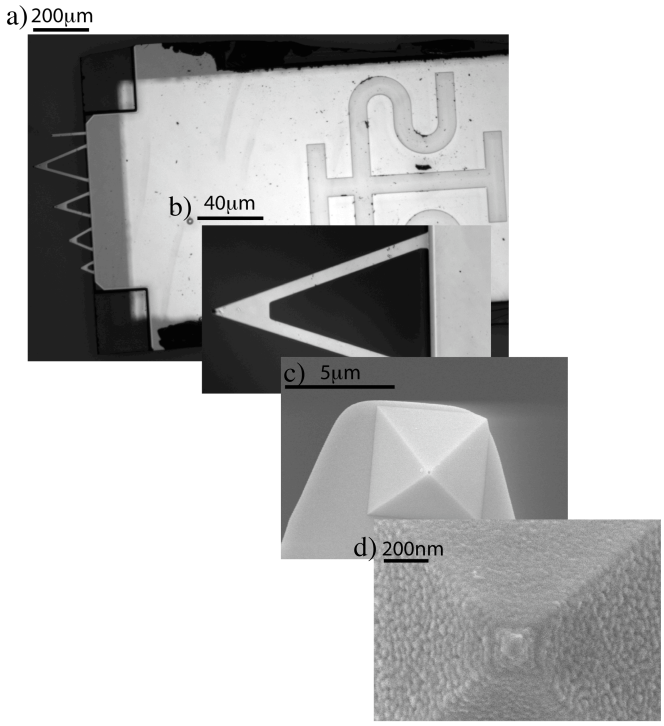

Abbildung 9: Siliziumnitrid-Spitze für das Kraftmikroskop. a): Siliziumnitrid Chip mit Cantilevern unterschiedlicher Länge (links); b): Einzelner Cantilever mit kleiner pyramidenförmiger Spitze (Länge ca. 200 μm); c): Pyramidenförmige Spitze (Durchmesser ca. 5 μm); d): Vergrößerung der pyramidenförmige Spitze.

Kraftmikroskop

In den 80er-Jahren gelang es erstmals, einzelne Atome in einer Oberfläche mithilfe eines Rasterkraftmikroskops abzubilden [6]. Dieses Mikroskop benutzt eine atomar scharfe Spitze am Ende einer extrem weichen Blattfeder (Cantilever, Abb. 9), um mit Piezostellgliedern die

Oberfläche abzutasten (AFM für Atomic Force Microscope) [13]. Mit einer Laseroptik wird die Auslenkung der Feder und aus dieser die Kraft bestimmt, die zwischen Spitze und Probe wirkt. Bei den besten heutigen Instrumenten ist die Positionierung bis auf Bruchteile von Atomdurchmessern genau möglich und die Kraftmessung ist nur durch thermisches Rauschen limitiert (Abb. 10).

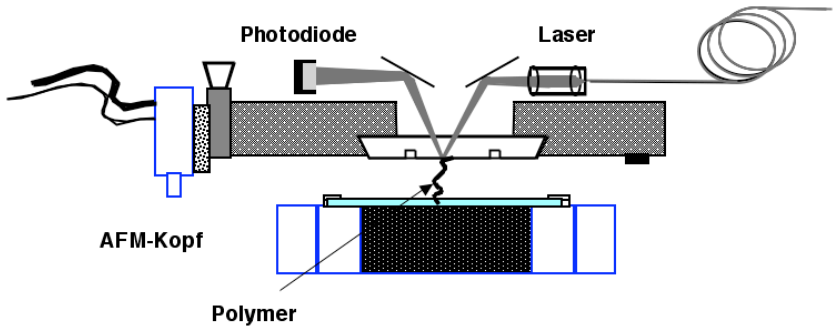

Abbildung 10: Typischer Aufbau eines Kraftspektrometers. Der Laserstrahl wird über eine Optik auf den Cantilever fokussiert, von dort reflektiert und mit einer Segment-Photodiode detektiert. Als Unterlage wird in der Regel ein Glasobjektträger verwendet, der mit einem Piezostellglied auf und ab bewegt wird.

Dieses Instrument eignet sich also auch ganz hervorragend dazu, gezielt und kontrolliert Kräfte auszuüben. Es hat sich deshalb als Basisinstrument für die molekulare Manipulation etabliert; die Einzelmolekül-Kraftspektroskopie hat sich daraus entwickelt. Bei geeigneter Modifikation der Spitze lassen sich mit solchen Instrumenten z. B. Kräfte zwischen einzelnen Molekülen bestimmen [14, 15], aber auch die Kräfte innerhalb großer Moleküle, wie etwa Biopolymere lassen sich als Funktion der Dehnung dieser Moleküle bestimmen [16–21]. Zu diesem Zweck bindet man die zu untersuchenden Moleküle, die zum einen auf ihrer Unterlage kovalent verankert sind, chemisch an die Spitze der AFM-Feder [16, 22–25].

In Abb. 11 ist solch ein Experiment schematisch dargestellt. Hier wurde eine bestimmte Art von Rezeptormolekülen an der Spitze des AFMs gekoppelt. Diese Spitze wurde dann der Oberfläche angenähert, auf der Ligandmoleküle mit langen polymeren Ankern gebunden sind. Die laterale Dichte dieser Liganden wurde dabei so gering gewählt, dass die Wahrscheinlichkeit, dass sich gleichzeitig mehrere Rezeptor-Ligand-Paare finden, sehr klein ist. Beim Zurückziehen der Spitze wird, falls ein molekularer Komplex gebildet wurde, zuerst der polymere Anker gedehnt, bis schließlich die Kraft im Rezeptor-Ligand-Komplex die Bindungskraft übersteigt und der Komplex zerfällt. Aus solchen Kraft-Dehn-Kurven können jetzt zum einen intramolekulare Prozesse, wie etwa die Entfaltung von Proteinen [19, 20] oder

auch das Aufspalten von DNA-Doppelsträngen [18, 25], herausgelesen und quantifiziert werden. Interessanterweise zeigt sich bei der Analyse einer großen Zahl verschiedener biologischer Systeme, dass mit den jeweils charakteristischen Kräften auch eine Längenskala verknüpft ist, auf der diese Prozesse ablaufen.

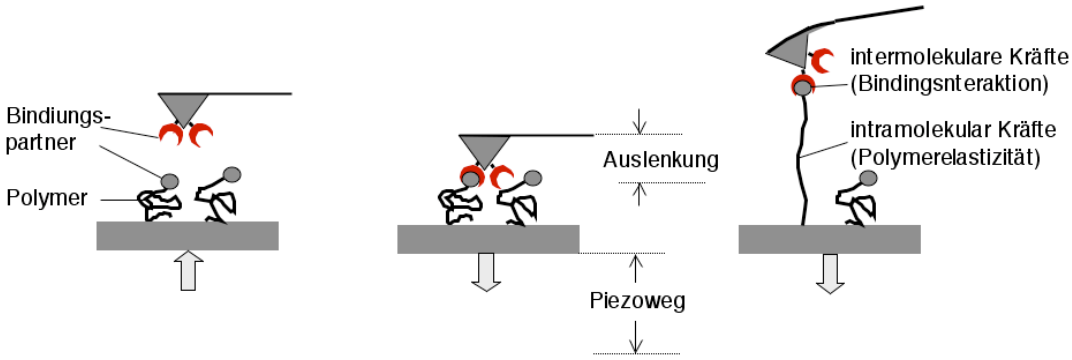

Abbildung 11: Prinzipieller Ablauf eines Kraftspektroskopie-Experiments. Die zu untersuchenden Kräfte unterteilt man in intramolekulare und intermolekulare Kräfte. Die intramolekularen Kräfte lassen Rückschlüsse auf die Polymerelastizität zu; die intermolekularen Kräfte sind z. B. Kräfte, die aufgewendet werden, um die Bindung des Rezeptor-und-Ligand-Komplexes zu öffnen. An der Spitze ist der Rezeptor angebunden und an der Unterlage ein Polymer mit dem Liganden. a): Das Substrat mit dem Liganden wird an die Spitze mit dem Rezeptor angenähert; b): Wechselwirkungen zwischen Rezeptor und Ligand finden statt; c): Entfernt man das Substrat von der Spitze, wird das Polymer gestreckt und die Bindung zwischen Rezeptor und Ligand belastet.

So braucht es zum Entknäueln eines Polymers Kräfte von wenigen Piconewton, und diese Knäuel haben typische Dimensionen von zig Nanometern. Das Entfalten von Proteinen hingegen verlangt Kräfte von einigen zig Piconewton, bei charakteristischen Dimensionen von wenigen Nanometern. Allen Prozessen ist gemein, dass sie auf der rechten Seite der "grünen Grenze" geschehen, die durch die thermische Energieskala 4 Piconewton · Nanometer bei Raumtemperatur definiert ist (Abb. 12) [14]. Alle Prozesse verlaufen offensichtlich nahe dem thermischen Gleichgewicht!

Hirarchy of Molecular Mechanics

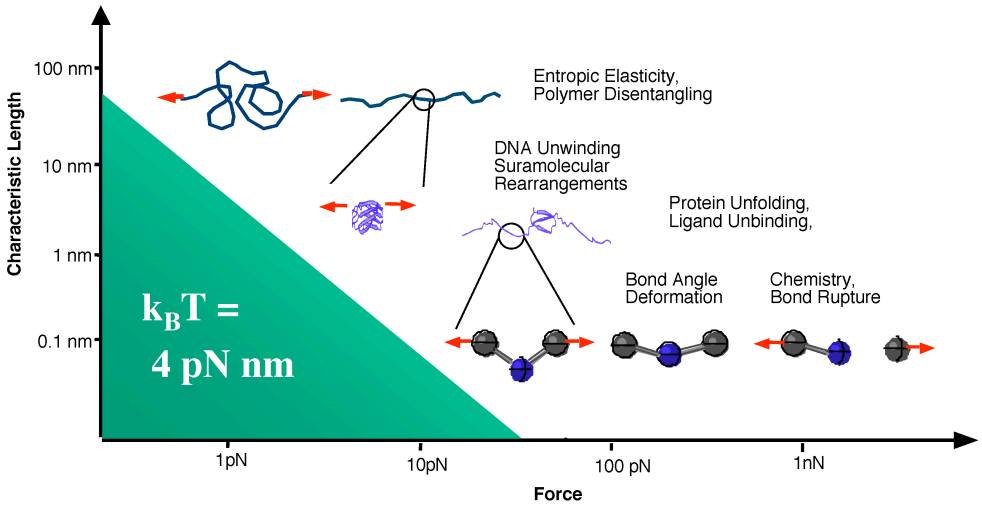

Abbildung 12: Übersicht über die zu untersuchenden Längen und Kraftbereiche oberhalb der thermischen Energiegrenze von k_BT = 4 pN nm

Carbon meets Silicon!

Licht-getriebene Einzelmolekülmaschine

Ein Beispiel einer solchen Kombination aus siliziumbasierten Nanostrukturen und kohlenstoffbasierten Funktionselementen ist in Abb. 13 gegeben. Hier wurde ein photoaktives Polymer kovalent zwischen einem Piezostellglied und einem AFM-Cantilever eingespannt. Das Polymer ist aus Azobenzol-Einheiten aufgebaut, die optisch durch Einstrahlen von Licht bestimmter Wellenlänge zwischen zwei stabilen Zuständen hin und her geschaltet werden können. Da sich beide Zustände durch die Längen der Monomereinheiten unterscheiden, kann das Polymer auf diese Weise verkürzt bzw. wieder verlängert werden. Das Polymer biegt durch seine Kontraktion den Cantilever, leistet also mechanische Arbeit. Mit dieser experimentellen Geometrie kann man also prinzipiell die direkte opto-mechanische Energie-Konversion an einem einzelnen Molekül untersuchen und technologisch nutzbar machen [22, 23].

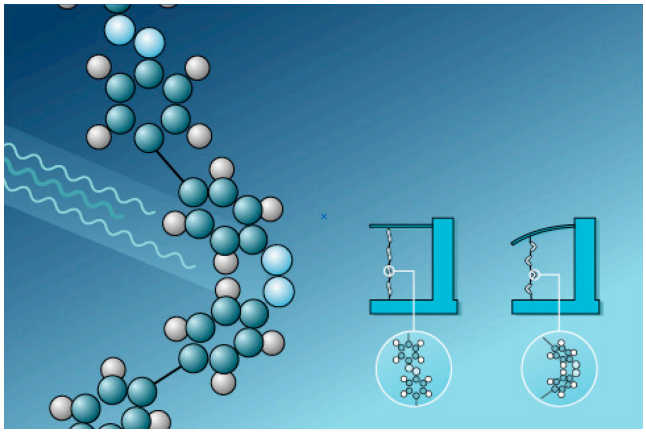

Abbildung 13: Prinzipieller Aufbau einer künstlichen Einzelmolekülmaschine, durch Licht angetrieben

In Abb. 14a ist schematisch dargestellt, wie ein optisch getriebener Einzelmolekülmotor funktionieren kann. Im Gedankenexperiment belasten wir das Polymer mit einer leeren Waagschale (Position (I)). Ein Gewicht, das wir auflegen, dehnt das Polymer gegen seine Entropieelastizität und wir erreichen Position (II). Jetzt wird das Polymer optisch um den Betrag δl (Länge 2 – Länge 1) kontrahiert, das Gewicht wird angehoben, die mechanische Arbeit F1 x δl wird dabei verrichtet (Position (III)). Das Gewicht wird von der Waagschale genommen, und das Polymer wird durch Belichten wieder in den expandierten Zustand zurückversetzt. Insgesamt ist also ein kompletter Zyklus durchlaufen worden, in dem optische Energie in mechanische Arbeit umgesetzt wurde.

Mit dem oben beschriebenen experimentellen Schema wurde das Gedankenexperiment realisiert. Wie in Abb. 14b dargestellt, wurde dabei das System Polymer/Cantilever durch das Piezostellglied in einem Kreisprozess getrieben, der hier in der Kraft-Dehnungsebene dargestellt wurde, dem eindimensionalen Analogon der sonst üblichen Druck-Volumen-Darstellungen bei makroskopischen Wärmekraftmaschinen. Faszinierenderweise folgt der optisch betriebene Motor einem Otto-Zyklus mit dem kleinen, aber energiefressenden Unterschied, dass statt des Öffnens des Auslassventils hier das Polymer optisch wieder in den Ursprungszustand versetzt werden muss (Abb. 14a).

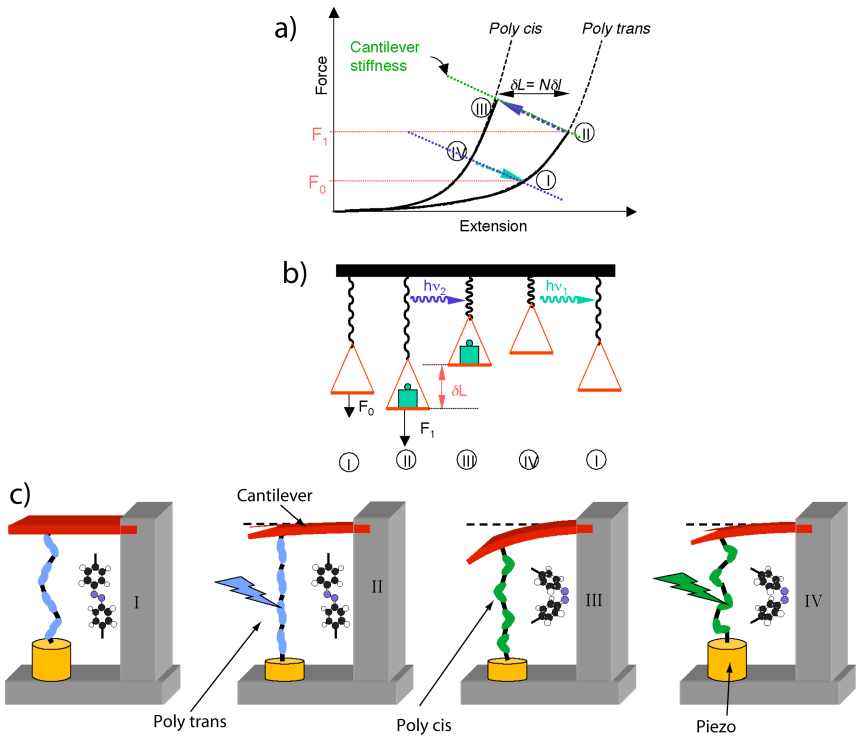

Abbildung 14: Experimentelle Realisierung der Einzelmolekülmaschine. a): Arbeitszyklus einer optisch angetriebenen Einzelmolekülmaschine in einem Kraft-Abstands-Diagramm; b): Illustration des Arbeitszyklus einer solchen Maschine. Die unterschiedlichen Federn stellen das Polymer im trans- und cis-Zustand dar. Das Gewicht beschreibt das Strecken des Polymers; c): Experimenteller Ablauf einer Einzelmolekülmaschine in einem Kraftspektroskopie-Experiment.

Insgesamt lassen sich die Ergebnisse dieser ersten Studie, an der optomechanische Konversion mit einzelnen Molekülen demonstriert wurde, so zusammenfassen, dass prinzipiell die Stellkräfte solcher Polymere, die bis zu mehreren hundert Piconewton betragen können, durchaus geeignet sind, um optisch geschaltete nanomechanische Funktionseinheiten auch technisch zu realisieren. Allerdings sind die Wirkungsgrade der Kreisprozesse von bisher noch weniger als 1 Prozent sehr verbesserungswürdig.

Strukturieren auf der Nanometerskala: die molekulare Werkzeugmaschine

Wie einführend beschrieben, wird das Kraftmikroskop vorwiegend zum Abbilden, optional aber auch zum Manipulieren und Strukturieren von Oberflächen benutzt. Von besonderem Vorteil ist dabei die extrem gute Positionspräzision der Spitze von Bruchteilen von Atomdurchmessern. Es ist durchaus nahe liegend, darüber zu fantasieren, ob es denn nicht möglich sein sollte, die Spitze durch ein intelligenteres Werkzeug zu ersetzen.
Mutter Natur hat solche Werkzeuge: Enzyme und Kinasen regeln durch gezielten Ab- und Aufbau die Entstehung lebender Systeme. Enzyme sind in der Lage, ihre Zielsubstanzen mit

extremer Präzision an einer genau vorbestimmten Stelle umzubauen, sie also auf molekularer Ebene zu bearbeiten. Solch ein Enzym an der Spitze der AFM-Nadel wäre die ultimative Miniaturisierung der maschinellen Bearbeitung, die molekulare Werkzeugmaschine.

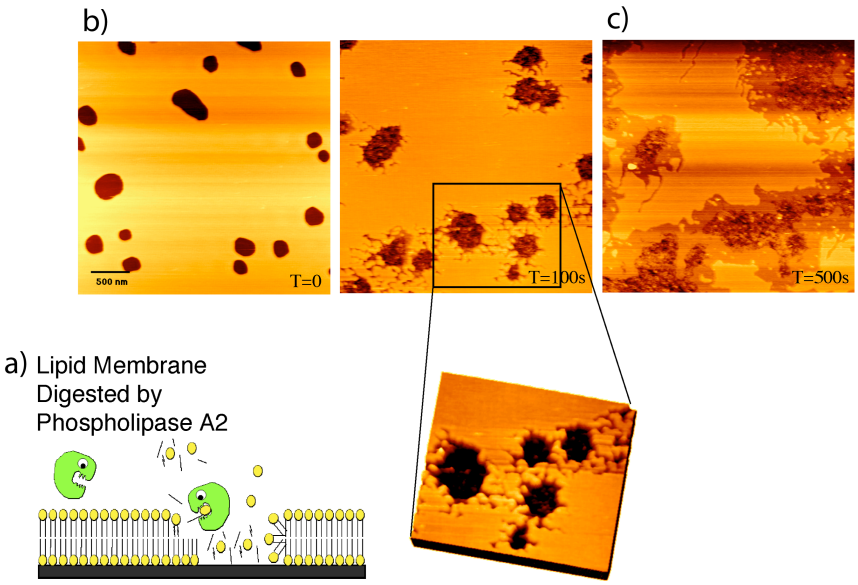

Abbildung 15: Phospholipase A2 (PLA2) bei der Arbeit. a): Die Phospholipase greift zuerst defekte Stellen in der Membran an; b, c): Rasterkraftmikroskopische Aufnahmen einer Lipid-Membran in Gegenwart von PLA2 bei verschiedenen Zeiten

Auf dem Weg dorthin sind noch viele Stolpersteine auszuräumen, aber einige Schlüsselexperimente wurden schon realisiert, die die prinzipielle Machbarkeit dieses Konzepts demonstriert haben. Eines davon ist in Abb. 15 skizziert. Hier wurde eine künstliche Membrandoppelschicht aus einem synthetischen Lipid auf einer Glimmeroberfläche mithilfe der Langmuir-Blodget-Technik übertragen und mit dem AFM abgebildet [13]. Die dunklen Flächen in der Membran sind Defekte, die bewusst als Angriffsstellen für eine Phospholipase eingebaut wurden. Phospholipasen sind Enzyme, die durch enzymatischen Abbau der Lipide biologische Membranen zerstören können, etwa als Bestandteil des Gifts der Klapperschlange. Eine derartige Lipase wurde der Modellmembran zugegeben mit dem Ergebnis, dass ausgehend von den Defekten die Membran zerfressen und aufgelöst wurde. Die Detailaufnahme zeigt sehr schön die dünnen Kanäle, durch die sich einzelne Lipasemoleküle bereits gefressen haben.

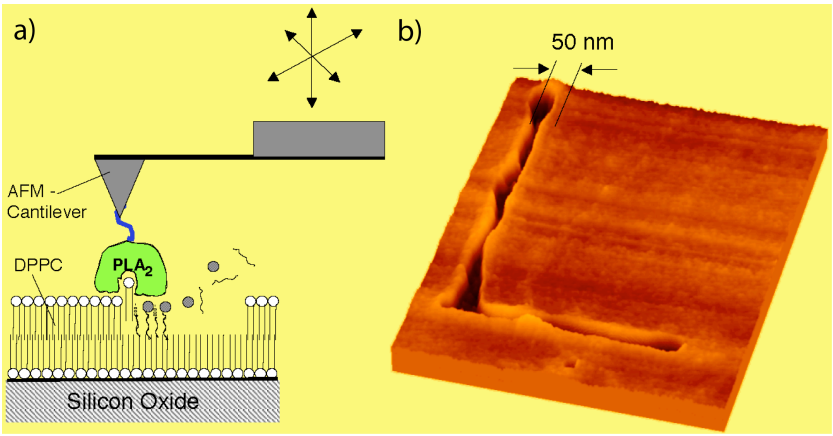

Abbildung 16: Nanostrukturierung einer Lipid-Membran mit Phospholipase, die an einem Cantilever angebunden ist. a): Cantilever mit Polymer (blau) und Phospholipase (grün) wird über eine DPPC-Membran bewegt; b): Ergebnis einer Nanostrukturierung mit der Phospholipase am Cantilever

Eine mögliche Realisierung der molekularen Werkzeugmaschine wäre also eine positionskontrollierte Lipase, z. B. gekoppelt an die AFM-Spitze [26]. Dieses Konzept wurde in ersten Modellexperimenten, wie sie in Abb. 16 gezeigt sind, bereits verwirklicht. Es zeigte sich zur großen Genugtuung, dass auf diese Weise die Aktivität der Phospholipase räumlich kontrolliert werden kann und dass in der Tat nanoskalige Strukturen in Lipidmembranen erzeugt werden können. Allerdings ergaben diese Messungen auch, dass die Kopplung zwischen Enzym und Siliziumspitze der neuralgische Punkt für Funktion, aber auch für technologische Praktikabilität ist und dass hier noch enormer Forschungsbedarf herrscht. Interessanterweise zeigt sich hier wieder, dass genau diese Grenze zwischen Silizium- und Kohlenstoffwelt wieder von größter Wichtigkeit ist und dass deren Beherrschung noch einiger Anstrengung bedarf.

Danksagung

Diese Arbeit beinhaltet eine Fülle von Darstellungen anderer Autoren, die dankenswerterweise durch anregende Diskussionen zum Entstehen dieses Manuskripts beigetragen haben.

Literatur

[1] Erbe, A., Weiss, C., Zwerger, W., Blick, R. H.: Nanomechanical resonator shuttling single electrons at radio frequencies. Phys. Rev. Lett. 87, 096106 (2001).

[2] Junge, W.: ATP synthase and other motor proteins. Proc. Natl. Adad. Sci. USA 96, 4735–4737 (1999).

[3] Berg, H. C.: Motile Behavior of Bacteria. Physics Today 24 (2000).

[4] Mehta, A. D., Rock, R. S., Rief, M., Spudich, J. A., Mooseker, M. S., Cheney, R. E.: Myosin-V is a processive actin-based motor. Nature 400, 590–593 (1999).

[5] Ashkin, A., Schütze, K., Dziedzic, J. M., Euteneuer, U., Schliwa, M.: Force generation of organelle transport measured *in vivo* by an infrared laser trap. Nature 348, 346–348 (1990).

[6] Binnig, G., Quate, C. F., Gerber, C.: Atomic force microscope. Phys. Rev. Lett. 56, 930 (1986).

[7] Noji, H., Yasuda, R., Yoshida, M., Kinosita, K.: Direct observation of the rotation of F-1-ATPase. Nature 386, 299–302 (1997).

[8] Itoh, H., Takahashi, A., Adachi, K., Noji, H., Yasuda, R., Yoshida, M., Kinosita, K.: Mechanically driven ATP synthesis by F-1-ATPase. Nature 427, 465–468 (2004).

[9] Yoshida, M., Muneyuki, E., Hisabori, T.: ATP synthase – A marvellous rotary engine of the cell. Nature Reviews Molecular Cell Biology 2, 669–677 (2001).

[10] Dogterom, M., Maggs, A. C., Leibler, S.: Diffusion and formation of microtubule asters: physical processes versus biochemical regulation. Proc. Natl. Acad. Sci. U S A 92, 6683–6688 (1995).

[11] Mehta, A. D., Rief, M., Spudich, J. A., Smith, D. A., Simmons, R. A.: Single-molecule biomechanics with optical methods. Science 283, 1689–1695 (1999).

[12] Hess, H., Bachand, G. D., Vogel, V.: Powering nanodevices with biomolecular motors. Chemistry 10, 2110–2116 (2004).

[13] Grandbois, M., Clausen-Schaumann, H., Gaub, H.: Atomic force microscope imaging of phospholipid bilayer degradation by phospholipase A2. Biophys. J. 74, 2398–2404, (1998).

[14] Clausen-Schaumann, H., Seitz, M., Krautbauer, R., Gaub, H.: Force spectroscopy with single bio-molecules. Curr. Op. Chem. Biol. 4, 524–530 (2000).

[15] Hugel, T., Seitz, M.: The Study of Molecular Interactions by AFM Force Spectroscopy. Macromol. Rapid Commun. 22, 989–1016 (2001).

[16] Hugel, T., Grosholz, M., Clausen-Schaumann, H., Pfau, A., Gaub, H., Seitz, M.: Elasticity of single polyelectrolyte chains and their desorption from solid supports studied by AFM based single molecule force spectroscopy. Macromolecules 34, 1039–1047 (2001).

[17] Oesterhelt, F., Oesterhelt, D., Pfeiffer, M., Engel, A., Gaub, H. E., Muller, D. J.: Unfolding pathways of individual bacteriorhodopsins. Science 288, 143–146 (2000).

[18] Rief, M., Clausen-Schaumann, H., Gaub, H. E.: Sequence dependent mechanics of single DNA-molecules. Nat. Struct. Biol. 6, 346–349 (1999).

[19] Rief, M., Fernandez, J. M., Gaub, H. E.: Elastically Coupled Two-Level-Systems as a Model for Biopolymer Extensibility. Phys. Rev. Lett. 81, 4764–4767 (1998).

[20] Rief, M., Gautel, M., Oesterhelt, F., Fernandez, J. M., Gaub, H. E.: Reversible unfolding of individual titin Ig-domains by AFM. Science 276, 1109–1112 (1997).

[21] Rief, M., Oesterhelt, F., Heymann, B., Gaub, H. E.: Single molecule force spectroscopy on polysaccharides by AFM. Science 275, 1295–1298 (1997).

[22] Holland, N. B., Hugel, T., Neuert, G., Cattani-Scholz, A., Renner, C., Oesterhelt, D., Moroder, L., Seitz, M., Gaub, H. E.: Single Molecule Force Spectroscopy of Azobenzene Polymers: Switching Elasticity of Single Photochromic Macromolecules. Macromolecules 36, 2015 (2003).

[23] Hugel, T., Holland, N. B., Cattani, A., Moroder, L., Seitz, M., Gaub, H. E.: Single-Molecule Optomechanical Cycle. Science 296, 1103 (2002).

[24] Grandbois, M., Beyer, M., Rief, M., Clausen-Schaumann, H., Gaub, H. E.: How Strong is a Covalent Bond? Science 283, 1727–1730 (1999).

[25] Clausen-Schaumann, H., Rief, M., Tolksdorf, C., Gaub, H. E.: Mechanical stability of single DNA molecules. Biophys. J. 78, 1997–2007 (2000).

[26] Clausen-Schaumann, H., Grandbois, M., Gaub, H. E.: Enzyme-assisted nanoscale lithography in lipid membranes. Advanced Materials 10, 949 (1998).

P2

“Single Molecule Force Spectroscopy of Azobenzene Polymers: Switching Elasticity of Single Photochromic Macromolecules“

N. B. Holland, T. Hugel, G. Neuert, A. Cattani-Scholz, C.Renner, D.Oesterhelt, L. Moroder, M. Seitz, and H. E. Gaub

Macromolecules 2003, 36, 2015-2023, 2003

Single Molecule Force Spectroscopy of Azobenzene Polymers: Switching Elasticity of Single Photochromic Macromolecules

Nolan B. Holland,[†,§] Thorsten Hugel,[†] Gregor Neuert,[†] Anna Cattani-Scholz,[‡] Christian Renner,[‡] Dieter Oesterhelt,[‡] Luis Moroder,[‡] Markus Seitz,[†] and Hermann E. Gaub*[,†]

Lehrstuhl für Angewandte Physik & Center for Nanoscience, Ludwig-Maximilians-Universität, Amalienstrasse 54, 80799 München, Germany, and Max-Planck-Institut für Biochemie, Am Klopferspitz 18 a, 82152 Martinsried, Germany

Received July 17, 2002; Revised Manuscript Received November 22, 2002

ABSTRACT: The reversible, optical switching of individual polymer molecules was observed using molecular force spectroscopy. We synthesized a polypeptide with multiple photoactive azobenzene groups incorporated in the backbone. The contour length of the polymer could be selectively lengthened or shortened by switching between the *trans*- and *cis*-azo configurations with 420 and 365 nm wavelength light, respectively. This *cis*- to *trans*-azo configurational transition induced by ultraviolet light resulted in a measurable change in polymer contour length. The contour length change was observed at low force and under external loads of up to 400 pN using a modified force spectrometer, in which the sample could be irradiated in total internal reflectance. The ability to shorten the polymer against an external load is the first demonstration of photomechanical energy conversion in an individual molecule. This is a significant milestone in the road toward molecular level machines.

Introduction

Reversible transformations in chemical species induced by photoexcitation have attracted much attention owing to their high potential for application in various optoelectronic devices, e.g., optical memory, photooptical switching, and display.[1−5] One such extensively studied molecular process is the *trans*/*cis* (or *E*/*Z*) configurational transition of double bonds, such as found in the stilbene or the azobenzene moiety. This photoinduced isomerization between the extended (*trans*) and the compact (*cis*) configurations is reversibly triggered at two different wavelengths of light and thus could be utilized as a light triggered switch.[2,6] It was the basis for the first artificial example of light-driven ion transport through membranes[7] and has since been frequently used in synthetic photoresponsive systems for regulating the geometry and function of biomolecules[8−10] and organic materials[4,5,11,12] as well as supramolecular complexes.[13−15]

In technological applications, the change in the absorptive properties upon photoisomerization has made azobenzene-based fast response liquid crystals successful for image storage devices,[16] and azobenzene sidechain polymers have proven to be an ideal material for erasable holographic data storage.[17−20] In addition, the reversible geometric change (lengthening and shortening) of the azobenzene chromophore upon photoisomerization may result in significant photomechanical effects, as this has been demonstrated for azobenzene polymers in bulk and solution.[21−27] For example, when azobenzene groups are incorporated into the backbone of a polymer, photoinduced changes in the hydrodynamic radius of the polymer coil were observed by viscosity measurements. Rigid linkers between the azobenzene moieties resulted in particularly large reversible changes of up to 60%.[23] While photomechanical effects have been utilized in bulk polymer materials, particular interest arises from their potential use for the construction of molecular machines in nanotechnology.

Biological molecular motors are capable of performing specific tasks in response to specific external energy sources in a highly sophisticated fashion[28−32] and thus may soon be utilized in nanoscopic devices. However, the design of synthetic molecular machines is just beginning to be explored.[33−39] Photons have been proposed as an ideal primary energy source because their application is fast, well controlled, and "clean"; i.e., it normally does not result in byproducts if used at moderate levels.[40] The ability to convert optical excitation energy into molecular motion thus makes photochromic molecules such as azobenzene highly promising for the development of synthetic molecular level machines.

The investigation and use of nanoscopic optomechanical energy transducers require interfacing them with the macroscopic world. In the past decade, mechanical experiments with single macromolecules in solution have become possible in a wide dynamic range and with an accessible force window from entropic forces at several femtonewtons (fN) to the rupture of covalent bonds above a nanonewton (nN).[41−51] It has been demonstrated for many systems that, with these tools, small differences in polymer length and minute forces generated by conformational changes can be directly measured; likewise, conformational transitions can be induced along polymer chains by mechanical stress, upon which the molecule's elastic properties may undergo marked changes.[51−54] Such transitions in the polymer chains have been described as a series of elastically coupled two-level systems, each representing

* To whom correspondence should be addressed: e-mail gaub@physik.uni-muenchen.de.
[†] Ludwig-Maximilians-Universität.
[‡] Max-Planck-Institut für Biochemie.
[§] Current address: Department of Physiology and Biophysics, Case Western Reserve University, 10900 Euclid Avenue, Cleveland, OH 44106.

10.1021/ma021139s CCC: $25.00
Published on Web 02/25/2003

one individual segment (or module) of the polymer chain.[55] These developments open the possibility of studying the photoisomerization of azobenzene by atomic force microscopy (AFM)-based force spectroscopy, when many chromophores are incorporated into a polymer backbone to amplify the photomechanical effect in a single chain.

In this paper, we describe the coupling of optical excitation with AFM force spectroscopy, utilizing an object slide as a waveguide. With this combined experimental setup, it is possible to measure the mechanics of single photochromic polymers precisely and simultaneously to their manipulation by optical excitation. We thoroughly characterized a polyazopeptide, observed reversible length changes of single chains as induced by light of different wavelengths, and also studied this process under the influence of an external stretching force. Our findings provide the first experimental basis for controlled optomechanical energy transduction and optical information storage at the level of individual molecules employing synthetic photochromic polymers.

Experimental Section

AFM Setup with Optical Excitation. Single molecule force spectroscopy was performed on a home-built instrument and a modified Molecular Force Puller (Asylum Research, Santa Barbara, CA). In each instrument the tip sample separation is controlled by a one-dimensional piezo equipped with a position detector. Using the measured value of the sample position allows us to eliminate any contribution of piezo drift to our measurements. Microlevers (Thermomicroscopes, Sunnyvale, CA; nominal spring constants: 13 and 30 mN/m) were coated by thermal evaporation with 5 nm of chrome−nickel (80:20) followed by 50 nm of gold to allow for the chemical binding of the thiol ends of the polymers. The spring constant of each cantilever was calibrated prior to use by measuring the amplitude of the thermal oscillations.[56]

We redesigned the sample stage in order to couple optical excitation with measurements of the mechanical response of a single polymer molecule. The general concept of the design is that the sample is attached to a glass microscope slide, which is used as a waveguide (Figure 1). The light of a xenon flashlamp JML-C1 (Rapp OptoElectronic, Hamburg, Germany) with a pulse length of 1 ms was filtered either by a 365 nm band-pass filter (band half-width = 12.2 nm, maximum pulse energy $E_{max} = 10$ mJ) for *trans*- to *cis*-azo switching or a GG 420 nm colorglass filter ($E_{max} = 100$ mJ) for *cis*- to *trans*-azo switching. In addition, a colorglass BG12 blocked long wavelength excitation. The light was focused onto the polished edge of the microscope slide. The energy of the light pulse before entering the object slide was measured by a Thermal Power Meter (Spectra Physics, model 407A). The evanescent wave from total internal reflection of the excitation light beam passing through the slide irradiates the sample while interactions with the cantilever are minimized. Total internal reflection was of crucial importance to eliminate the deleterious effects of absorption by and thermal heating of the cantilevers. The measurements were performed in dimethyl sulfoxide (DMSO), which has a refractive index of 1.48; therefore, high refractive index flint glass slides (F-2, Schott Glas Mainz, Hellma Optik GmbH Jena, $n_D \sim 1.666$) were necessary to satisfy conditions for total internal reflection as well as to provide high transmission in the UV.

Various test measurements were performed to exclude artifacts which might arise from several sources, including solvent effects and cantilever response to excitation light. The effect of a light pulse on the deflection signal in the absence of any polymer molecule was analyzed. Direct illumination of the sample resulted in such a strong interaction with the cantilever that the resulting cantilever deflection (corresponding to several nanonewtons of force) would result in a rupture of polymer attachment. This is why the total internal reflection

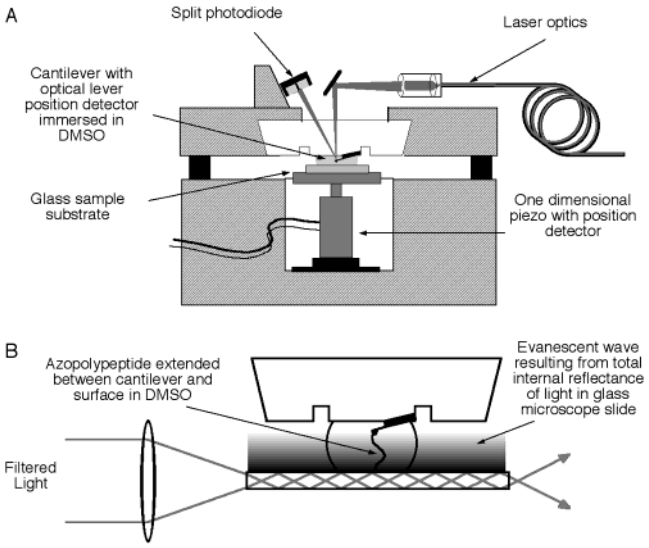

Figure 1. Schematic of the optomechanical experimental setup. A flint glass microscope slide is used in a dual role as a sample substrate for the force spectrometer (A) and as a waveguide for generating an evanescent field to excite the polymer sample (B). Light is generated using a flash lamp, and the desired ultraviolet wavelengths are chosen with band-pass filters. An additional high pass filter eliminates low-frequency radiation. The filtered light is directed into a polished end of the microscope slide at a low enough angle to result in total internal reflectance. The polymer sample, which is covalently attached to the cantilever spring tip and the glass slide, is excited by the evanescent wave while its mechanical properties are probed using the force spectrometer.

geometry is necessary. With the given length of the cantilever tip of several microns, the penetration depth of the evanescent field (wavelength $(\lambda)/2\pi \sim 50$ nm) is short enough to prevent interaction with the cantilever itself. Nonetheless, we observed further artifacts in the deflection signal from the lamp (Figure 2A,B), which were eliminated with careful experimental setup (Figure 2C,D) as described below in detail. No matter how carefully the light was coupled into the sample, stray light during the pulse reaches the photodiode, which detects the cantilever position. This appears as a 1 ms spike in the deflection signal but does not correspond to any cantilever motion or interfere with our measurements. A second artifact was observed as a small deflection which decays back to equilibrium on a time scale of seconds. As this only occurred in certain instances, when the light was not coupled well into the sample slide, it is believed to be caused by light energy being absorbed by the cantilever, resulting in a thermal bimetal effect. The final artifact was a damped oscillation in the deflection-time signal starting a few milliseconds after the light pulse and lasting several hundred milliseconds. This was caused by acoustic and vibrational noise from the flash lamp. By acoustically and mechanically decoupling the lamp from the AFM and shielding all light that is not coupled into the flint glass, we were able to reduce the detrimental artifacts below the thermal noise level (Figure 2C,D).

Further control experiments were performed to identify possible thermal side effects on the force vs extension curves of single polymer chains, which may be a result of the ultraviolet irradiation. While any thermal energy deposited on the molecule directly would be dissipated into the bulk medium at frequencies much faster than the time scale of our experiments, thermal effects resulting from heating of solvent or glass substrate cannot be excluded a priori. To fully exclude such thermal effects (as well as other possible irradiation artifacts affecting the measurement of single chain elasticity), control measurements were performed on polysaccharides, which do not contain photochromic molecular units. No measurable effects were observed in the force−extension curves of these polymers (Figure 3). These data also demon-

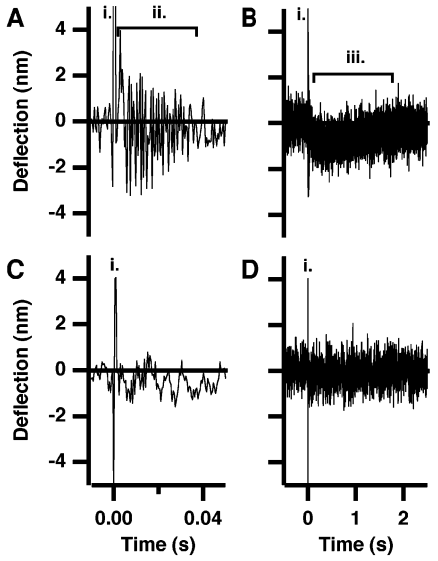

Figure 2. Interaction of light pulse with cantilever beam. The deflection signal of the cantilever probe vs time when a single flash of 420 nm wavelength light is coupled into the spectrometer reveals the successful isolation of the cantilever from the excitation. A setup where the coupling of the light into the sample slide is not ideal (A, B) shows significant interactions with the cantilever, including the initial light pulse impinging on the position sensing photodiode at $t = 0$ (i), the mechanical and acoustic noise arriving several milliseconds after the pulse (ii), and a presumably thermal interaction occurring on the time scale of seconds (iii). When the light pulse is well-coupled (C, D), the only signal observed is light pulse reaching the photodiode (i). The deleterious interactions with the cantilever are eliminated.

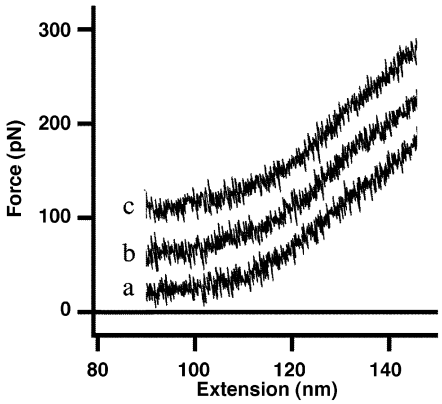

Figure 3. Effect of light pulses on polysaccharide molecule force traces. Three traces of the same polysaccharide molecule before excitation (a) and after excitation with light pulses of 365 and 420 nm wavelength (b and c, respectively) show no significant change in the force profile. This clearly demonstrates that the light pulse has no effect for a nonphotoactive molecules. Force trace (b) and (c) have been shifted by 40 and 80 pN, respectively.

strate that the trace to trace variability of measurements on the same chain is quite low. We estimate that we can effectively measure differences in persistence lengths of <0.2 nm and that the trace to trace variability is below this level in a well-controlled experiment.

Polymer Synthesis and Bulk Characterization. The preparation of optically switchable polymers for direct observation in molecular force spectroscopy was directed by three basic design parameters: the desire to maximize the potential length change upon irradiation, the need to chemically attach a chain both to the AFM probe tip and to the glass slide substrate, and the need for a sufficiently long chain. The polymer, which we prepared, is a sequential polypeptide with

Scheme 1. Synthesis of Azobenzene Containing Polypeptides

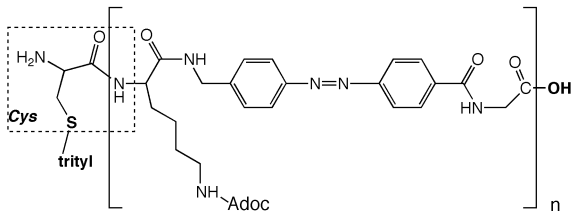

H-Gly-OH → H-AMPB-Gly-OPfp → H-Lys(Adoc)AMPB-Gly-OPfp·HCl
(1)

(1) → H-[Lys(Adoc)-AMPB-Gly]$_n$-OH → H-Cys(Trt)-[Lys(Adoc)-AMPB-Gly]$_n$-OH
(2)

multiple azobenzene moieties incorporated in the backbone. A heterobifunctionality of the N- and C-termini of the polypeptide chain provides for a gold−cysteine bond to the probe tip and an amide bond to an amino-functionalized surface.

For the incorporation of multiple azobenzene moieties into a linear polymer a sequential polypeptide approach based on polycondensation of tripeptide monomers containing (4-aminomethyl)phenylazobenzoic acid (AMPB)[57,58] was selected. For this purpose, the pentafluorophenyl ester of the pseudotripeptide **1** was synthesized in stepwise manner by classical procedures in solution (Scheme 1) and isolated as hydrogen chloride salt (homogeneous on HPLC: $t_R = 10.4$ min [Nucleosil 100-5 C18 (Macherey & Nagel, Germany); linear gradient of 2% H_3PO_4/acetonitrile from 95:5 to 10:90 in 13 min]; ESI-MS: m/z 785.4 [M + H]; M_r 784.3 calculated for $C_{39}H_{41}N_6O_6F_5$). Polycondensation of **1** was allowed to proceed in DMF at 0.4 M concentration and at room temperature for 24 h upon addition of 1.2 equiv of triethylamine. The resulting crude polymer was reacted with an excess of Fmoc-Cys(Trt)-OSu in DMF, and after 24 h, the reaction mixture was chromatographed on a phenogel 1K-75K (Phenomenex, Germany) column (300 × 7.8 mm) with DMF at 60 °C as eluent. The main fraction of ∼25 kDa molecular weight was collected and reacted with diethylamine for cleavage of the *N*-Fmoc group and generation of polymer **2**. Quantitative comparison of NH and $C^{\alpha}H$ proton signals in ^1H NMR spectra of the carboxy-terminal glycine residue with those of all other glycines allowed to estimate an average polycondensation degree of 28. NMR spectra also confirmed hydrolysis of the carboxy-terminal pentafluorophenyl ester during workup and isolation steps of the polymer.

From studies performed on azobenzene[59] as well as on peptides containing the AMPB moiety,[60,61] it is known that *cis*/*trans* photoisomerization of the azobenzene unit is reversible upon irradiation at $\lambda = 365$ and 450 nm, respectively. However, although the *trans*-azo isomer is obtained upon thermal relaxation in the dark, because of the spectral overlap of the excitations of *cis*- and *trans*-azo isomers, complete photoisomerization upon optical pumping is not possible. The maximum populations that are typically obtained in azobenzene-containing peptides are 70−80% of the *trans*- or *cis*-azo isomer;[58] for convenience, here, we refer to the saturated extended and the saturated short polymer configurations, as the dominant *trans*-azo state and *cis*-azo state, respectively. Upon thermal relaxation into the *all-trans*-azo configuration, the average contour length of the polymer was estimated at 54 nm.

Sample Preparation and Optomechanical AFM Experiments on Polyazopeptides. A stepwise attachment of the azobenzene containing polypeptide was utilized to prepare the sample for force measurements. The polymer was first attached to a gold-coated probe tip via the thiol group of the amino-terminal cysteine residue, and then the carboxy-terminal end was covalently bound to amino functionalities on the sample slide. Polymer chains were coupled to the probe tip by first physisorbing them to the cantilevers in DMSO solution, followed by deprotection of the cysteine thiol group

using 5% trifluoroacetic acid in CH_2Cl_2. The proximity of the deprotected thiol groups to the gold surface resulted in chemisorption of the polypeptides to the gold-coated tip via the formation of a covalent Au−S bond.

Flint glass microscope slides were functionalized with *N*′-[3-(trimethoxysilyl)propyl]diethylenetriamine (Aldrich) to introduce amino groups. A drop of silane was placed on the slides, which were then placed in a 90 °C oven for 15 min. The slides were rinsed with ethanol followed by water and then placed in 90 °C water for 30 min.

After mounting a polymer modified cantilever chip in the force spectrometer, the carboxy termini of the polypeptides were activated by the addition of 10 μL of a 100 mM *N*-hydroxysuccinimide (NHS) and 1-ethyl-3-(3-(dimethylamino)propyl)carbodiimide (EDC) (NHS and EDC in 1:1 molar ratio) solution in DMSO to promote the formation of an amide bond with the amino groups on the glass slide surface. The cantilever tip with the activated, chemisorbed polymers was brought into contact with the amino-functionalized slide. The formation of a covalent bond was reflected by rupture forces in the nanonewton range,[46] which allowed us to stretch and hold the polymers with a force of several hundred piconewtons for several minutes without bond rupture. Adhesion of short strands of nonspecifically bound polymer was ruptured until a single covalently bound strand remained, at which point we could irradiate and make multiple measurements on a single polymer molecule.

We observed that the stability of the tip and surface attachment of single polypeptide chains is drastically reduced if the polymer is kept at elevated forces for prolonged times. The reported value of 1.4 nN for the failure of gold−sulfur bonds[46] provides an upper limit of the forces we can expect to obtain with the current bifunctional attachment system. If one considers the occurrence of occasional mechanical noise and the addition of mechanical energy to the system from the light pulse, it is not surprising that, on time scales of the experiments, we are limited to forces on the order of 1 nN. Indeed, as the force applied in the experiment rose above 500 pN, the stability of polymer attachment was observed to decrease substantially. Nonetheless, with care we were able to keep an individual chain attached for more than an hour of continuous measurements.

Data Collection and Analysis. The data were collected as cantilever deflection and measured piezo position at rates as high as 5 kHz. These data were converted to force and tip−sample separation using the measured spring constant, sensitivity, and point of tip−sample contact. We collected data in Igor Pro (Wavemetrics) as individual force curves or, alternatively, collected 5−10 min of continuously streamed data. The advantage of continuously collecting data was the ability to accurately account for instrument drift during and between many force curves without having to come into contact with the surface between each trace. Corrections in the data were made for low-frequency noise, i.e., thermal effects and instrument creep.

To determine the contour lengths of stretched polypeptide chains, the experimental curves were fitted by an extended wormlike chain (WLC) model including linear elastic contributions arising from the stretching of bond angles and covalent bonds.[62]

$$F\frac{L_P}{k_BT} = \frac{R_z}{L} - \frac{F}{K_0} + \frac{1}{4(1 - R_z/L + F/K_0)^2} - \frac{1}{4} \qquad (1)$$

In this expression, R_z is the measured end−end distance at any given force, F, and L is the contour length of the stretched chain (polymer strand) under zero force ($F = 0$). The polymer's bending rigidity is expressed by the chain's persistence length, L_P, and the chain's extensibility upon stretching is described by the segment elasticity, K_0, which is introduced into eq 1 as a linear term. (K_0 can be understood as the inverse of the normalized compliance of a Hookean spring; the spring constant of the polymer chain is given by K_0/L.) Note that eq 1 is only based on an approximation to the exact solution of the WLC model, which is valid in the range of low and high forces (in the regimes $F < 1$ pN and $F > 20$ pN), but may differ in the intermediate regime by as much as 10%.[63] It has been suggested that the extensibility of the polymer chain may be determined from the slope of the linear regime found at forces above several hundred piconewtons,[64] but as this regime is not always accessed, the established WLC fits were used to make comparisons in this investigation.

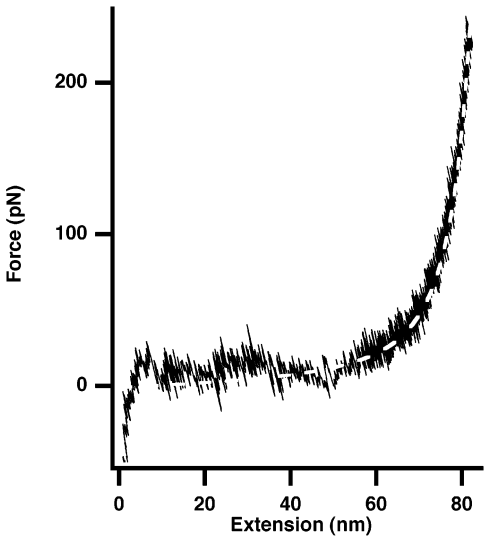

Figure 4. Force vs extension trace of a *trans*-azo polypeptide. A wormlike chain (WLC) fit shown by the dashed line reveals a contour length of 89.1 nm, a persistence length of 0.5 nm, and a segment elasticity of 20 000 pN.

Results

Mechanical Characterization of *all-trans*-Azobenzene Polymers. The characteristic shape of a single azobenzene containing polypeptide was established by obtaining numerous force spectra of several individual chains. Figure 4 shows a typical force vs extension plot of a polyazopeptide in the *trans*-azo state; that is its fully extended configuration. The polymer exhibits no measurable conformational transitions, indicating that no significant thermal activation barriers are overcome along the trajectory of mechanical stretching.

The measure for the contour length of a stretched chain is obtained from the extended wormlike chain fit (WLC), after the two other free parameters, persistence length L_P and segment elasticity, K_0, were determined. For the force profile of the polyazopeptide in its extended state, we obtained reasonable WLC fits with $L_P = 0.5$ nm and $K_0 = 20\,000$ pN. (For the particular polymer molecule shown in this trace, the contour length of $L =$ 89.1 nm was fit; note that the deviation from the average length is due to the molecular weight distribution of the material.) We assumed that the *trans*/*cis* isomerization does not significantly affect these two parameters, so they were held fixed in all fits to the experimental force−extension curves in order to obtain precise relative values for the contour lengths of polyazopeptides in different configurational states.

Reversible Optical Switching at Low Force. Figure 5A shows typical data obtained in a force experiment during which optical excitation was coupled into the sample. The traces are extracted from data streams of cantilever deflection vs time that are recorded. In the time traces, individual light pulses can be observed as spikes in the deflection data. The reader

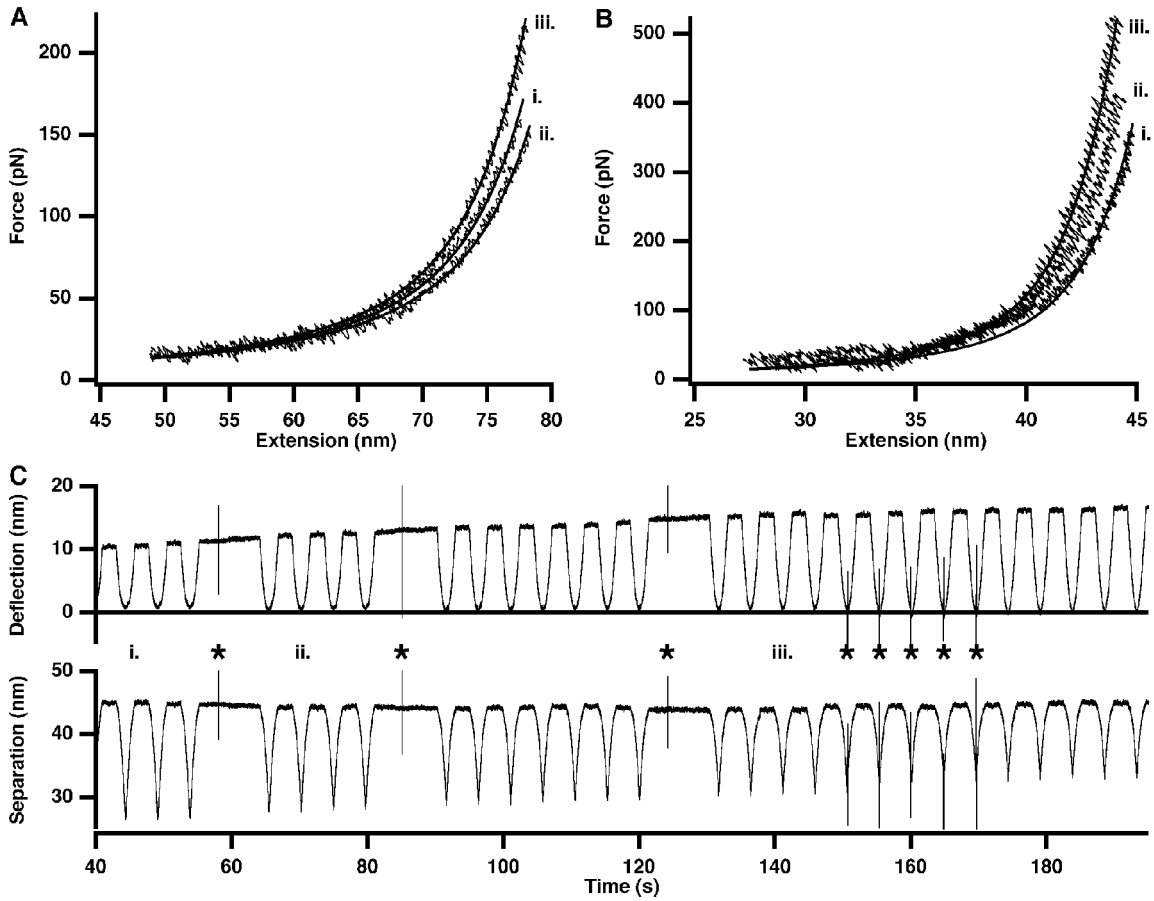

Figure 5. Switching azobenzene configurations. (A) Reversible switching of contour length at low forces is demonstrated by the conversion of these data to force vs extension revealing the original trace (i), the more extended trace (ii) after pulses of 420 nm wavelength light drove the polymer to the *trans*-azo configuration, and a shortened trace (iii) after pulses of 365 nm wavelength drove the polymer to its *cis*-azo configuration. (B) A similar extent of shortening of the polymer chain is observed for a polymer held under external force during excitation. The polymer initially driven to the *trans*-azo state by 420 nm wavelength light (i) is shortened (ii) upon a single flash of 365 nm wavelength light. Two more flashes result in slightly more shortening. Five further flashes at low force do not alter the length. (C) The cantilever deflection vs time for the data displayed in (B) shows the time course of the experiment. Force curves are observed as the gradual increase and decrease in deflection, while the sharp spikes (noted with stars) indicate the light pulses.

is reminded that these spikes result from stray light reflected onto the photodiode and *not* from actual cantilever movement (see experimental part for detailed discussion of artifacts). This signal provides a convenient marker for when the light pulses occurred.

The effect of the light pulses on a single azobenzene polymer can be observed by comparing the force−extension traces extracted prior to and after irradiation of the sample. At the beginning of the experiment, the polymer sample assumed an undefined configurationally mixed state owing to the absorbed ambient radiation. Trace i in Figure 5A is the polymer in this initial mixed state. After five pulses of 430 nm wavelength light, the polymer chain was driven into the saturated extended *trans*-azo state. Trace ii illustrates the lengthening of the polymer due to this switch. The polymer was then driven into the saturated *cis*-azo state by irradiation of five pulses of 365 nm wavelength light. As a result, the polymer exhibited marked shortening as observed in trace iii. Such lengthening and shortening could be repeated several times before the polymer or its attachment to tip or substrate ruptured. The intensity of the light pulses from the flash lamp on the molecule varies to some degree, and so the direct correlation of molecular length change to the number or relative intensity of the light flashes has not yet been possible. However, we could use several flashes to drive the system into an equilibrium state. We observed that three flashes were enough to reach such a photochemical equilibrium.

Repeated measurements of a particular configurational state of the same polyazopeptide molecule (i.e., no optical excitation between successive measurements) resulted in identical force−extension, even when the time span between successive measurements was minutes. The drift stability of the experimental setup is therefore sufficient to ensure the accurate determination of contour lengths of different polymer configurations based on the WLC fit as described above. A contour length, $L_{cis} = 83.7$, was obtained by fitting the *cis*-azo state trace in Figure 5A with a persistence length $L_p = 0.5$ nm and a polymer segment elasticity of $K_o = 20\,000$ pN as described above. From this, the difference in contour lengths (ΔL) between the saturated *trans*- and *cis*-azo states was measured to be 2.8 nm, which corresponds to a relative length change ($\Delta L/L_{trans}$) of ∼3%. Interestingly, stretching of the polymer in its saturated short conformation, despite being the thermodynamically unfavored state, does not result in any mechanically induced configurational transition. The lifetime of the *cis* state is thus still high enough to provide mechanical stability of the short polymer configuration on the time scale of the AFM experiment even

at elevated forces up to 1 nN. The *cis*/*trans* isomerization of polyazopeptides does not result in different shape characteristics of the force curves and is therefore only identified by the relative length changes prior to and after optical irradiation.

Reversible Optical Switching against External Mechanical Force. Further experiments were carried out to test whether the configuration of the azo units could be optically switched, while holding the polymer under relatively high tension. Under this condition, optical switching is of particular interest, as the contraction of a polymer chain against an external force may be employed for an optomechanical energy conversion at the single-molecule level. Figure 5B,C shows the results of one such experiment. The streamed deflection and molecular extension data are displayed in Figure 5C. The sharp spikes show the points when light was flashed into the system. The labeled force curves showing decreases in extension correspond to the extracted force curves displayed in Figure 5B. Prior to the experiment, we drove the polymer into the saturated *trans*-azo conformation with five consecutive flashes at 420 nm. Trace i reveals that, in the saturated *trans*-azo state, this polymer molecule's contour length is 47.7 nm. The molecule was stretched to a force of about 350 pN, and a single 365 nm pulse at constant tip−sample separation resulted in a shortening by about 1.0 nm, as measured from trace ii. Two further pulses holding the polymer at the slightly higher force resulted in an additional shortening by 0.9 nm observed in trace iii. Since five additional 365 nm wavelength pulses at low force did not result in further shortening, the polymer was assumed to be in the saturated *cis*-azo state. The relative length change observed here against external force between the two saturated states corresponds well with the value found for *trans*- to *cis*-azo switching at low force ($\Delta L/L_{trans} \sim 3\%$). Only at very high forces do we find hints for a suppression of the optical *trans*/*cis* isomerization reaction. However, because of the limited stability of polymer−surface attachment at high forces, we have relatively few data at these high forces. The highest force at which contraction of polymer was clearly observed was 400 pN.

Discussion

Mechanical Stability of Azobenzene Configurations. The rate at which an equilibrium is reached (i.e., the lifetime, τ, of any initially populated configurational state) depends on the activation barrier of the transition between the different states, ΔG^*. For AMPB peptides in DMSO an activation energy barrier for thermal reisomerization from the *cis*- to the *trans*-isomer of $\Delta G^* = 44 \pm 2\ k_BT$ has been determined.[60] The experimentally determined lifetime of the *cis*-azo configuration at 301 K is 120 h.[60]

At the time scale of a single AFM stretching experiment, any state with τ_0 greater than 1 min can be considered "stable". However, the mechanical energy applied by stretching alters the conformational potential landscape by effectively tilting it along the stretching coordinate. This reduces the activation barrier of any transition that proceeds in the direction of a path nonorthogonal to the applied force. Therefore, the probability, and thus also the rate, of such a transition increases as the lifetime of the initial state decreases. It can be estimated from the Bell equation[65]

$$\tau_F = \tau_0 \exp[(-F_z \Delta z^*)/k_B T] \qquad (2)$$

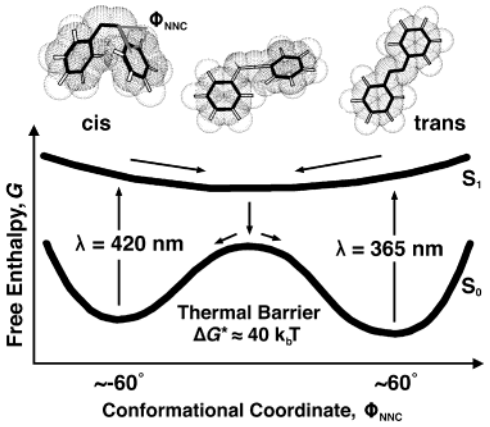

Figure 6. Schematics of a cut through the potential energy landscape of the reversible azobenzene *cis*/*trans* transition along the inversion pathway. The relevant conformational coordinate is the bond angle which changes from about −60° to +60° for an in-plane transition of the right phenyl ring from the *cis*- to the *trans*-azo position.[60,66,67] The transition can be induced by optical excitation (*cis*-azo form at 420 nm; *trans*-azo form at 365 nm). Typically, the *trans*-azo form is thermally favored. (The graph is based on previous theoretical[66] and experimental data.[68,69])

in which F_z is the projection of the applied force along the internal transition coordinate z and Δz^* is the "width" of the conformational transition potential. The length difference in the end-to-end distance of a single azobenzene unit in the *cis*- and *trans*-azo states was calculated ab initio using the INSIGHT II software ($l_{trans} \sim 1.9$ nm, $l_{cis} \sim 1.65$ nm, and therefore $\Delta l \sim 0.25$ nm). Then assuming a symmetric potential, Δz^* is ~ 0.13 nm. According to the Bell equation, the lifetime of the excited *cis*-isomer is reduced to $\tau_F \sim 100$ ms, once the projection of the stretching force on the coordinate describing the trajectory of the *cis*/*trans* transition exceeds 400 pN. While this force is well within the range of stretching forces applied in our AFM experiments, the saturated *cis*- and *trans*-azo configurations were both found mechanically stable to all experimental pulling forces on the time scale of the experiment. For the lower energy *trans*-azo configuration, this is expected, as it represents the equilibrium configurational state.

A likely explanation for the somewhat surprisingly high stability of the *cis*-azo configuration is that the force-induced transition proceeds along a pathway nearly orthogonal to the thermal *cis*/*trans* isomerization. The activation barrier and thus the thermal lifetime of the *cis*-azo configuration would remain unaltered. Note that the thermal *cis*/*trans* isomerization is suggested to proceed along an isomerization pathway in which the dihedral angle Φ_{NNC} is the relevant configuration coordinate (Figure 6)[60,66−69] and that, the azo groups are not all aligned with the stretching coordinate. A more generalized view of this effect would be that the forced transition occurs on a pathway ensemble whose width in conformation space is drastically restricted by the external force acting along the polymer backbone. The thermal transition, however, samples the whole conformation space and may reach saddles and low-energy barriers, which are not accessible for the forced transition. This would to a certain degree correspond to the conformationally locked interaction found in certain biopolymers, e.g., actin filaments, which are known to withstand forces of up to 100 pN for seconds although their equilibrium constant is in the millimolar range.

If there is such a separate mechanical pathway, our measurements allow us to set a lower bound for the lifetime, $\tau_{0,z}$, of the *cis*-azo state when restricted to this path along the stretching coordinate z. With eq 2 and the observation that a molecule can be held in the *cis*-azo state at forces of ~1 nN for longer than a second, it is estimated as $\tau_{0,z} \sim 3 \times 10^{13}$ s (i.e., ~1 million years). The lifetime of a state, τ_0, is correlated with the energy barrier of the escape path, ΔG^*, via $\tau_0 = (1/\nu_0) \exp(+\Delta G^*/k_B T)$,[70] where ν_0 may be seen as a characteristic frequency of the transition.[71] If ν_0 is assumed independent of the pathway, the energy barrier ΔG_Φ^* along the configurational coordinate Φ_{NNC} and the energy barrier ΔG_z^* along the stretching coordinate z are related by

$$\Delta G_z^* = \Delta G_\Phi^* + k_B T \ln(\tau_{0,z}/\tau_{0,\Phi}) \qquad (3)$$

Thus, $\Delta G_z^* \sim 62\ k_B T$; i.e., the energy barrier is increased by approximately 18 $k_B T$ when the molecules' escape path is restricted to the stretching coordinate. However, these estimates are based on the assumption that the natural frequency ν_0 is the same in the forced and the thermal process. This need not necessarily be the case. Particularly on top of the saddle where the state density is drastically reduced, the transition state theory may break down. Our finding of the unexpected stability of the *cis*-azo state against external force may reflect this effect.

Photochemically Induced Length Changes and Mechanical Work. The lengths of a single azotripeptide unit in the *cis*- and the *trans*-azo state from theoretical calculations are $l_{trans} \sim 1.9$ nm and $l_{cis} \sim 1.65$ nm. As discussed above, the spectral overlap of the excitations of *cis*- and *trans*-azo configurations limits the photochemical switching of polyazopeptides to shifting the average configurational populations between the two limits ~80% *trans*-azo and ~75% *cis*-azo state.[60] From this, we may give an "average monomer length" in the polymer's saturated *trans*-azo state as $\langle l_{trans} \rangle \sim 1.85$ nm. In the saturated *cis*-azo state, a total average of 55% azobenzene units change their configuration, which corresponds to an average contraction, $\langle \Delta l \rangle \sim 0.14$ nm, or an average monomer length in the polymer's saturated *cis*-azo state, $\langle l_{cis} \rangle \sim 1.71$ nm.

The fitted contour length of the polyazopeptide molecule in Figure 5A is $L_{trans} \sim 86.5$ nm in its saturated *trans*-azo state, as obtained from the WLC fit to our data. This corresponds to 46 azotripeptide monomers. Considering the theoretical contraction per monomer of 0.14 nm, a maximum contraction, ΔL_{max}, of 6.4 nm, a relative change of 7.4%, could be expected by optical pumping at 365 nm. The actual length change measured at saturation at low forces is 2.8 nm (~3%), which is considerably less than this upper limit. The difference may reflect the fact that some parts of the polymer chain are not excited by the evanescent field. More importantly, the above calculations on the monomer lengths do not directly correlate to the contour length of the polymer chain. Intrinsic viscosity measurements on azobenzene polymers have shown the largest effects of optical excitation on the end−end distance of the polymer coils in solution, when the photoactive units were connected by stiff rather than flexible chain segments.[22,23] In our experiments, the polymer chains are fixed between tip and substrate and stretched beyond the coil regime. While this geometry is thus more comparable with photoactive bulk polymer networks, which may show considerable length changes upon optical switching,[27] the remaining conformational freedom of the polypeptide backbone may compensate for some of the azobenzene shortening by rotations around single backbone bonds.[60]

In other words, orientational rearrangement of the azobenzene units, such as a change in their tilt angle with respect to the polymer main axis, remain possible in order to compensate for some of the conformational strain induced by the configurational change. Additionally, the *cis*-azo configuration could have a lower chain elasticity than the *trans*-azo configuration, which would result in lower measured length change upon extension than expected. As a result, the maximum contraction of the azobenzene unit Δl is thus not entirely projected onto the stretching axis. The experimentally measured absolute length change of the polyazopeptide relates to an averaged contraction of $\langle \Delta l \rangle = 0.06$ nm per monomer in contour length. As only 55% of the azobenzene units change their configuration, the length change of a single azobenzene unit upon *trans*- to *cis*-azo switching, which is detectable along the stretching axis, is estimated as $\Delta l^z = 0.11$ nm.

Efficiency of Converting Optical Excitation Energy to Mechanical Work. It is instructive to have a look at the efficiency of the optomechanical energy conversion in the limit of all light reaching the polymer in order to describe the experimental limit of efficiency. In Figure 5A, contraction against a force of about 400 pN is shown, resulting in an average shortening of 0.12 nm per azobenzene monomer. When one assumes that each switching of a single azobenzene unit is initiated by a single photon carrying an energy of $h\nu = 5.5 \times 10^{-19}$ J ($\lambda = 365$ nm), the conversion of this photon to mechanical work has an efficiency of about 10%.[72] This estimate neglects that the azobenzene is not excited by every photon that it interacts with. (The quantum yield is about 10% for *trans*- to *cis*-azo.) In addition, to lengthen the shortened polymer and complete a cycle, a second photon ($h\nu = 4.7 \times 10^{-19}$ J, $\lambda = 430$ nm) is absorbed at a quantum yield of about 50%. With about 10 azobenzene units in the chain measured in the cycle,[72] about 120 photons or an energy of 6.6×10^{-17} J is needed for one complete cycle. The total mechanical energy transduced to the cantilever is about 5×10^{-20} J (estimated from the area of the cycle). This results in a total efficiency of about 7.5×10^{-4} for this extremely simple optomechanical motor. This is only a rough estimate of efficiency, and we recognize that there are many other effects that will complicate more accurate estimates of efficiency, including thermal back-relaxation, the field strength, and orientation dependency of excitation efficiency, etc.

Conclusions

We have demonstrated the incorporation of a chromophore into a polymer chain allowing controlled lengthening and shortening of the chain contour length and the ability to read out this change in a single polymer with a macroscopic device. Not only was this accomplished in a relaxed chain, but also while the chain was held extended by an external force. In the extended state, the shortening transition was able to convert the absorbed optical energy into mechanical work performed on the system. We demonstrated that such a molecule could be used for a molecular switch via length change or to perform work on a system.

The use of optomechanical energy conversion for molecular switches is promising since the light can be

applied in a controlled, clean manner. One must only be concerned with thermal effects. The coupling of optical excitation into polymer mechanics therefore seems to be the most attractive approach for the general study of energy transductions at the single molecule level. We have recently demonstrated that the mechanical stability of the two different azobenzene configurations is sufficient to operate the experiment in an optomechanical cycle and thus to perform work at the molecular level.[72]

Our results prepare the way for the development of improved optomechanical switches with higher activation barriers, such as could be provided by structural units, in which covalent bonds are formed and cleaved during the reversible photochemical process. Most prominent examples are spiropyranes and spirooxazines, fulgides and fulgimides, and some diarylethene derivatives, but their introduction into polymer main chains (which would be needed for their study by AFM force spectroscopy) appears synthetically much more demanding.

Not to be overshadowed by the thoughts of building nanomachines, this experimental system is a promising method for quantifying how an applied force can alter the energy landscape of chromophore transitions. This could provide new fundamental insights into the course of photoreactions under external loads. Investigating the dependence of the transitions on the excitation wavelength and external load will require carefully planned experiments since the complexity of the potential mechanisms is confounded by contributions of alignment of the chromophores, the exponentially decaying field strength (in addition to the possibility of near field amplification of the light by the AFM probe), and the small contour length changes. But a systematic wavelength-dependent analysis would allow the mapping of the energy landscape as a function of external force and chromophore substitution pattern.

Acknowledgment. We thank R. Netz, H. Grubmüller, J. Kreuzer, and W. Zinth for helpful discussions as well as Asylum Research for technical support. The study was supported by the Deutsche Forschungsgemeinschaft (DFG), the Humboldt Foundation, and the Fonds der Chemischen Industrie.

References and Notes

(1) Brown, C. H. *Photochromism*; Wiley-Interscience: New York, 1971.
(2) Rau, H. In *Photochromism: Molecules and Systems*; Dürr, H., Bouas-Laurent, H., Eds.; Elsevier: Amsterdam, 1990; Vol. 40, pp 165−192.
(3) Irie, M. *Photoreactive Materials for Ultrahigh-Density Optical Memory*; Elsevier: Amsterdam, 1994.
(4) Feringa, B. L.; Jager, W. F.; de Lange, B. *Tetrahedron* **1993**, *49*, 8267−8310.
(5) Tamai, N.; Miyasaka, H. *Chem. Rev.* **2000**, *100*, 1875−1890.
(6) Hartley, G. S. *Nature (London)* **1937**, *140*, 281.
(7) Shinkai, S.; Manabe, O. *Top. Curr. Chem.* **1984**, *121*, 67−104.
(8) Willner, I. *Acc. Chem. Res.* **1997**, *30*, 347−356.
(9) Ulysse, L.; Cubillos, J.; Chmielewski, J. *J. Am. Chem. Soc.* **1995**, *117*, 8466−8467.
(10) Asanuma, H.; Ito, T.; Yoshida, T.; Liang, X.; Komiyama, M. *Angew. Chem., Int. Ed.* **1999**, *38*, 2393−2395.
(11) Kumar, G. S.; Neckers, D. C. *Chem. Rev.* **1989**, *89*, 1915−1925.
(12) Irie, M. *Adv. Polym. Sci.* **1990**, *94*, 27−67.
(13) Vögtle, F. *Supramolecular Chemistry*; Wiley: New York, 1991.
(14) Würthner, F.; Rebek Jr., J. *J. Chem. Soc., Perkin Trans. 2* **1995**, 1727−1734.
(15) Archut, A.; Azzellini, G. C.; Balzani, V.; De Cola, L.; Vögtle, F. *J. Am. Chem. Soc.* **1998**, *120*, 12187−12191.
(16) Ikeda, T.; Tsutsumi, O. *Science* **1995**, *268*, 1873−1875.
(17) Eich, M.; Wendorff, J. H.; Reck, B.; Ringsdorf, H. *Makromol. Chem. Rapid Commun.* **1987**, *8*, 59−63.
(18) Eich, M.; Wendorff, J. H. *Makromol. Chem. Rapid Commun.* **1987**, *8*, 467−471.
(19) Bieringer, T.; Wuttke, R.; Gessner, U.; Rübner, J.; Haarer, D. *Macromol. Chem. Phys.* **1995**, *196*, 1375−1390.
(20) Zilker, S. J.; Bieringer, T.; Haarer, D.; Stein, R. S.; van Egmond, J. W.; Kostromine, S. G. *Adv. Mater.* **1998**, *10*, 855−859.
(21) Eisenbach, C. D. *Polymer* **1980**, *21*, 1175−1179.
(22) Blair, H. S.; Pogue, H. I.; Riordan, E. *Polymer* **1980**, *21*, 1195−1198.
(23) Irie, M.; Hirano, Y.; Hashimoto, S.; Hayashi, K. *Macromolecules* **1981**, *14*, 262−267.
(24) Strzegowski, L. A.; Martinez, M. B.; Gowda, D. C.; Urry, D. W.; Tirrell, D. A. *J. Am. Chem. Soc.* **1994**, *116*, 813−814.
(25) Lagungé Labarthet, F.; Bruneel, J. L.; Buffeteau, T.; Sourisseau, C.; Huber, M. R.; Zilker, S. J.; Bieringer, T. *Phys. Chem. Chem. Phys.* **2000**, *2*, 5154−5167.
(26) Schulz, B. M.; Huber, M. R.; Bieringer, T.; Krausch, G.; Zilker, S. J. *Synth. Met.* **2001**, *124*, 155−157.
(27) Finkelmann, H.; Nishikawa, E.; Pereira, G. G.; Warner, M. *Phys. Rev. Lett.* **2001**, *87*, 015501−015504.
(28) Oster, G.; Wang, H. In *ATP Synthase: The rotary molecular motors working together*; Creighton, T., Ed.; Wiley: New York, 1999.
(29) Vale, R. D.; Milligan, R. A. *Science* **2000**, *288*, 88−95.
(30) Keller, D.; Bustamante, C. *Biophys. J.* **2000**, *78*, 541−556.
(31) Bustamante, C.; Keller, D.; Oster, G. *Acc. Chem. Res.* **2001**, *34*, 412−420.
(32) Howard, J. *Mechanics of Motor Proteins and the Cytoskeleton*; Sinauer Assoc.: Thunderland, MA, 2001.
(33) Balzani, V.; Credi, A.; Raymo, F. M.; Stoddart, J. F. *Angew. Chem., Int. Ed.* **2000**, *39*, 3348−3391.
(34) Feringa, B. L.; van Delden, R. A.; Koumura, N.; Geertsema, E. M. *Chem. Rev.* **2000**, *100*, 1789−1816.
(35) Collin, J. P.; Dietrich-Buchecker, C.; Gaviña, P.; Jimenez-Molero, M. C.; Sauvage, J. P. *Acc. Chem. Res.* **2001**, *34*, 477−487.
(36) Pease, A. R.; Jeppesen, J. O.; Stoddart, J. F.; Luo, Y.; Collier, C. P.; Heath, J. R. *Acc. Chem. Res.* **2001**, *34*, 433−444.
(37) Schalley, C. A.; Beizai, K.; Vögtle, F. *Acc. Chem. Res.* **2001**, *34*, 465−476.
(38) Shipway, A. N.; Willner, I. *Acc. Chem. Res.* **2001**, *34*, 421−432.
(39) Balzani, V.; Credi, A.; Venturi, M. *Proc. Natl. Acad. Sci. U.S.A.* **2002**, *99*, 4814−4817.
(40) Ballardini, R.; Balzani, V.; Credi, A.; Gandolfi, M. T.; Venturi, M. *Acc. Chem. Res.* **2001**, *34*, 445−455.
(41) Kishino, A.; Yanagida, T. *Nature (London)* **1988**, *334*, 74−76.
(42) Ashkin, A.; Schütze, K.; Dziedzic, J. M.; Euteneuer, U.; Schliwa, M. *Nature (London)* **1990**, *348*, 346−348.
(43) Smith, S. B.; Finzi, L.; Bustamante, C. *Science* **1992**, *258*, 1122−1126.
(44) Sheetz, M. P. *Laser Tweezers in Cell Biology*; Academic Press: New York, 1997.
(45) Binnig, G.; Quate, C. F.; Gerber, C. *Phys. Rev. Lett.* **1986**, *56*, 930−933.
(46) Grandbois, M.; Beyer, M.; Rief, M.; Clausen-Schaumann, H.; Gaub, H. E. *Science* **1999**, *283*, 1727−1730.
(47) Viani, M. B.; Schaffer, T. E.; Paloczi, G. T.; Pietrasanta, L. I.; Smith, B. L.; Thompson, J. B.; Richter, M.; Rief, M.; Gaub, H. E.; Plaxco, K. W.; Cleland, A. N.; Hansma, H. G.; Hansma, P. K. *Rev. Sci. Instrum.* **1999**, *70*, 4300−4303.
(48) Clausen-Schaumann, H.; Seitz, M.; Krautbauer, R.; Gaub, H. *Curr. Opin. Chem. Biol.* **2000**, *4*, 524−530.
(49) Janshoff, A.; Neitzert, M.; Oberdörfer, Y.; Fuchs, H. *Angew. Chem., Int. Ed.* **2000**, *39*, 3212−3237.
(50) Hugel, T.; Seitz, M. *Macromol. Rapid Commun.* **2001**, *22*, 989−1016.
(51) Rief, M.; Oesterhelt, F.; Heymann, B.; Gaub, H. E. *Science* **1997**, *275*, 1295−1297.
(52) Smith, S. B.; Cui, Y.; Bustamante, C. *Science* **1996**, *271*, 795−799.
(53) Rief, M.; Clausen-Schaumann, H.; Gaub, H. E. *Nat. Struct. Biol.* **1999**, *6*, 346−349.
(54) Oesterhelt, F.; Rief, M.; Gaub, H. E. *New J. Phys.* **1999**, *1*, 6.1−6.11.

(55) Rief, M.; Fernandez, J. M.; Gaub, H. E. *Phys. Rev. Lett.* **1998**, *81*, 4764−4767.
(56) Butt, H. J.; Jaschke, M. *Nanotechnology* **1995**, *6*, 1−7.
(57) Behrendt, R.; Renner, C.; Schenk, M.; Wang, F.; Wachtveitl, J.; Oesterhelt, D.; Moroder, L. *Angew. Chem., Int. Ed.* **1999**, *38*, 2771−2773.
(58) Behrendt, R.; Schenk, M.; Musiol, H. J.; Moroder, L. *J. Pept. Sci.* **1999**, *5*, 519−529.
(59) Rau, H., Rabek, J. F., Eds.; CRC Press: Boca Raton, FL, 1989; Vol. 2, pp 119−141.
(60) Renner, C.; Cramer, J.; Behrendt, R.; Moroder, L. *Biopolymers* **2000**, *54*, 501−514.
(61) Renner, C.; Behrendt, R.; Heim, N.; Moroder, L. *Biopolymers* **2002**, *63*, 382−393.
(62) Bustamante, C.; Marko, J. F.; Siggia, E. D.; Smith, S. *Science* **1994**, *265*, 1599−1600.
(63) Bouchiat, C.; Wang, M. D.; Allemand, J.-F.; Strick, T.; Block, S. M.; Croquette, V. *Biophys. J.* **1999**, *76*, 409−413.
(64) Livadaru, L.; Netz, R. R.; Kreuzer, J., submitted to *Macromolecules*.
(65) Bell, G. I. *Science* **1978**, *200*, 618−627.
(66) Monti, S.; Orlandi, G.; Palmieri, P. *Chem. Phys.* **1982**, *71*, 87−99.
(67) Robertson, J. M. *J. Chem. Soc.* **1939**, 232−236.
(68) Rau, H. *J. Photochem.* **1984**, *26*, 221−225.
(69) Nägele, T.; Hoche, R.; Zinth, W.; Wachtveitl, J. *Chem. Phys. Lett.* **1997**, *272*, 489−495.
(70) Arrhenius, S. *Z. Phys. Chem.* **1889**, *4*, 226.
(71) Hänggi, P.; Talkner, P.; Borkovec, M. *Rev. Mod. Phys.* **1990**, *62*, 251−341.
(72) Hugel, T.; Holland, N. B.; Cattani, A.; Moroder, L.; Seitz, M.; Gaub, H. E. *Science* **2002**, *296*, 1103−1106.

MA021139S

P3

“Elasticity of Poly(azobenzene-peptides)“

G. Neuert, T. Hugel, R. R. Netz and H. E. Gaub

Submitted to Macromolecules

Elasticity of Poly(azobenzene-peptides)

Gregor Neuert[*], *Thorsten Hugel*[§†], *Roland R. Netz*[†] *and Hermann E. Gaub*[*]

[*]Lehrstuhl für Angewandte Physik & Center for Nanoscience, Ludwig-Maximilians-Universität, Amalienstrasse 54, 80799 München, Germany

[†]Physics Department, TU-München, 85748 Garching, Germany

[§] Zentralinistitut für Medizintechnik, 85748 Garching, Germany

RUNNING HEAD: Switching and ab-initio modeling of Photoswitchable Polymers

*To whom correspondence should be addressed: email: gaub@physik.uni-muenchen.de

Abstract

Since the mechanical properties of individual polymers have become accessible with single molecule force spectroscopy, detailed insight was gained into the molecular origin of their elasticity. Active, optically switchable polymers were introduced as photonic muscles and used in single molecule motors. Here, we present experimental data and calculations to describe the mechanical properties of poly(azobenzene-peptides) in the complete force regime accessible by AFM. The high force regime is very well described by ab-initio quantum mechanical calculations, while for the low force regime we combine ab-initio calculations with a description of the entropic forces based on the freely rotating chain model. Finally, a one-parameter fit for the different configurations of the poly(azobenzene-peptide) and a quantitative description of the optically induced actuation are given.

KEYWORDS AFM; protein; polymer elasticity; conformational transitions; opto-mechanical coupling; molecular machines; energy cycle; molecular switches, azobenzene, FRC, WLC, ab-initio

Introduction

Single molecule force spectroscopy has provided a very detailed insight into the mechanics of individual polymers. Proteins were unfolded [1-5], nucleic acids were unzipped [6-13], synthetic polymers were disentangled [14-18] and peeled from surfaces [14,19-21] . Interactions within and between molecules were analyzed and quantified with unparalleled resolution and sensitivity. Different techniques evolved for different applications. Optical traps [11,22-26], magnetic tweezers [11,12] and vesicle pipette [27-29] techniques have been optimized for low force applications in the range well below 100 pN at the expense of spatial resolution and dynamic range. Cantilever based techniques with their sub-nanometer spatial resolution were found to be ideally suited for applications starting from several piconewton (pN) up to the nanonewton (nN) regime, where covalent bond rupture occurs [14,30-34].

At low forces the intramolecular conformations of polymers are found to be governed by entropic effects, whereas at high forces the backbone deformations prevail [35]. The crossover regime was found to be dominated by supramolecular rearrangements such as folding in proteins [1,3], hybridization on nucleic acids [6,9,36,37] or solvent interactions [34]. This regime provided a richness of fingerprints specific for the chemical nature of the polymer and its particular material properties or its biological function [1,3,6,15,16,18,34,38].

The elastic response of simple polymers with negligible supramolecular rearrangements was in the past successfully modeled by either the worm like chain (WLC) model [3,5,13,14,39,40] or the freely jointed chain (FJC) model [14,34,40,41], both with modifications to account for the backbone elasticity and the resulting softening of the entropic spring at higher forces. Recently, a parameter-free description of the elasticity of three standard polymers: polypeptides, polynucleic acid and polyethylene, based on a combination of statistical mechanics and quantum mechanics was introduced [35,42]. The backbone elasticity, which dominates the elastic response of the polymers at higher forces, was calculated with ab-initio quantum mechanical (QM) methods [35,40,43-46]. The low force contributions were described by the freely rotating chain (FRC) model [40,43]. As a result a convincing fit of experimental force extension curves in a force

regime from 10pN to 2 nN was obtained for polyvinylamine. These studies were partly motivated by findings that weak interaction of the polymer with the solvent as low as one k_BT per monomer unit could be determined and the accuracy was limited more by the quality of the model than by the precision of the experimental data [34,43]. [4]

In addition, single polymers are the ultimate milestone in miniaturization of materials, and in combination with molecular actuators, or of active devices. In a previous study we had shown that a single poly(azobenzene-peptide) might be operated in a repetitive expansion contraction cycle in close analogy to an Otto-Cycle [15,16]. The action may also be seen as a photonic muscle, converting optical energy into mechanical work upon contraction. Such optically driven devices are generally regarded as promising candidates for the realization of nano-scale motors, since optical agitation and fuelling offers striking advantages both in speed and versatility, compared to electrical wiring or slow diffusive transport of chemicals [47-59] In this study the precision of the data analysis was largely hampered by the empiric model used for the fit of the force extension curves before and after optical switching[16]. The quantum efficiency of the opto-mechanical conversion, which is the major target for further improvement in applications of this system as photonic muscle, could only be estimated based on relative measurements [15,16]. Here, a parameter-free fit of the force extension curves as a function of the number of cis and trans azobenzene units is clearly a desirable goal.

Furthermore, our previous experimental studies revealed an unexpectedly high potential barrier between the cis and the trans conformation, indicating that the thermally activated conversion pathway between the two conformations is not collinear with the forced pathway [16,60]. Our quantum chemical calculation of the molecular conformations under external mechanical tension in fact lead to further insights with respect to the forced transition pathway. It is pointed out that the mechanical stretching modulus of the transition state is an important parameter which describes to what degree the conversion between two molecular states is in induced or slowed down by the action of external forces. We believe that this finding applies quite generally and might be of importance for other systems as well.

Experimental Section

Sample Preparation

The azobenzene-tripeptide building block was synthesized as described in [16,61], it was then polymerized and functionalized on the N-terminus with a trityl-protected cystein [15,16]. For the attachment onto the cantilever, the non-polar poly(azobenzene-peptide) was dissolved in dimethyl-sulfoxide (DMSO) and physisorbed on a cantilever tip (Microlevers, Park Scientific Instruments, Sunnyvale, CA), which was evaporated with 0.5 nm CrNi and 50 nm gold [15] . The trityl-protected thiol group of the cystein was deprotected with trifluoroacetic acid / CH_2Cl_2 resulting in chemisorption of the poly(azobenzene-peptide) to the tip via the formation of a covalent Au-S bond. The C-terminal end of the polymer was coupled in situ to a flint glass slide (Schott), previously amino functionalized by silanisation with N'-[3-(trimethoxysilyl)propyl]-diethylene-triamine (Aldrich) [38]. The amide bond was formed in the presence of 100 mM N-hydroxysuccinimid (NHS) and 1-ethyl 3-(3-(dimethylamine)propyl)carbodiimide (EDC) (NHS and EDC in 1:1 molar ratio) in DMSO [15,16] .

The non-polar homo-bifunctional C-(GVGVP)nx251-C polypeptide (kindly provided by Dan Urry) were immobilized on a gold-coated glass slide by incubation and picked up with a gold-coated cantilever tip (Olympus Biolever) [17]. Both, the Si_3N_4 cantilever tips as well as the glass slide were evaporated with 0.5 nm CrNi and 30 nm gold [17]. These measurements were performed in Millipore water and at room temperature [15].

Optical switching of the poly(azobenzene-peptide) was achieved by coupling light from a xenon flash lamp (Rapp OptoElectronic, Hamburg, Germany) into the polished flint glass slide (F-2, Schott Glass Mainz, Hellma Optic GmbH, Jena, Germany, n_D = 1.666) via total internal reflection (TIR). A band pass filter at 365 nm (FWHM 12.2 nm) and a filter setup at 430 nm (high pass GG420 in combination with BG 12) were placed between the flash lamp and the flint glass slide to excite the azobenzene unit and switch between the cis and the trans conformation. To achieve high transmission in the UV, it was necessary to use flint glass slides. DMSO (Aldrich, München, Germany, n_D=1.48) was used as a solvent [15,16] .

The technique of atomic-force-microscopy (AFM) based force spectroscopy and the instrumental set-up have been described in detail elsewhere [15,16,30,35,62]. The cantilever tip used in our experiments had spring constants of 10, 14.5 and 35 mN m $^{-1}$. The spring constant of each cantilever was individually calibrated by measuring the amplitude of their thermal oscillations [63]. The sensitivity of the optical lever detection was measured by indenting the cantilever tip into a hard surface.

Data collection and analysis

The data collection and correction of the traces analysed in this paper are described in detail elsewhere [16]. Stretching the same molecule several times in series made it possible to average over three to five force curves resulting in an improved signal to noise ratio. The averaged force curves were smoothed by a three-point sliding average procedure before fitting.

Theoretical description

Ab–initio quantum mechanical model

In the last years the mechanical response of single molecules under stretching forces has been extensively investigated with ab-initio quantum chemistry [35,40,43-46,64]. Ab-initio methods are performed at zero temperature, and therefore miss entropic effects due to conformational fluctuations. These fluctuations become irrelevant at high stretching forces. Therefore, ab-initio methods become very accurate at high stretching force. We have recently shown, how to combine entropic effects, embodied in the freely rotating chain model, with ab-initio predictions and achived a fit function for polyvinylamine in the whole force range accessible by AFM [35]. In this section we present results for azobenzene molecules under tension. As described before, azobenzene exists in a trans and cis conformation [60]. By performing an unconstrained geometry search for a single azobenzene unit, we identified even further local minima conformations. In Figure 1a we show the energy of five different conformations as a function of the distance between the two outer carbon atoms.

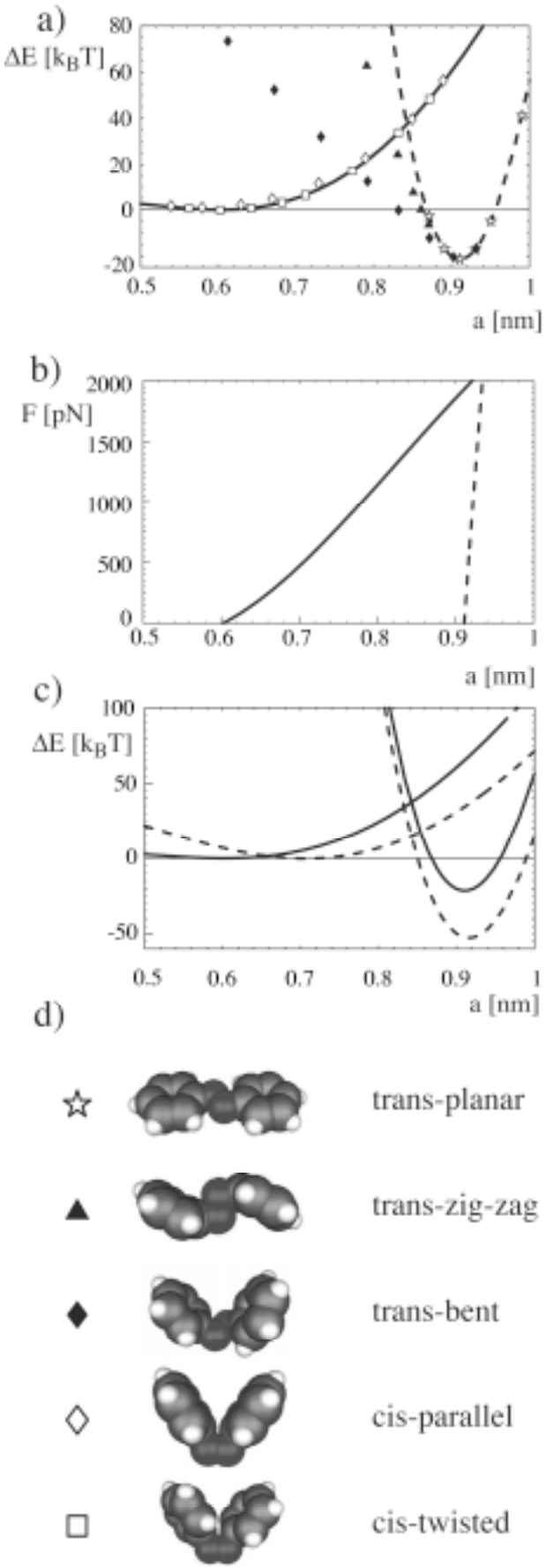

Figure 1: Force dependent energy landscape of azobenzene.

a) Energies of different locally stable configurations as a function of the distance, a, between the two outer carbon atoms. The solid line denotes fits of the cis-twisted and the trans-planar conformation (dashed line). b) Force-Extension curves of the cis-twisted conformation (solid line) and the trans-planar conformation (dashed line). c) Plot of the energy curves for the cis and trans state in the absence of force (solid lines) and in the presence of an external force of 500 pN (broken line). d) Different configurations are trans-planar (open stars), trans-zig-zag (filled triangles), trans-bent (filled diamonds), cis-parallel (open diamonds), cis-twisted (open squares).

For convenience, we measure all energies relative to the ground-state energy of the cis-twisted conformation. All calculations are performed on the quite restricted 6-Gaussian level [35,44]. However, our estimated cis-trans energy difference, which is of the order of 21 k_BT, compares quite well with experimental measurements which find this energy difference to be of the order of 17-20 k_BT [65]. In previous calculations, we have shown that although the absolute energy difference between different basis sets can be considerable, forces depend significantly less on basis set quality (and on including electronic correlations) since they correspond to energy differences [35,44]. All different conformations are quite stable, meaning that they are separated by large barriers in the multidimensional conformation space (which we will discuss later on). The geometries are schematically depicted in Figure 1d. For further analysis, we concentrate on the cis-twisted conformation and on the trans-planar conformation (note that the trans-zig-zag conformation and the trans-bent conformation become degenerate with the trans-planar conformation at distances larger than the equilibrium distance in the trans conformation, which means under extensional forces). The lines in Figure 1a denote polynomial fits for trans (dashed line) and cis (solid line) conformations according to the formula

$$\Delta E = \sum_{n=0}^{\infty} c_n a^{n+1}/(n+1) \qquad (1)$$

where a denotes the distance between the outer carbon atoms in the azobenzene unit. All energies are measured relative to the ground state of the cis-state. The choice of unit cell reflects the chemistry of the used azobenzene molecules, where spacer groups (peptide units) are linked to the azobenzene extremities (Figure 2).

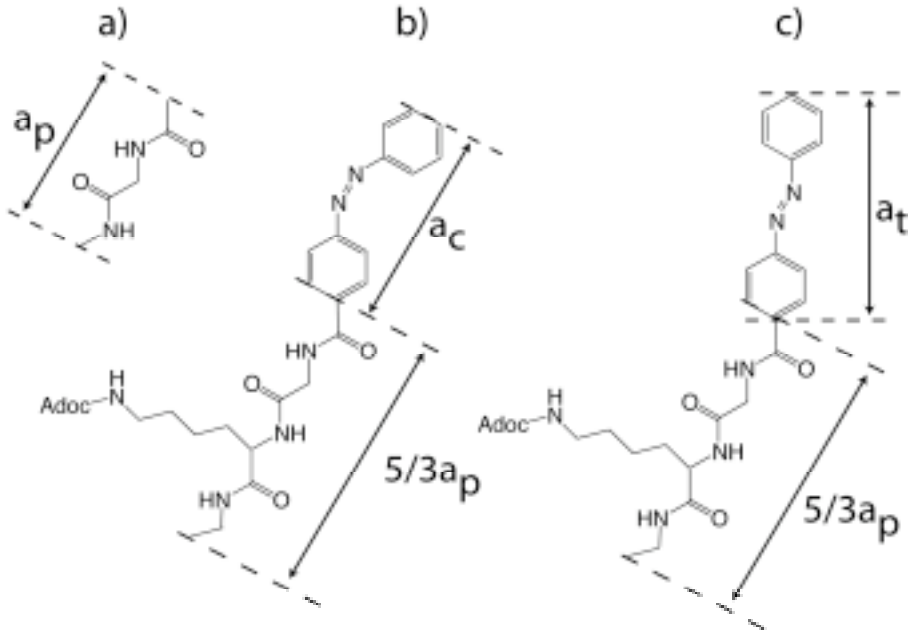

Figure 2. Chemical structures of a non-polar dipeptide (a) and the non-polar azobenzene-tripeptide in the cis (b) and the trans (c) conformation.

For the FRCQM-fits, the polymer is separated into building blocks of azobenzene-cis (unit length a_c=0.6027 nm), azobenzene-trans (unit length a_t=0.9106 nm), and tripeptide (unit length 5/3 a_p=1.2166 nm).

Our fitting results for the elastic coefficients c_n are given in Table 1. The experimentally measurable quantity is the force, which follows from Equation 1 by a derivative

$$F = \frac{\partial \Delta E}{\partial a} = \sum_{n=0}^{\infty} c_n a^n \qquad (2)$$

and is shown in Figure 1b for the trans (dashed line) and cis (solid line) conformations. The equilibrium extension follows from Equation 2 by setting F=0 and is denoted by a_0. Note that Equation 2 gives the force of a single azobenzene unit, which can be generalized for a polymer of arbitrary length by writing

$$F = \sum_{n=0}^{\infty} d_n (a/a_0)^n = \sum_{n=0}^{\infty} d_n (L/L_0)^n \qquad (3)$$

where $d_n=(a_0)^n c_n$. The results for the coefficients d_n are given in Table 2. Yet another way of expressing the force response is obtained by re-expanding Equation 3 around the equilibrium length, leading to the expression

$$F = \sum_{n=1}^{\infty} \gamma_n (a/a_0 - 1)^n \qquad (4)$$

Two mechanisms of conversion between the cis and trans have been discussed in the literature, namely the in-plane inversion of the N-N double bond and the rotation around the dihedral angle [60]. Our results in Figure 1a show that the inversion path way is faced with an activation barrier with a height of at least 35 $k_B T$ (note that the crossing of the two locally stable conformational branches does not correspond to the true transition state, which most likely is of higher energy). It is important to note that the cis state is much softer than the trans state, and thus yields quite easily to extensional forces. This is demonstrated in Figure 1c, where we plot the energy curves for the cis and trans state in the absence of force (solid lines) and in the presence of an external force of 500 pN (broken line). It is seen that the length of the cis state increases substantially in the presence of an external force, and, as a result, the barrier decreases less than it would in the absence of elasticity effects. For a force of 500 pN, the barrier height has decreased to 20 $k_B T$. Experimentally, there is evidence that the actual conversion pathway involves a rotation of the N-N dihedral bond angle [66]. Therefore, we study the rotation under extensional force in the following.

	c_0 (nN)	c_1 (nN/nm)	c_2 (nN/nm^2)	c_3 (nN/nm^3)	a_0 (nm)
azobenzene-trans	-826.66	2,342.8	-2,254.2	745.0	0.9106
azobenzene-cis	9.992	-45.93	64.35	-25.942	0.6027

Table 1. Shown are all elastic constants obtained from the ab-initio calculation for a unit cell of azobenzene in the cis and in the trans conformation.

	d_0 (nN)	d_1 (nN)	d_2 (nN)	d_3 (nN])	a_0 (nm)
azobenzene-trans	-826.66	2,133.9	-1,869.1	562.49	0.9106
azobenzene-cis	9.992	-27.689	23.378	-5.68	0.6027

Table 2: Shown are the rescaled elastic constants obtained from the ab-initio calculation for a unit cell of azobenzene in the cis and in the trans conformation.

The transition between cis and trans conformations can be visualized by a rotation around the dihedral angle ϕ at the nitrogen-nitrogen bond by 180 degrees. In Figure 3a we show the energy as a function of this angle.

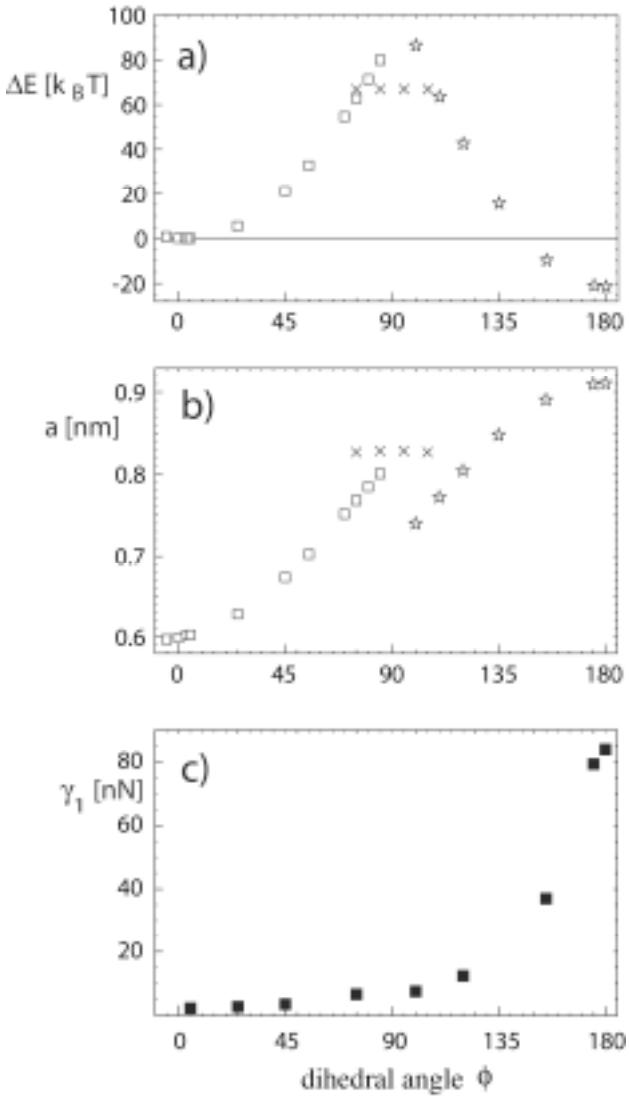

Figure 3. The transition between the cis and trans conformation is visualized by a rotation around the dihedral angle ϕ at the nitrogen-nitrogen bond by 180 degrees.

a) The energy as a function of this angle is plotted. The cis-twisted geometry (denoted by squares) becomes instable at dihedral angles above roughly ϕ=85 degrees. Likewise, the trans conformation (star) loses stability at angles below ϕ=105 degrees. At the crossover between the cis and trans conformation, an intermediate structure (cross) appears. This demonstrates that close to the barrier many competing and locally stable structures exist. b) The distance between the two outer carbon atoms as a function of the dihedral angle ϕ is plotted for the cis conformation (squares), the trans conformation (star) and the intermediate stae (cross). The unit cell size of the barrier state is roughly intermediate between the unit cell size in the cis and trans conformations. c) The stretching modulus of the azobenzene as a function of the dihedral angle is plotted. It is seen that as the dihedral angle increases, the molecules becomes stiffer, meaning that in the cis conformation the molecule easily yields to the externally applied force.

In the calculation, we have only fixed the dihedral angle, but have otherwise optimized the geometry of the whole molecule. The distance between the two outer carbon atoms as a function of the dihedral angle is plotted in Figure 3b. In Figure 3c, the stretching modulus γ_1 of the azobenzene as a function of the dihedral angle is plotted.

Further, we investigated the influence of force on the energy as a function of the angle ϕ. The force-dependent energy for F=0nN, F=0.5nN and F=1nN is calculated by equation (5) and shown in Figure 4a.

$$\Delta\tilde{E}(F) = \Delta E - (a[\phi] - a_{0,cis})F \qquad (5)$$

In Figure 4b we include the stretching modulus γ_1 of the azobenzene, which is given in Figure 3c, the energy can then be written as

$$\Delta\tilde{E}(F) = \Delta E - (a[\phi] - a_{0,cis})F - \frac{1}{2}F^2/\gamma[\phi] \qquad (6)$$

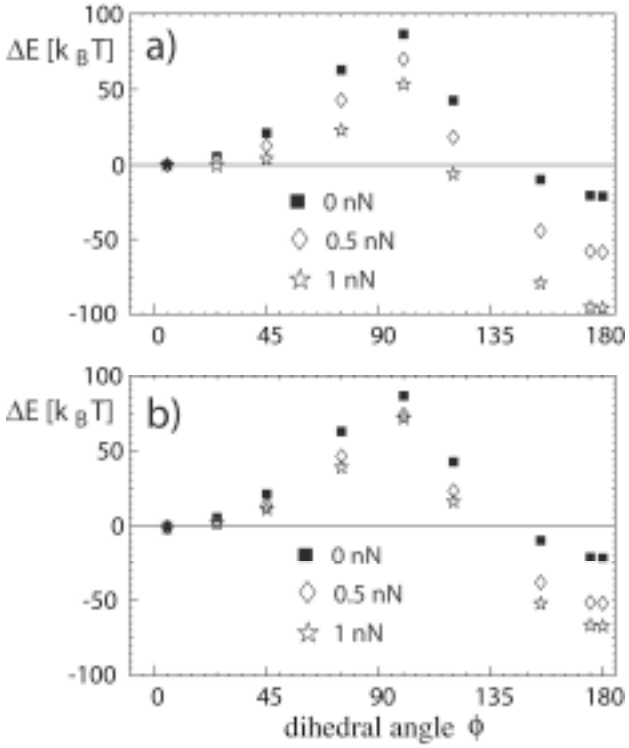

Figure 4.

a) The energy relative to the cis ground state as a function of the dihedral angle is plotted at forces corresponding to 0 nN, 0.5 nN and 1 nN.

b) Here, the elastic effects from Figure 3c are included via Equation 6.

Including elasticity effects changes the energy of the extended states considerably. In specific, the reduction of the barrier height under applied force is considerably reduced.

Freely Rotating Chain model

The freely rotating chain (FRC) model consists of segments with fixed length b that are freely rotating at a fixed angle with respect to each other, as illustrated in the insert in Figure 5.

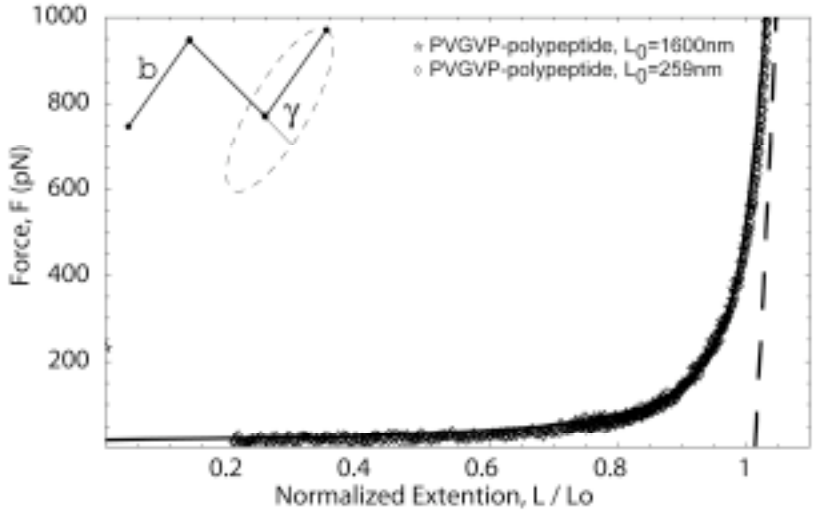

Figure 5. FRCQM fit (solid trace) and normalized force extension traces measured with two different chains (diamond and star) of the non-polar poly-GVGVP. The slope in the high force regime (> 800 pN) of the two force vs. extension curves were first fitted with the ab-initio calculated elasticity for a dipeptide (long dash line). From this fit, the resulting contour length for the chains at zero force was determined to be L_0=259 nm (diamond) and L_0=1600 nm (star), respectively. These zero force contour lengths were used to normalize the measured curves. The ab-initio elasticities combined with the FRC-model (FRCQM) and a bond length of b_p=0.12 nm were found to fit the low, medium and high force range of the normalized experimental curves over the whole force range (solid line).

Insert: Geometric configuration of the FRC-model with segments of a fixed bond length, b, rotating freely around the bond axis at fixed angles γ [40].

The full force-distance relation is involved and has only recently been numerically determined. For high forces, the FRC model is asymptotically described by Equation 7 [40].

$$\frac{R_z(f)}{L_0(N_p)} = 1 - \left(\frac{2 \cdot f \cdot b_p}{k_B T} \right)^{-1} \qquad (7)$$

In this Equation $R_z(f)$ is the chain length, $L_0(N_p) = N_p\, a_{p0} / 2$ is the contour length at zero force, k_B is the Boltzmann constant, T is the temperature, f is the force, N_p is the number of monomers, $a_{p0}/2$ is the unit length at zero force from the ab-initio calculation and b_p the bond length.

In this study we fit the poly(azobenzene-peptide) by dividing it into three units: peptide, azobenzene-trans and azobenzene-cis. Assuming that the behavior of the single units is additive, Equation 7 was expanded as a sum over all units:

$$\frac{R_z(f, N_t, N_c)}{L_0(N_t, N_c)} = \sum_{i=1}^{3} \left(\frac{L_{i0}(N_t, N_c)}{L_0(N_t, N_c)} \cdot \left(1 - \left(\frac{2 \cdot f \cdot b_i}{k_B T} \right)^{-1} \right) \right) \qquad (8)$$

Here, i=1 indicates peptide, i=2 azobenzene-trans and i=3 azobenzene-cis. $L_0(N_t, N_c)$ is the contour length at zero force of the poly(azobenzene-peptide) (Equation 9d). $L_{i0}(N_t,N_c)$ is the sum of all unit length at zero force from one species in the polymer (Equation 9a-c).

The pre-factor $L_{i0}(N_t, N_c) / L_0(N_t, N_c)$ is a weighting factor dependent on the amount of one species in the polymer.

Equation 8 includes now three different bond lengths b_i, namely the bond length for peptide $b_1=b_p$, azobenzene-trans $b_2=b_t$ and azobenzene-cis $b_3=b_c$.

The contour length $L_0(N_t, N_c)$ of the poly(azobenzene-peptide) is separated into peptide $L_1=L_{p0}(N_t, N_c)$, azobenzene-trans $L_2=L_{t0}(N_t)$, azobenzene-cis monomers $L_3= L_{c0}(N_c)$:

$$L_1 = L_{p0}(N_p) = N_p \cdot a_{p0} / 2 = (N_t + N_c) \cdot 5/3 \cdot a_{p0} \qquad (9a)$$

$$L_2 = L_{t0}(N_t) = N_t \cdot a_{t0} \qquad (9b)$$

$$L_3 = L_{c0}(N_c) = N_c \cdot a_{c0} \qquad (9c)$$

$$L_0(N_t, N_c) = L_{p0}(N_t, N_c) + L_{t0}(N_t) + L_{c0}(N_c) \qquad (9d)$$

Here a_{p0} is the peptide unit length at zero force (Figure 2a), a_{c0} is the azobenzene-cis unit length at zero force (Figure 2b) and a_{t0} is the azobenzene-trans unit length at zero force (Figure 2c). N_p, N_t and N_c are the number of peptide, azobenzene-trans and azobenzene-cis monomers, respectiveley.

Combined freely rotating chain-ab-initio quantum mechanical model

In the combined FRC-ab-initio QM (FRCQM) model, the unit length a_i is force dependent because $a_i(f)$ is the inverse function for the ab-initio stretching force $F(a_i)$ as described in the ab-initio section above (see Equation 3) [35] .

$$a_i(f) = f^{(-1)}(a_i) \tag{10}$$

Therefore, all the unit length become force dependent and Equations 7-9 are rewritten as:

$$\frac{R_z(f)}{L_0(N_p)} = \frac{L_0(f,N_p)}{L_0(N_p)}\left(1-\left(\frac{2\cdot f\cdot b_p}{k_BT}\right)^{-1}\right) \tag{11}$$

$$\frac{R_z(f,N_t,N_c)}{L_0(N_t,N_c)} = \sum_i\left(\frac{L_i(f,N_t,N_c)}{L_0(N_t,N_c)}\cdot\left(1-\left(\frac{2\cdot f\cdot b_i}{k_BT}\right)^{-1}\right)\right) \tag{12}$$

$$L_p(f,N_p) = N_p\cdot a_p(f)/2 = (N_t+N_c)\cdot 5/3\cdot a_p(f) \tag{13a}$$

$$L_t(f,N_t) = N_t\cdot a_t(f) \tag{13b}$$

$$L_c(f,N_c) = N_c\cdot a_c(f) \tag{13c}$$

$$L_0(f,N_t,N_c) = L_p(f,N_t,N_c) + L_t(,f,N_t) + L_c(f,N_c) \tag{13d}$$

With this combined FRCQM model the experimental force curves are fitted in the following way:

The high force range of the non-polar polypeptide chain was fitted first with the ab-initio Equation 13a. In this fit, only the number of monomers (peptides) was varied and no bond length b_p was involved. From this fit the contour length at zero force and zero temperature was extracted ($L_0(f=0, N_p)$) and the force curves were normalized with this contour length.

Applying Equation 11 to the normalized poly-GVGVP force curves results in the fitted bond length b_p, this length was later also used for the peptide bonds in the poly(azobenzene-peptide). After fitting the bond length b_p, the effects of fluctuations are taken into account (Equation 11), which results in a length increase of the fitted contour length (Figure 5, solid line). Note: Therefore, the dashed line in Figure 5 hits the x-axis at $L/L_0>1$ [35].

Following the procedure above, Equation 13d was used to fit the high force range of the non-polar poly(azobenzene-peptide) to extract the contour length at zero force and zero temperature. In this Equation

combinations of N_t and N_c were used to fit the high force range. The fit yields the number of azobenzene-trans and azobenzene-cis monomers.

To determine the difference between trans and cis due to optical switching, the number of azobenzene units was kept constant (N_t+N_c=costant) and only the ratio between trans and cis was varied (N_t / N_c=variable).

In the last step, the bond length for azobenzene-trans b_t and for azobenzene-cis b_c was ajusted to fit the whole force range for a wide range of conformational changes in the poly(azobenzene-peptide) (Figure 6-8).

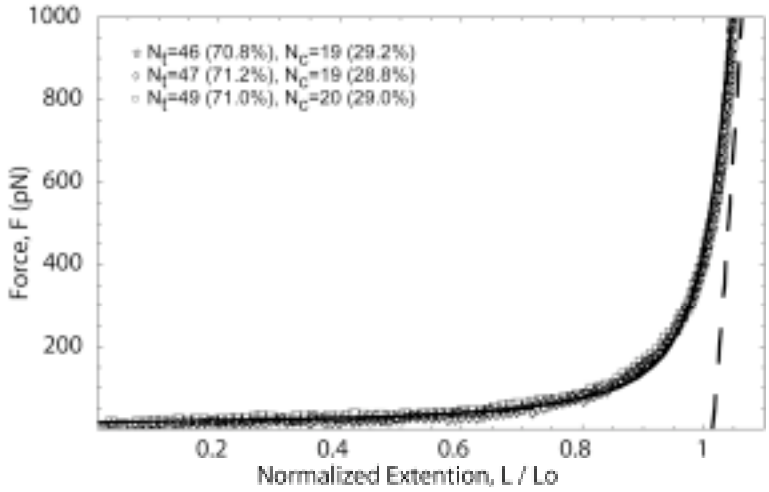

Figure 6. Poly(azobenzene-peptide) force curves compared with FRCQM prediction.

Three force curves of non-polar poly(azobenzene-peptide) containing about the same amount of trans and cis azobenzene are superimposed. Their good agreement shows, that a change in curve shape does not result from uncertainties in the experiment (but reflects a switching of the polymers elasticity). The contour length L_0 for the polymer is extracted from the ab-initio fit in the high force range (black dashed line). Now the number of azobenzene monomers in the trans and in the cis conformation can be calculated. The resulting FRCQM fit (solid line) uses the following bond lengths: azobenzene trans (b_t=0.11 nm), azobenzene cis (b_c=0.30 nm) and peptide (b_p=0.12 nm).

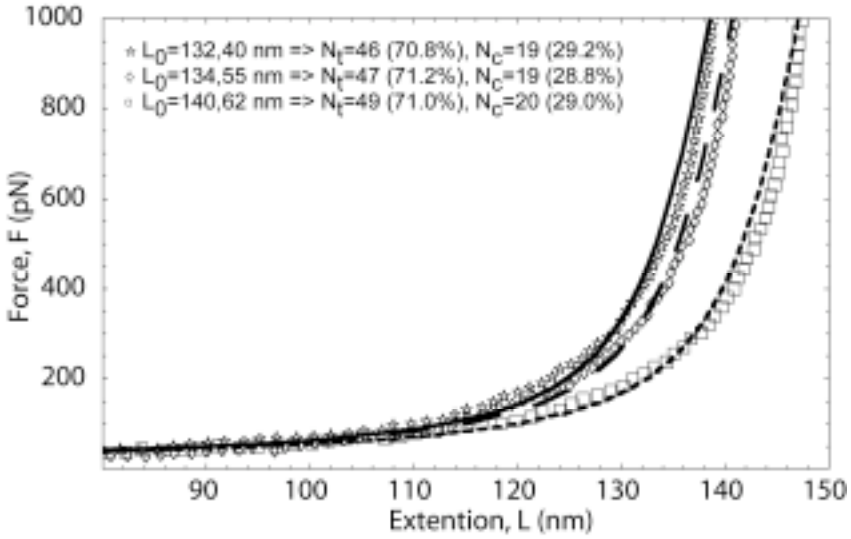

Figure 7. Non-normalized force vs. distance curves as used in Figure 6.

The three curves from Figure 6 are fitted here with different contour length and the above calculated amount of azobenzene monomers in the trans and cis conformation. Short curve: Data: star, fit: solid line; L_0=132,4 nm <=> N_t=46 (70.8%), N_c=19 (29.2%), Medium curve: Data: diamond, fit: long dash line; L_0=134,55 nm <=> N_t=47 (71.2%), N_c=19 (28.8%), Long curve: Data: square, fit: short dash line; L_0=140,62 nm <=> N_t=49 (71.0%), N_c=20 (29.0%)

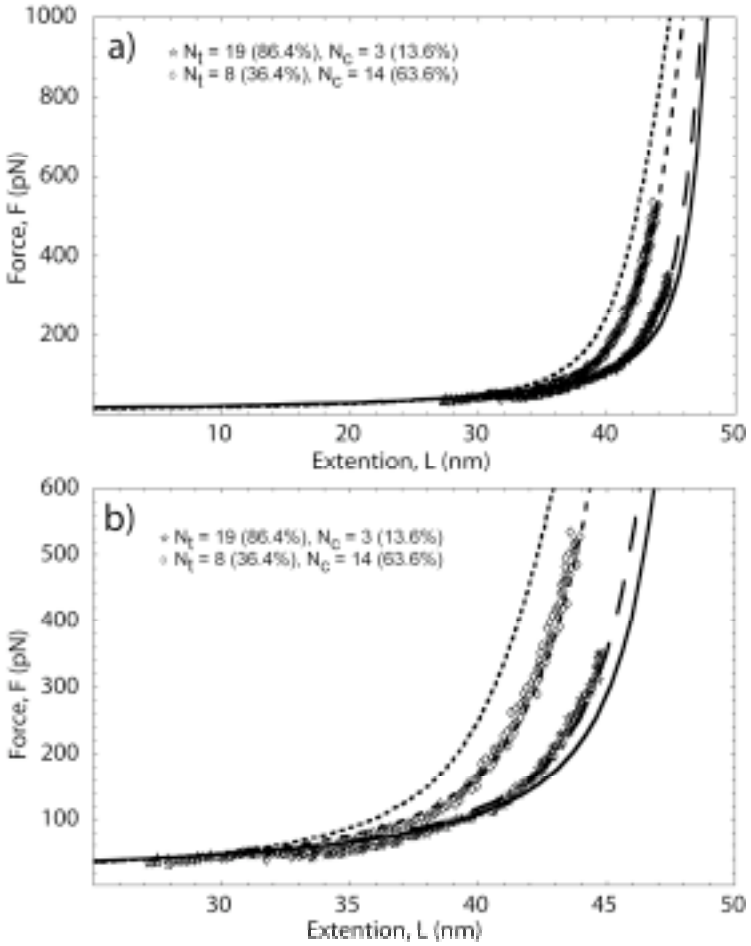

Figure 8. Light induced switching of poly(azobenzene-peptide) compared to the theoretical prediction.

a) Experimentally observed optical switching of poly(azobenzene-peptide) from 86.4% trans (star) to 36.4% trans (diamond).

The theoretical predicted FRCQM calculation is plotted for 86.4% trans (long dash line, N_t=19, N_c=3) and for 36.4% trans (short dash line, N_t=8, N_c=14). A theoretical all trans (solid line, N_t=22, N_c=0) and all cis (dot line, N_t=0, N_c=22) conformation of the poly(azobenzene-peptide) is plotted to present the upper und lower limit for the length change. b) Magnification of Figure 8 highlights the one-parameter fit and illustrates the excellent match between experiment and theory.

Force curves shown in Figure 5 and 6 are selected on the basis of maximum force (to get a very precise L_0) and maximum polymer contour length (to have the elasticity of the polymer much smaller than the elasticity of the cantilever). The curves in Figure 8 were selected to demonstrate the FRCQM model over a large length change due to optical switching of the azobenzene monomers.

Results and discussion

Since the poly(azobenzene-peptide) backbone predominantly consists of peptide bonds, the accuracy of the freely rotating chain-ab-initio quantum mechanical (FRCQM) model was first demonstrated with a fit of the force extension traces of two non-polar polypeptide chains with different length (Figure 5). Following the procedure given above, the contour lengths were determined at zero force and zero temperature (see Equation 13a, diamond, $L_0(f=0)=259$ nm, star, $L_0(f=0)=1600$ nm) and the experimental curves were normalized with these contour length and plotted on top of each other together with the theoretical curve based on the FRCQM model (Equation 11, parameters from [35]). As can be seen, the accuracy of the calculated force curve is striking with a bond length of $b_p=0.12$ nm = a_0 / 6 (Figure 5) [35]which is similar to the bond length of a single peptide bond in an uncharged polypeptide chain.

Next, the ab-initio quantum mechanical calculations at zero temperature for the azobenzene were performed as described above resulting in free energies of the different azobenzene-conformations as a function of their end-to-end distances (see Figure 1a). From these the molecular elasticity's were derived and plotted in Figure 1b. This results in stretching moduli of $\gamma_1=82.5\ nN$ for the trans conformation and $\gamma_1=2.02\ nN$ for the cis conformation according to Equation 4. The enormous difference in stretching modulus reflects the different architecture of the conformations: the trans conformation is straightened out and any lengthening of the molecule either deforms the nitrogen bonds (which is costly), distorts the benzene rings or changes the length of a bond. In the cis conformation, the total molecule is bent and the force acting on the outer carbon atoms produces an enormous torque at the center. This means that not only the length per unit upon optical switching, but also the elasticity of the polymer changes.

The transition between the cis and the trans state is visualized by the rotation around the dihedral angle ϕ at the nitrogen-nitrogen bond by 180 degrees. As shown in Figure 3a, the cis-twisted geometry (denoted by squares) becomes instable at dihedral angles above roughly $\phi=85$ degrees. Likewise, the trans conformation loses stability at angles below $\phi=105$ degrees. In between, an intermediate structure appears. We have not been able to determine the saddle-point, which is probably caused by the near-degeneracy of

many local minima close to the energy barrier [67]. Nevertheless, we estimate the barrier to be of the order of the energy of the cis and trans conformations where they almost cross.

In Figure 3b we plot the distance between the two outer carbon atoms an as a function of the dihedral angle ϕ. At distances corresponding to the barrier state, the distance *a* is roughly intermediate between the unit cell size in the cis and trans conformations. This suggests that under an applied force, the barrier height should be substantially decreased and thus a mechanic pulling experiment should be able to induce the transition from the cis to the trans conformation at large enough forces. To test this, we plot in Figure 4a the force-dependent energy for forces corresponding to 0 nN, 0.5 nN and 1 nN (c.f. Equation 5). It can be seen that the barrier height decreases from about 85 k_BT to about 55 k_BT. If, in addition, the angle dependence of the stretching modulus γ_1 (c.f. Figure 3c) is included (according to Equation 6), the barrier stays even above 70 k_BT (Figure 4b). This explains the, on first sight unexpected, high stability of the cis conformation against an external force, which was observed in the experiments.

This result can be generalized: pulling a soft molecule over a free-energy barrier into a stiff state becomes increasingly difficult when the transition state is stiffer than the starting conformation. Conversely, it would be easy to push azobenzene from the trans conformation into the cis conformation [60].

Comparing these calculated values for the barrier height with experimental results is not straightforward, be cause the experimental analysis usually employs Kramers theory which strictly holds only in a one-dimensional configuration space for a reaction path, however the actual path is in a multidimensional configuration space and degrees of freedom that are orthogonal to the reaction path become important (e.g. translocational vibration which are characterized by the longitudinal stretching modulus γ_1 – see Figure 3c). In addition, the ab-initio calculation is performed with the very restrictive 6G-basis set, and the saddle point of the transition is not determined. The values that can be extracted from the data in Figure 4 should therefore only be regarded as a rough estimate.

The main goal of this project is highlighted in Figure 6. It shows three normalized force extension traces measured on polymers of different length but equivalent cis to trans ratio of about 29:71 together with the

predicted curve (solid line). These ratios and the total number of azobenzene-cis N_c and azobenzene-trans N_t -are a result of the fit in the high force range (Equation 13d), they result in the contour length at zero force.

As can be seen the FRCQM model (Equation 12) provides an excellent agreement between experiment and theory with a bond length b_t=0.11 nm for azobenzene-trans and b_c=0.3 nm for azobenzene-cis. Figure 7 shows the same curves but not normalized (star, solid fit: L_0=132,40 nm, N_t=46, N_c=19; diamond, long dash fit: L_0=134,55 nm, N_t=47, N_c=19; square, short dash fit: L_0=140,62 nm, N_t=49, N_c=20). In the appendix we give some arguments why for polymer that consists of bonds different length and different bond angles the effective bond length will tend to be smaller than the true bond length, in agreement with what we observed in our fits.

In Figure 8a this model was used to quantify the conversion ratio for a particular poly(azobenzene-peptide), which was switched back and forth optically. Two traces were picked and analyzed after the procedure given above. The best fit in the high force range was given for N_t=19 and N_c=3 (N_t+N_c=22), resulting in a contour length of 45.9 nm (Equation FRC 8d) and a trans to cis ratio of 86:14 (star, long dash line). After UV exposure it contracted into the state fitted best by the short dash line where the fraction of trans units was reduced to 36.4% (N_t=8, N_c=14, N_t+N_c=22, L_0=42.5 nm, diamond, short dash line). The extremes of 0 and 100% conversion are shown as doted (N_t=22, N_c=0, L_0=46.8 nm) and solid (N_t=0, N_c=22, L_0=40.0 nm) lines respectively. Figure 8b is a magnification of Figure 8a and illustrates the large change from a most trans to the most cis conformation in the single molecule poly(azobenzene-peptide) experiment. This conversation rate is similar to the one observed in ensemble measurements [68].

Conclusions

We have demonstrated that a new statistical model for the analysis of experimental force-extension data of poly(azobenzene-peptide)s can yield the precise number of units in the cis and trans conformation. The model is a combination of the freely rotating chain model and ab-initio quantum mechanical calculations (FRCQM) for azobenzene and peptide units. The experimental data were analyzed in three steps. In the first step, force curves of non-polar poly-peptide chains were fitted with the FRCQM model and result in a bond length of b_p=0.12 nm. In the second step, poly(azobenzene-peptide) force curves were fitted and

resulted in bond length for azobenzene-trans of b_t=0.11 nm and for azobenzene-cis of b_c=0.3 nm. In the third step this parameter-free model was used to analyze the switching of the poly(azobenzene-peptide) from 86.4% trans to 36.4% trans.

As can be seen the model allows a one-parameter analysis of the degree of optical conversion and so for a determination of the quantum efficiency of the opto-mechanical transformation. Experiments of this kind in connection with this data analysis will be the basis of further development of the photonic muscle.

Beside the FRCQM model, the quantum mechanical calculations reveal that the forced conversion path is orthogonal or at least has no prominent co-linear component to the thermal unfolding path. In other words, pulling at the ends of the azobenzene group does not help the rotation around the N-N double bond. As a result the force acting along the polymer backbone does not reduce the remaining activation barrier for the thermal conformational transition and as a consequence the force does not significantly reduce the lifetime of the cis conformation. This explains why the known thermal relaxation of the cis conformation within fractions of hours is not speeded to a timescale comparable to the force ramp in the experiment. This is why forces as high as 500 pN can be applied for many seconds to a mostly cis configuration without switching it to the trans conformation.

Acknowledgements

This work was supported by the Deutsche Forschungsgemeinschaft. Helpful discussion with Markus Seitz and Dan Urry are gratefully acknowledged. The Azo-polymers were kindly provided by Louis Moroder.

Appendix: High-force limit of freely-rotating chain model

We present here a generalization of the scaling arguments already displayed in a previous publication [69]. Consider a freely rotating chain model under large extensional forces. In this high force limit, the chain will adopt an extended conformation, and we only consider small librational fluctuations around this ground state. In the previous publication, all bonds had the same length and bond angle. Now, we show a slightly more general model where the chain consists of two bonds of different length and in principle also of

different bond angle. Figure 9 depicts two bonds that might make up the chain and all the relevant variables.

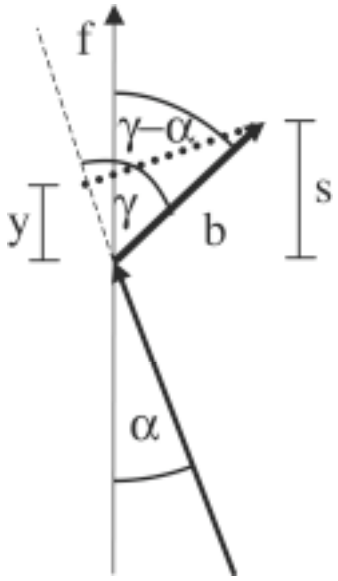

Figure 9. High-force limit of freely-rotating chain model.

Shown is a general model where the chain consists of two bonds of different length and in principle also of different bond angle. The upper bond makes an angle γ with the lower bond and an angle γ–α with the vertical axis. The torsional angle ϕ determines angular fluctuations away from the ground state. Where $y = b\cos\gamma\cos\alpha$ and $s = b\cos(\gamma-\alpha)$ and b is the bond length.

The vertical axis denotes the direction along which the external force acts. The upper bond (the vertical orientation of which we want to calculate) makes an angle γwith the lower bond and an angle γ–αwith the vertical axis. The torsional angle ϕdetermines angular fluctuations away from the ground state. The projected length along the force direction is given by

$$z = y + (s-y)\cos\phi$$

where $y = b\cos\gamma\cos\alpha$ and $s = b\cos(\gamma-\alpha)$ and b is the bond length. The fluctuation of the upper bond are determined by the partition function

$$Z = \int_0^{2\pi} d\phi \exp\{zf/k_BT\} \approx \sqrt{2\pi k_BT/(f(s-y))}\exp(fs/k_BT)$$

from which the vertical extension follows by a partial derivative as $\langle z \rangle = \partial \ln Z / \partial (f / k_B T)$. Dividing the vertical extension <z> by the projected bond length *s*, we obtain finally

$$\frac{\langle z \rangle}{s} = 1 - \frac{k_B T}{2 f b \cos(\gamma - \alpha)}.$$

The new result is the factor cos(γ–α), which amounts to a reduction of the effective bond length by a geometric factor. A bond that is oriented closely to the force axis will only be subject to a small correction, but for bonds that are oriented at a large angle γ–α away from the force axis the correction term will be important. The main result is that the effective bond length will be reduced, and this effect might be especially important for polymer, which consist of bonds of different length and different bond angles. This observation is in accord with the results obtained in this paper based on the fits of experimental data, where the effective bond lengths were found to be substantially smaller than the geometric bond lengths obtained within the ab-initio calculation. An explanation could be that some of the bonds make large angles with the force axis.

References

(1) Rief, M.; Gautel, M.; Oesterhelt, F.; Fernandez, J. M.; Gaub, H. E. *Science* **1997**, *276*, 1109-1112.

(2) Rief, M.; Fernandez, J. M.; Gaub, H. E. *Physical Review Letters* **1998**, *81*, 4764-4767.

(3) Oesterhelt, F.; Oesterhelt, D.; Pfeiffer, M.; Engel, A.; Gaub, H. E.; Muller, D. J. *Science* **2000**, *288*, 143-146.

(4) Kessler, M., Gaub H.E. *Nat. Struct. & Mol. Biol.* **2005**, *submitted.*

(5) Kellermayer, M. S. Z.; Smith, S. B.; Granzier, H. L.; Bustamante, C. *Science* **1997**, *276*, 1112-1116.

(6) Rief, M.; Clausen-Schaumann, H.; Gaub, H. E. *Nature Structural Biology* **1999**, *6*, 346-349.

(7) Smith, S. B.; Finzi, L.; Bustamante, C. *Science* **1992**, *258*, 1122.

(8) Bustamante, C.; Smith, S. B.; Liphardt, J.; Smith, D. *Current Opinion in Structural Biology* **2000**, *10*, 279-285.

(9) Clausen-Schaumann, H.; Rief, M.; Gaub, H. E. *Biophysical Journal* **1999**, *76*, A151-A151.

(10) Albrecht, C.; Blank, K.; Lalic-Multhaler, M.; Hirler, S.; Mai, T.; Gilbert, I.; Schiffmann, S.; Bayer, T.; Clausen-Schaumann, H.; Gaub, H. E. *Science* **2003**, *301*, 367-370.

(11) Bockelmann, U. *Current Opinion in Structural Biology* **2004**, *14*, 368-373.

(12) Allemand, J. F.; Bensimon, D.; Croquette, V. *Current Opinion in Structural Biology* **2003**, *13*, 266-274.

(13) Bouchiat, C.; Wang, M. D.; Allemand, J.-F.; Strick, T.; Block, S. M.; Croquette, V. *Biophys. J.* **1999**, *76*, 409-413.

(14) Hugel, T.; Seitz, M. *Macromolecular Rapid Communications* **2001**, *22*, 989-1016.

(15) Hugel, T.; Holland, N. B.; Cattani, A.; Moroder, L.; Seitz, M.; Gaub, H. E. *Science* **2002**, *296*, 1103-1106.

(16) Holland, N. B.; Hugel, T.; Neuert, G.; Cattani-Scholz, A.; Renner, C.; Oesterhelt, D.; Moroder, L.; Seitz, M.; Gaub, H. E. *Macromolecules* **2003**, *36*, 2015-2023.

(17) Urry, D. W.; Hugel, T.; Seitz, M.; Gaub, H. E.; Sheiba, L.; Dea, J.; Xu, J.; Parker, T. *Philosophical Transactions of the Royal Society of London Series B-Biological Sciences* **2002**, *357*, 169-184.

(18) Rief, M.; Oesterhelt, F.; Heymann, B.; Gaub, H. E. *Science* **1997**, *275*, 1295-1297.

(19) Friedsam, C.; Becares, A. D.; Jonas, U.; Seitz, M.; Gaub, H. E. *New Journal of Physics* **2004**, *6*.

(20) Friedsam, C.; Seitz, M.; Gaub, H. E. *Journal of Physics-Condensed Matter* **2004**, *16*, S2369-S2382.

(21) Seitz, M.; Friedsam, C.; Jostl, W.; Hugel, T.; Gaub, H. E. *Chemphyschem* **2003**, *4*, 986-990.

(22) Ashkin, A.; Schütze, K.; Dziedzic, J. M.; Euteneuer, U.; Schliwa, M. *Nature* **1990**, *348*, 346.

(23) Bustamante, C.; Bryant, Z.; Smith, S. B. *Nature* **2003**, *421*, 423-427.

(24) Neuman, K. C.; Block, S. M. *Review of Scientific Instruments* **2004**, *75*, 2787-2809.

(25) Lang, M. J.; Fordyce, P. M.; Engh, A. M.; Neuman, K. C.; Block, S. M. *Nature Methods* **2004**, *1*, 133-139.

(26) Sheetz, M. P., Ed. *Laser tweezers in cell biology*; Academic Press: New York, 1997.

(27) Merkel, R.; Nassoy, P.; Leung, A.; Ritchie, K.; Evans, E. *Nature* **1999**, *397*, 50-53.

(28) Evans, E. *Annual Review of Biophysics and Biomolecular Structure* **2001**, *30*, 105-128.

(29) Evans, E.; Ritchie, K. *Biophysical Journal* **1997**, *72*, 1541-1555.

(30) Clausen-Schaumann, H.; Seitz, M.; Krautbauer, R.; Gaub, H. E. *Current Opinion in Chemical Biology* **2000**, *4*, 524-530.

(31) Gaub, H. E. *Abstracts of Papers of the American Chemical Society* **2000**, *220*, U260-U260.

(32) Grandbois, M.; Beyer, M.; Rief, M.; Clausen-Schaumann, H.; Gaub, H. E. *Science* **1999**, *283*, 1727-1730.

(33) Rief, M.; Grubmuller, H. *Chemphyschem* **2002**, *3*, 255-261.

(34) Oesterhelt, F.; Rief, M.; Gaub, H. E. *New J. Phys.* **1999**, *1*, 6.1.

(35) Hugel, T.; Rief, M.; Seitz, M.; Gaub, H. E.; Netz, R. R. *Physical Review Letters* **2005**, *94*.

(36) Krautbauer, R.; Pope, L. H.; Schrader, T. E.; Allen, S.; Gaub, H. E. *Febs Letters* **2002**, *510*, 154-158.

(37) Krautbauer, R.; Rief, M.; Gaub, H. E. *Nano Letters* **2003**, *3*, 493-496.

(38) Hugel, T.; Grosholz, M.; Clausen-Schaumann, H.; Pfau, A.; Gaub, H.; Seitz, M. *Macromolecules* **2001**, *34*, 1039-1047.

(39) Odijk, T. *Macromolecules* **1995**, *28*, 7016-7018.

(40) Livadaru, L.; Netz, R. R.; Kreuzer, H. J. *Macromolecules* **2003**, *36*, 3732-3744.

(41) Friedsam, C.; Wehle, A. K.; Kühner, F.; Gaub, H. E. *Journal of Physics-Condensed Matter* **2003**, *15*, S1709-S1723.

(42) Kreuzer, H. J.; Wang, R. L. C.; Grunze, M. *New Journal of Physics* **1999**, *21*, 1367-2630.

(43) Livadaru, L.; Netz, R. R.; Kreuzer, H. J. *Journal of Chemical Physics* **2003**, *118*, 1404-1416.

(44) Netz, R. R. *Macromolecules* **2001**, *34*, 7522-7529.

(45) Rohrig, U. F.; Troppmann, U.; Frank, I. *Chemical Physics* **2003**, *289*, 381-388.

(46) Rohrig, U. F.; Frank, I. *Journal of Chemical Physics* **2001**, *115*, 8670-8674.

(47) Finkelmann, H.; Nishikawa, E.; Pereira, G. G.; Warner, M. *Phys Rev Lett* **2001**, *87*, 015501.

(48) Brown, C. H., Ed. *Photochromism*; Wiley-Interscience: New York, 1971.

(49) Tamai, N.; Miyasaka, H. *Chem. Rev.* **2000**, *100*, 1875.

(50) Irie, M. In *Photoreactive Materials for Ultrahigh-Density Optical Memory*; Irie, M., Ed.; Elsevier: Amsterdam, 1994; p 1.

(51) Rau, H. In *Photochromism: Molecules and Systems*; Dürr, H.; Bouas-Laurent, H., Eds.; Elsevier: Amsterdam, 1990; p Ch. 4.

(52) Rau, H. *J. Photochem.* **1984**, *26*, 221.

(53) Shinkai, S.; Manabe, O. *Topics Curr. Chem.* **1984**, *121*, 67-104.

(54) Willner, I. *Acc. Chem. Res.* **1997**, *30*, 347-356.

(55) Archut, A.; Vögtle, F.; De Cola, L.; Azzellini, G. C.; Balzani, V.; Ramanujam, P. S.; Berg, R. H. *Chem Eur. J.* **1998**, *4*, 699-706.

(56) Strzegowski, L. A.; Martinez, M. B.; Gowda, D. C.; Urry, D. W.; Tirrell, D. A. *J. Am. Chem. Soc*. **1994**, *116*, 813-814.

(57) Lagungé Labarthet, F.; Bruneel, J. L.; Buffeteau, T.; Sourisseau, C.; Huber, M. R.; Zilker, S. J.; Bieringer, T. *PhysChemChemPhys* **2000**, *2*, 5154-5167.

(58) Feringa, B. L.; Jager, W. F.; de Lange, B.; Meijer, E. W. *J. Am. Chem. Soc*. **1991**, *113*, 5468-5470.

(59) Feringa, B. L.; van Delden, R. A.; Koumura, N.; Geertsema, E. M. *Chem Rev* **2000**, *100*, 1789-1816.

(60) Monti, S.; Orlandi, G.; Palmieri, P. *Chem. Phys*. **1982**, *71*, 87.

(61) Behrendt, R.; Renner, C.; Schenk, M.; Wang, F.; Wachtveitl, J.; Oesterhelt, D.; Moroder, L. *Angew. Chem. Intl. Ed*. **1999**, *38*, 2771-2773.

(62) Binnig, G.; Quate, C. F.; Gerber, C. *Phys. Rev. Lett*. **1986**, *56*, 930.

(63) Butt, H. J.; Jaschke, M. *Nanotechnology* **1995**, *6*, 1-7.

(64) Kreuzer, H. J.; Grunze, M. *Europhysics Letters* **2001**, *55*, 640-646.

(65) Adamson, A. W.; Vogler, A.; Kunkely, H.; Wachter, R. *Journal of American Chemical Society* **1978**, *100*, 1298.

(66) Nerbonne, J. M.; Weiss, R. J. *Journal of American Chemical Society* **1978**, *100*, 5953.

(67) Frank, I. *to be published*.

(68) Renner, C.; Cramer, J.; Behrendt, R.; Moroder, L. *Biopolymers* **2000**, *54*, 501-514.

(69) Aktah, D.; Frank, I. *Journal of the American Chemical Society* **2002**, *124*, 3402-3406.

P4

“Dynamic force spectroscopy of the digoxigenin - antibody complex“

G. Neuert, C. Albrecht, E. Pamir and H. E. Gaub

Submitted to FEBS Letter

Dynamic force spectroscopy of the digoxigenin - antibody complex

G. Neuert, C. Albrecht, E. Pamir and H. E. Gaub

Lehrstuhl für Angewandte Physik & Center for Nanoscience, Ludwig-Maximilians-Universität, Amalienstrasse 54, 80799 München, Germany.

Abstract:

Small ligands and their receptors are widely used non-covalent couplers in various biotech applications: the digoxigenin-antibody complex is a prominent example. Here we employed single molecule force spectroscopy to investigate the mechanical stability of this complex in order to validate its potential applications in biomolecular assemblies under force load. We found a pronounced loading rate dependence of the rupture force, which we analyzed based on the well established Bell-Evans-model with two subsequent unbinding barriers. We could show that the first barrier has a width of Δx=1.15nm and a spontaneous rate of k_{off}=0.015s^{-1} and the second has a width of Δx=0.35nm and a spontaneous rate of k_{off}=4.56s^{-1}. In the crossover region between the two regimes we found a marked discrepancy between the predicted bond rupture probability density and the measured rupture force histograms which we discuss as non-Markovian contribution to the unbinding process.

Keywords: AFM, force spectroscopy, digoxigenin, antibody, loading rate, PEG, nanostructure, epoxy silane

1. Introduction:

Affinity conjugation of biomolecules has found widespread applications for *in vitro* diagnostics substituting radioactive labeling [1]. Especially protein receptors, which bind to small molecules with high affinity, are the molecules of choice for biomolecular assays [1].

Prominent examples are the avidin-biotin and the anti-digoxigenin antibody - digoxigenin system [2]. Both consist of a small molecule ligand that possesses a functional moiety, which protrudes out of the binding pocket of the protein receptor. By means of this moiety the ligand can be coupled covalently to other molecules or to a solid support [1,3]. For example, for non-radioactive southern blotting a DNA probe that is specific for the gene of interest is labeled with digoxigenin [2]. The sample DNA is fixed to a solid support, and after the probe was hybridized to it, a conjugate of an anti-digoxigenin antibody to a reporter enzyme is incubated on the sample. Now, the reporter enzyme is used to generate a dye that indicates the existence of the gene of interest in the sample. Also ELISA assays can be performed according to this principle. Here the digoxigenin is connected to an antibody, which is specific for the analyte [2].

Affinity conjugation for diagnostic assays heavily relies on the low spontaneous off-rate of the complexes formed. In contrast to that, biophysical experiments often involve loading or even forced unbinding of receptor ligand bonds. Due to the application of an external force the off-rate (k_{off}) can be reduced tremendously. This has first been demonstrated for the forced unbinding of streptavidin-biotin with AFM force spectroscopy [4-8]. These experiments have also proved, that slow natural off-rates correlate with high unbinding forces [9].

There are many examples using affinity conjugation to investigate the binding properties of receptor-ligand interactions under an applied external force. In one example it has been exploited for unbinding experiments of double stranded DNA with the optical trap [10]. The DNA strand was immobilized to a surface bound anti-digoxigenin antibody via a digoxigenin-label. To measure a setup like this it is important to choose an appropriate holding force for the immobilization of the DNA, which can potentially be higher than the rupture force of the bond under investigation [11-19].

A deeper insight into the strength and behavior of a receptor-ligand interaction under force was described by Bell and decribed in detail by Evans [5,20]. These studies have shown, that the force that holds a receptor-ligand pair together, depends strongly on the applied load. Therefore, studies over a large range of loading rates reveal new insights in the energy landscape of a receptor – ligand interaction.
As long the applied force does not exceed a critical range, the affinity conjugation has to be stable under load for the time span of an experiment.

In another example, a differential force assay, biotin has been used to immobilize DNA duplexes to a streptavidin coated silicone stamp. This method is based on the direct comparision of two DNA duplexes, potential rupture sites assembled in series. Upon application of an external force, one of the duplexes under investigation will break, but not the biotin-streptavidin bond which is in a much higher force regime than the DNA-duplex [21,22].

Since the digoxigenin-antidigoxigenin interaction is of high practical importance, in particular for use in affinity coupling, it would be desirable to gain deeper insight into the energy landscape of this system. Therefore, we report in this publication the measurement of forced unbinding of digoxigenin-antidigoxigenin with the AFM spectroscope over a large range of loading rates. We can show that the natural dissociation $k_{off}=0.015s^{-1}$ measured with AFM are in good agreement with bulk measurements on Fv-fragments [23].

2. Material and Methods

2.1 Slide preparation

Commercial epoxy functionalized slides (Schott, Nexterion, Mainz, Germany) were used for covalent coupling of di-amino-polyethylenglycole (di-NH_2-PEG, MW 6000g/mol, Rapp Polymere, Freiburg, Germany). An amount of 75mg of di-NH_2-PEG was homogenously distributed over the whole epoxy slide and heated at 95°C for 15min until melting. To obtain a thin PEG layer, a second epoxy slide was placed up side down onto the first one. This "sandwich" was heated at 95°C for 24h. After carefully separating the slides, they were rinsed with Millipore water several times to wash away unbound di-NH_2-PEG and dried afterwards with N_2 [24].

The NH_2 functional PEG surface was then converted into a COOH surface by covering the surface with a 200μl solution of 2g/ml glutaric anhydride ($C_5H_6O_3$, Aldrich) in N, N-Dimethylformamide (DMF, $HCON(CH_3)_2$, Aldrich). A second NH_2 functional PEG slide was placed onto the slide to cover it completely with glutaric anhydride. This sandwich was incubated at room temperature for 12h in a DMF atmosphere. After incubation, the slides were washed with DMF, Millipore water and finally dried in the oven. The PEG slides with the COOH functionalized surface were stored in an Ar-atmosphere until activation.

2.2 Cantilever preparation

The cantilevers (Bio-lever, Olympus, Tokio, Japan) were cleaned in sulfuric acid (H_2SO_4, 95%, Fluka, Germany) containing 17mg/ml potassium dichromate ($K_2Cr_2O_7$, Sigma, Germany) for 10min, then washed in Millipore water and dried. Silanization was achieved by keeping the cantilevers in concentrated 3-Glycidoxypropyl-trimethoxysilan (Sigma, München, Germany) for 1-2min. After that, they were washed with toluol (Sigma, München, Germany) and Millipore water and heated at 95°C for 30min, which finally results in epoxy

functionalized tips [25]. The PEG melting described before was also applied to the epoxy functionalized cantilevers.

For each cantilever 50mg of di-NH_2-PEG were put in adequate holes of a Teflon block and heated until melting. Now the cantilevers were placed carefully in the liquid di-NH_2-PEG drops and heated at 95°C for 12h. Finally, the cantilevers were washed several times in hot Millipore water and subsequently dried. As a result of this procedure the cantilever tips are now passivated and amino-functional.

2.3 Anti-digoxigenin antibody and digoxigenin coupling

The activation of COOH groups on the PEG glass slide was performed with 1-Ethyl-3-(3-Dimethylaminopropyl) carbodiimide hydrochlorid (EDC, Sigma) and 3-O-methylcarbonyl-aminocaproic acid-N hydroxysuccinimide ester (NHS). For each slide 200μl of a 1:1 solution of 100mM EDC and 100mM NHS in Millipore water were put onto the slide and covered with a thin glass cover slide. The slide was incubated for 30min in an H_2O-atmosphere, afterwards washed with Millipore water and dried in a stream of N2. Monoclonal nti-digoxigenin antibody from mouse (IgG1, clone 1.71.256, Roche, Germany) with a concentration of 100μg/ml (in 10mM potassium phosphate buffer, 75mM NaCl, 5% raffinose, 0.01% 2-methylisothiazolone (MIT), pH 7.8) was spotted onto the pre-activated COOH surface. Then incubated for 1h in H2O-atmosphere to allow for the reaction of the amino groups of the antibody with the pre-activated COOH groups forming a covalent bond. Finally, the slide was washed with PBS (phosphate buffered saline, pH 7.4) to remove non-covalently attached antibody and then stored in PBS at 4°C until use.

The cantilever tips were incubated for 1h in 20μl drops of the digoxigenin-3-O-methylcarbonyl-aminocaproic acid-N hydroxysuccinimide ester solution (10mM digoxigenin-NHS solved in sodium borate, 100mM, pH 8.5), to allow for a covalent reaction with the NH_2

groups of the PEG spacer. Finally, the cantilevers were washed with Millipore water to remove non-covalently attached digoxigenin-NHS and stored in Millipore water at 4°C until use.

Figure 1:
Schematic view of AFM-tip, PEG spacer, digoxigenin, anti-digoxigenin antibody and slide.

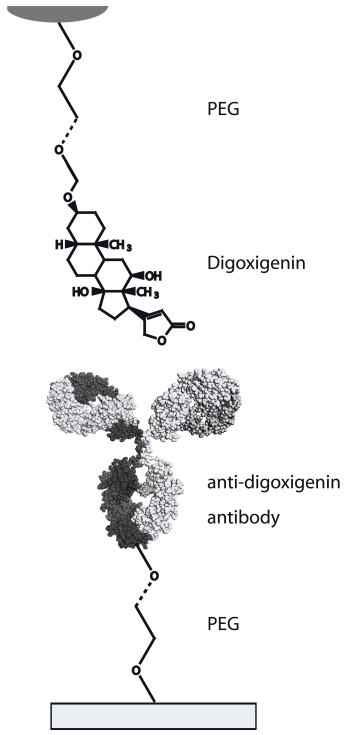

2.4 Dynamic force spectroscopy

All AFM measurements were performed at room temperature in PBS with a homebuilt instrument [26]. Cantilevers with spring constants of 6pN/nm, 8.08pN/nm (A – Bio-Lever) and 50pN/nm (B-Bio-Lever) were used. The spring constants were measured in each experiment as described previously [27,28]. During the experiment the retract velocity was held constant, whereas the contact time and the approach velocity were adjusted in order to obtain single binding events. Several hundreds of approach and retract cycles have been carried out to achieve good statistics. For each experiment, a broad distribution of loading rates was obtained by varying the retract velocities between 20nm/s and 20μm/s [5].

2.5 Data extraction

The data obtained were converted into force against extension curves (Figure 2). Each experiment consists of several hundreds of force distance curves measured at one constant retract velocity. These curves were analyzed all together to obtain both, the rupture force (the force at which the antigen-antibody bond breaks) and the loading rate dF/dt. The loading rate describes how much force was applied to the bond at a certain time shortly before the rupture event occurs. The rupture force was determined as described previously [29,30]. The loading rate was determined with a line-fit of the force curve prior to rupture, according to previous studies [29,30].

2.6 Data analysis:

Rupture forces and appropriate loading rates were then plotted in two histograms for each experiment with a constant retract velocity.

These histograms were analyzed in a two-step procedure. In the first step, the force and the loading rate histograms with the same retract velocity were fitted with a gauss distribution to find the maximum of the histograms. This was done for all measured histograms of the different experiments with retract velocities between 20nm/s and 20μm/s. The maximum values of the gauss fits were plotted in a force vs. logarithmic loading rate diagram.

The maximum obtained from the force histogram represents the most probable rupture force F*.

$$F^* = \frac{k_B T}{\Delta x} \ln \frac{\dot{F} \Delta x}{k_B T \cdot k_{off}^*} \quad (1)$$

with k_b- Boltzmann constant, T – temperature, k_{off} – natural dissociation rate at zero force, Δx potential width between the bound and the transition state and $\dot{F}$ = dF/dt the loading rate. A linear fit of the force vs. logarithm of the loading rate according to equation 1 reveals the

natural dissociation rate at zero force k_{off} and the potential width Δx for the digoxigenin-antidigoxigenin complex.

In the second step, the force histogram was normalized to be comparable with the probability density function p(F) containing k_{off} and Δx [5,29-31].

$$p(F) = k_{off}^{*} \exp\left(\frac{F\Delta x}{k_B T}\right)\frac{1}{\dot{F}} \exp\left(-k_{off}^{*}\int_0^F dF' \exp\left(\frac{F\Delta x}{k_B T}\right)\frac{1}{\dot{F}}\right) \quad (2)$$

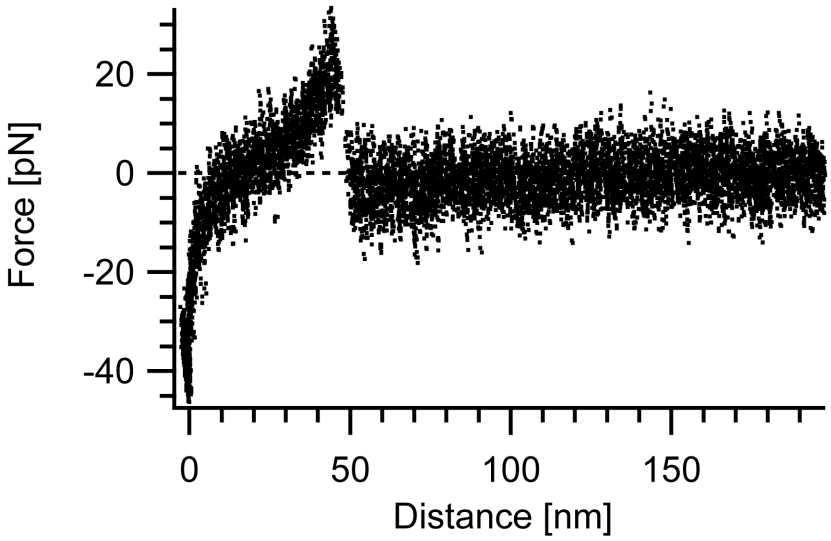

Figure 2:

Force against distance curve. The values of the rupture force, the rupture length and the loading rate were obtained from these curves as described in the text.

3. Results and discussion

This study was carried out in order to gain insight into to the energy landscape of the digoxigenin-antibody complex as a prerequsite for the estimation of its mechanical stability in molecular assemblies under a broad range of force loading rates. Therefore rupture forces have been extracted from force curves in a range of 30pN/s up to 63000pN/s. The maximum of the rupture force histograms was plotted against the corresponding loading rate dF/dt (figure 3) in order to extract k_{off} and Δx. The diagram shows a non-linear behaviour of the

force as a function of the logarithm of the loading rate. This diagram was therefore fitted with two lines. The line fit for low loading rates (figure 3, dash line) reveals a dissociation rate at zero force of $k_{off}=0.015s^{-1}$ and a potential width of $\Delta x=1.15nm$. This natural dissociation rate corresponds very well to the literature value of $k_{off}=0.023\ s^{-1}$ received from bulk measurements of comparable anti-digoxigenin Fv-fragments [23]. At high loading rates a $k_{off}=4.56s^{-1}$ and $\Delta x=0.35nm$ was deduced (figure 3, solid line). According to Merkel [5], who has investigated the unbinding of biotin – streptavidin, the two regions correspond to two barriers in the energy landscape of the complex.

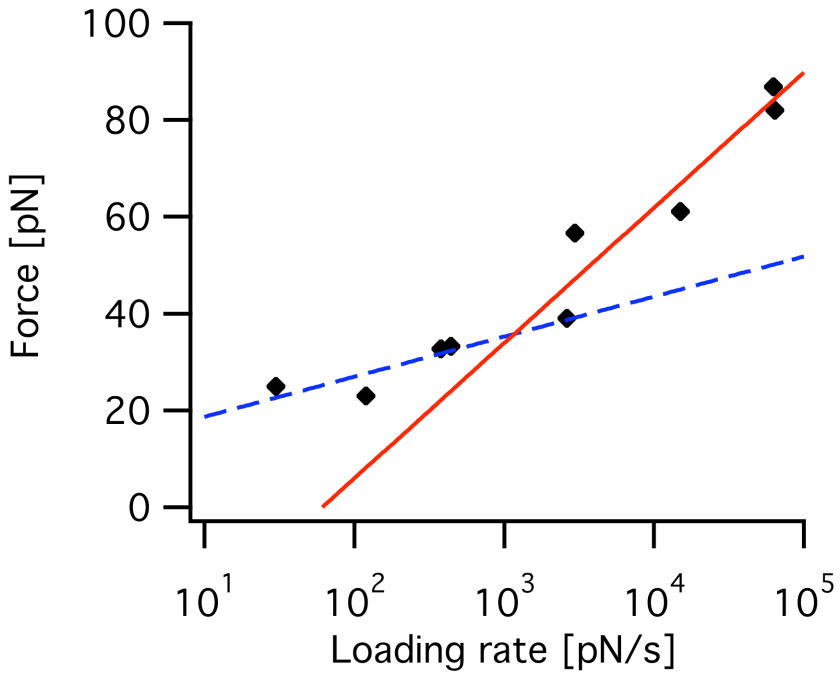

Figure 3.

Most probable rupture force F* plotted against the logarithm of the loading rate. Each point in the diagram represents the most probable rupture force F* and the related most probable loading rate dF/dt. The maximum was determined by a Gaussian fit to the force and the loading rate histogram at a constant retraction speed (black diamonds). Two distinct regions are observed and fitted with two line fits according to equation 1. The low loading rate region can be described with $\Delta x=1.15nm$ and $k_{off}=0.015s^{-1}$ (dash line) and the high loading rate region can be described with $\Delta x=0.35nm$ and $k_{off}=4.56s^{-1}$ (solid line).

Given that these values represent the energy landscape of the anti-digoxigenin antibody - digoxigenin interaction, it should be possible to extract similar k_{off} and Δx value directly from the force histogram [30,31]. Therefore, the probability density function p(F) of equation 2 should fit the observed force histograms in order to proof if it is possible to describe the force as a function of loading rate over the whole force range.

Therefore, we fitted the probability density function p(F) to the observed normalized last rupture force histogram as shown in figure 4. This histogram was measured at a loading rate of 120pN/s and can be fitted with the calculated probability density function p(F) using $k_{off}=0.015s^{-1}$ and $\Delta x=1.15nm$ (dash line).

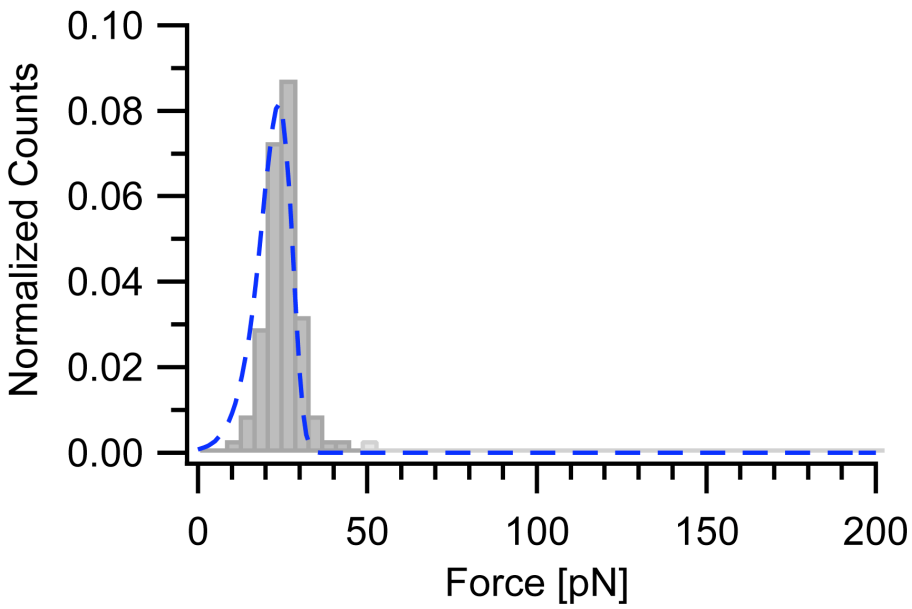

Figure 4.

Force histogram at a low loading rate.

Rupture forces for 85 force curve are plotted in a histogram (bars) and compared with the calculated probability density function p(F) (dash line) with $\Delta x=1.15nm$, $k_{off}=0.015s^{-1}$ at a loading rate of 120pN/s.

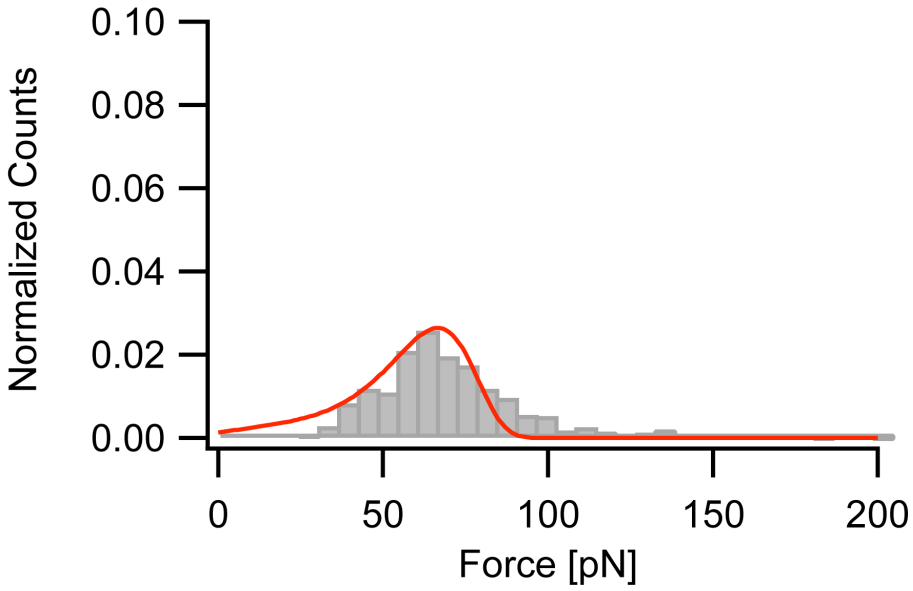

Figure 5.

Force histogram at a high loading rate.

Rupture forces for 644 force curves are plotted in a histogram (bars) and compared with the calculated probability density function p(F) (solid line) with Δx=0.35nm, k_{off}=4.56s^{-1} at a loading rate of 14950pN/s.

For high loading rates, the measured force histogram (loading rate of 14950pN/s) can also be fitted with the probability density function p(F) using k_{off}=4.56s^{-1} and Δx=0.35nm as shown in figure 5 (solid line). These two histograms at different loading rates describe the two regions in good accordance.

We tried to apply this analysis at very high loading rates and at the interception between the two line fits as seen in figure 3. For a loading rate of 63000pN/s the measured force histogram (figure 6) is broader compared to the calculated probability density function (solid line). These differences are dramatic, because the shape of the probability density function p(F) depends heavily on the natural dissociation rate at zero force k_{off} and the potential width Δx. For a good match of the measured force histogram and the calculated probability function p(F) totally different values for k_{off} and Δx have to be used.

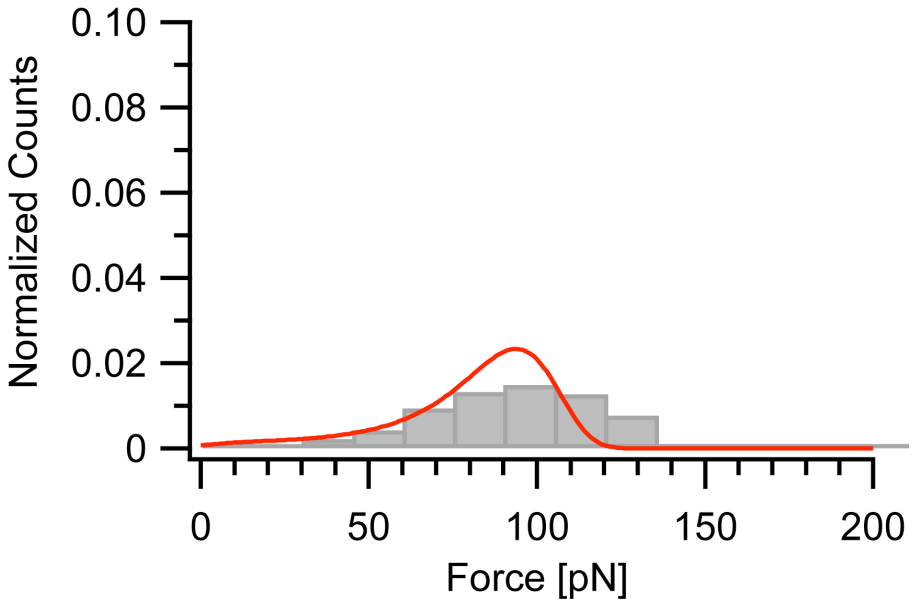

Figure 6.

Force histogram at a very high loading rate.

Rupture forces for 155 force curves are plotted in a histogram (bars) and compared with the calculated probability density function p(F) (solid line) with Δx=0.35nm, k_{off}=4.56s^{-1} at a loading rate of 63000pN/s.

The other interesting section is near the interception of the two line fits in figure 3. The force histogram shown in figure 7 was measured at a loading rate of 440pN/s and compared with two possible probability density functions. The first probability density function uses the k_{off} and Δx values observed at low loading rates (dash line) and the second probability density function uses the k_{off} and Δx values observed at high loading rates (solid line). It is clear that both probability density functions cannot fit the observed force histogram. Only by using again totally different values for k_{off} and Δx, the experimental force histogram can be fitted adequately. Therefore we conclude, that the analysis based on the assumptions of two barriers in the energy landscape of the receptor ligand pair [5,29], can potentially be misleading. In particular at the intermediate regime, large deviations occur between the measured data and the obtained fits. This indicates that perhaps the underlying dissociation mechanism might deviate from the simplistic two-barrier model at this region.

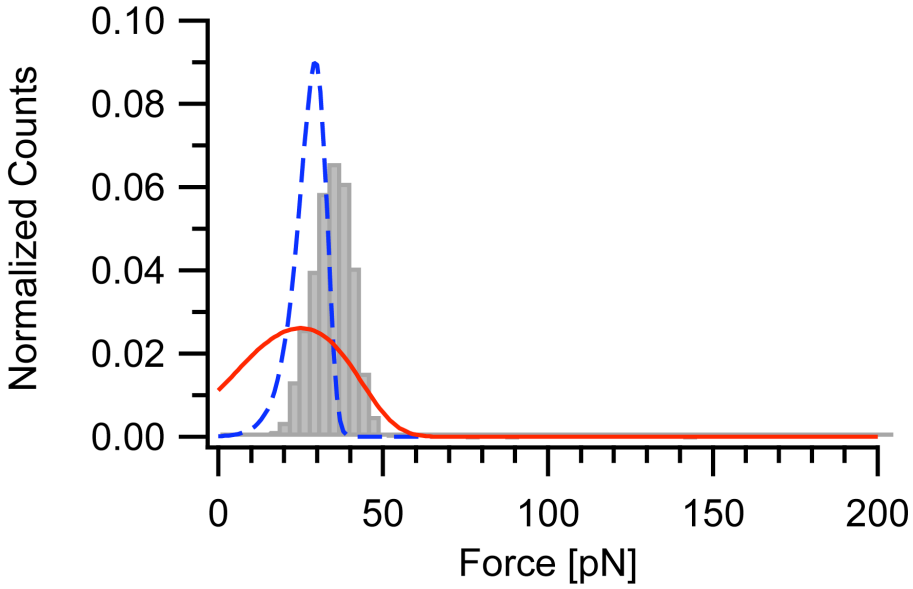

Figure 7.

Force histogram near the interception of the two regions.

Rupture forces for 925 force curves are plotted in a histogram (bars) and compared with the calculated probability density function p(F) for the low loading rate region (dash line: $k_{off}=0.015s^{-1}$, $\Delta x=1,15nm$) and for the high loading rate region (solid line: $k_{off}=4.56s^{-1}$, $\Delta x=0.35nm$).

One reason for the misleading analysis might be the assumption made in this model, that the energy wells are deep and the distance Δx between the minima and the transition state are fixed during the applied load [5,29,32-34]. Because in this study we applied large external forces that maybe alter the energy landscape of the complex dramatically. Therefore we can not assume a Makovian like behavior of two distinct states anymore. One possible way of resolving these differences is to take an energy landscape into account that describe the force histogram in a better way. This can be done by applying Kramers theory to a probable energy landscape at each external force [34]. To give a full description of the measured force histogram, further theoretical investigations are needed.

The practical implication of the above findings for experiments under force load can be illustrated by a gedankenexperiment: A receptor-ligand complex under investigation was

immobilized by the digoxigenin-antibody complex. At low loading rate of 120pN/s the maximum of the rupture force of digoxigenin – antidigoxygenin is 24pN as shown in figure 4. At a given rupture force of the complex under investigation of 10pN, the probability for bond breakage of digoxigenin- anti digoxigenin still is 10% compared to 100% probability at 24pN (dashed line in figure 4). Consequently the measurement of a force of 10pN in a setup that uses the anti-digoxigenin antibody - digoxigenin system as affinity conjugation under the above conditions, result in a 10% rupture probability of the affinity conjugation complex and a 90% rupture probability of system under investigation.

Especially for dynamic force spectroscopy where the loading rate and the rupture forces vary over a large range, this system has to be chosen carefully.

The problem however could be overcome by using multiple affinity tags in parallel which give rise to avidity effects and a highly decreased k_{off}, as demonstrated for the His-tags system [1].

4. Acknowledgements

We thank Thomas Nicolaus for technical assistance in preparing the surfaces and Julia Sedlmair, Julia Morfill, Kerstin Blank and Kay Gottschalk for helpful discussions. This work was supported by the Deutsche Forschungsgemeinschaft.

5. References

[1] Hermanson, G. (1996), pp. 785 Academic Press.
[2] Kessler, C., Holtke, H.J., Seibl, R., Burg, J. and Muhlegger, K. (1990) Biol Chem Hoppe Seyler 371, 917-27.
[3] Grandbois, M., Beyer, M., Rief, M., Clausen-Schaumann, H. and Gaub, H.E. (1999) Science 283, 1727-1730.
[4] Grubmüller, H., Heymann, B. and Tavan, P. (1996) Science 271, 997-999.
[5] Merkel, R., Nassoy, P., Leung, A., Ritchie, K. and Evans, E. (1999) Nature 397, 50-53.
[6] Florin, E.L., Rief, M., Lehmann, H., Ludwig, M., Dornmair, C., Moy, V.T. and Gaub, H.E. (1995) Biosensors & Bioelectronics 10, 895-901.

[7] Izrailev, S., Stepaniants, S., Balsera, M., Oono, Y. and Schulten, K. (1997) Biophysical Journal 72, 1568-1581.
[8] Lee, G.U., Kidwell, D.A. and Colton, R.J. (1994) Langmuir 10, 354-357.
[9] Moy, V.T., Florin, E.L. and Gaub, H.E. (1994) Science 266, 257-9.
[10] Lang, M.J., Fordyce, P.M., Engh, A.M., Neuman, K.C. and Block, S.M. (2004) Nature Methods 1, 133-139.
[11] Bockelmann, U. (2004) Current Opinion in Structural Biology 14, 368-373.
[12] Allemand, J.F., Bensimon, D. and Croquette, V. (2003) Current Opinion in Structural Biology 13, 266-274.
[13] Bryant, Z., Stone, M.D., Gore, J., Smith, S.B., Cozzarelli, N.R. and Bustamante, C. (2003) Nature 424, 338-341.
[14] Liphardt, J., Onoa, B., Smith, S.B., Tinoco, I. and Bustamante, C. (2001) Science 292, 733-737.
[15] Ha, T. (2001) Current Opinion in Structural Biology 11, 287-292.
[16] Quake, S.R., Babcock, H. and Chu, S. (1997) Nature 388, 151-154.
[17] Shaevitz, J.W., Abbondanzieri, E.A., Landick, R. and Block, S.M. (2003) Nature 426, 684-687.
[18] Koch, S.J., Shundrovsky, A., Jantzen, B.C. and Wang, M.D. (2002) Biophysical Journal 83, 1098-1105.
[19] Williams, M.C. and Rouzina, I. (2002) Current Opinion in Structural Biology 12, 330-336.
[20] Evans, E., Leung, A., Hammer, D. and Simon, S. (2001) Proceedings of the National Academy of Sciences of the United States of America 98, 3784-3789.
[21] Albrecht, C. et al. (2003) Science 301, 367-370.
[22] Blank, K. et al. (2003) Proceedings of the National Academy of Sciences of the United States of America 100, 11356-11360.
[23] Chen, G., Dubrawsky, I., Mendez, P., Georgiou, G. and Iverson, B.L. (1999) Protein Engineering 12, 349-356.
[24] Piehler, J., Brecht, A., Valiokas, R., Liedberg, B. and Gauglitz, G. (2000) Biosens Bioelectron 15, 473-81.
[25] Hugel, T., Grosholz, M., Clausen-Schaumann, H., Pfau, A., Gaub, H. and Seitz, M. (2001) Macromolecules 34, 1039-1047.
[26] Holland, N.B. et al. (2003) Macromolecules 36, 2015-2023.
[27] Butt, H.J. and Jaschke, M. (1995) Nanotechnology 6, 1-7.
[28] Hugel, T. and Seitz, M. (2001) Macromolecular Rapid Communications 22, 989-1016.
[29] Evans, E. and Ritchie, K. (1999) Biophysical Journal 76, 2439-2447.
[30] Friedsam, C., Wehle, A.K., Kühner, F. and Gaub, H.E. (2003) Journal of Physics-Condensed Matter 15, S1709-S1723.
[31] Kühner, F., Costa, L.T., Bisch, P.M., Thalhammer, S., Heckl, W.M. and Gaub, H.E. (2004) Biophysical Journal 87, 2683-2690.
[32] Evans, E. (2001) Annu Rev Biophys Biomol Struct 30, 105-28.
[33] Bell, G.I. (1978) Science 200, 618-627.
[34] Hänggi, P. and Talkner, P. (1990) Review of Modern Physics 62, 251-341.

P5

“Modular multichannel surface plasmon spectrometer“

G. Neuert, S. Kufer, M. Benoit and H.E.Gaub

Review of scientific instruments, 76, 054303, 2005

Modular multichannel surface plasmon spectrometer

G. Neuert,[a] S. Kufer, M. Benoit, and H. E. Gaub
Lehrstuhl für Angewandte Physik & Center for Nanoscience, Ludwig-Maximilians Universität, Amalienstrasse 54, 80799 München, Germany

(Received 3 December 2004; accepted 6 March 2005; published online 22 April 2005)

We have developed a modular multichannel surface plasmon resonance (SPR) spectrometer on the basis of a commercially available hybrid sensor chip. Due to its modularity this inexpensive and easy to use setup can readily be adapted to different experimental environments. High temperature stability is achieved through efficient thermal coupling of individual SPR units. With standard systems the performance of the multichannel instrument was evaluated. The absorption kinetics of a cysteamine monolayer, as well as the concentration dependence of the specific receptor-ligand interaction between biotin and streptavidin was measured. © *2005 American Institute of Physics.* [DOI: 10.1063/1.1899503]

I. INTRODUCTION

Receptor ligand interactions are the hallmark of life. Surface plasmon resonance (SPR) spectroscopy was established in recent years as a standard method for the quantification of such interactions. This optical technique uses an evanescent wave to measure changes in the refractive index at a metal—typically gold—surface. One of the binding partners is immobilized at this metal surface. Binding of the other partner results in an increase of the surface concentration, and as a consequence, in a change of the refractive index. Such measurements are performed in real time and the amount of bound ligand as well as association and dissociation rates are determined.[1]

Several commercial instruments are available,[2] which may be operated with little training on day to day basis with acceptable throughput.[3] However, these instruments can hardly be modified to suite the needs in a combined experimental setup, e.g., in combination with an atomic force microscope (AFM) or a second optical device accessing the same metal surface. The SPREETA-sensor from Texas Instruments (Dallas, Texas) is a fully integrated one-chip surface plasmon device.[4] As such it is easy to modify and may therefore be used for a wide range of application.[5] Furthermore it is inexpensive compared to the established standard systems.

Here we describe the design of a multichannel SPR spectrometer based on such sensor chips. This spectrometer is modular and the entire half space above the gold surface is available for additional experiments. The performance of our instrument is demonstrated with binding assays of different standard systems.

II. DESCRIPTION OF THE EXPERIMENT

A. SPR-sensor chip

The basis of this SPR system is the SPREETA-Sensor from Texas Instruments [4,5] (Fig. 1). This sensor consists of a light-emitting diode (LED) whose light is reflected from the gold film onto a linear camera. The camera signal is digitized with 12-bit resolution by a digital signal processor (DSP) (Normadics, Stillwater, Oklahoma) and transferred via a serial interface to a personal computer. The initiation and data collection is controlled with EVM software (Normadics, Stillwater, Oklahoma).

The sensor is initially covered by a gold layer, which was removed by dipping the sensor into solution out of 3/4 hydrochloric acid and 1/4 nitric acid. Afterwards, it was rinsed extensively with double deionized water (ddH_2O). The sensor was now cast with an epoxy resin (Robnor Resins, UK) into an aluminium block. Multiples of these units are combined to form a multichannel block. For multichannel operation each chip was operated by its own DSP controller, and analyzed in multiple windows of EVM software.

B. Gold-coated cover slips and surface functionalization

In order to allow for the sensor to be reused also with different surfaces, the initial single-use gold surface of the sensor was removed. Instead gold-coated glass cover slips were optically coupled with index matching oil to the surface of the sensor. These gold-coated cover slips are prepared as follows: cover slips (Roth, Karlsruhe, Germany) were cleaned once in 2% Helmanex-solution (Helma, Germany) for 15 min. and then two times for 15 min. in ddH_2O. All steps were performed in an ultrasonic bath. Afterward, the cleaned cover slips were dried in an oven at 75 °C overnight. The clean and dry glass cover slips were covered with 10 Å chrome/nickel (80% Cr / 20% Ni, GoodFellow, GB) as adhesive layer and 500 Å gold (99,99% pure, Leybold Optics, Germany) by thermal evaporation.

For surface functionalization the coated glass slips were transferred immediately after evaporation into a ddH_2O solution containing 20 mM cysteamine (2-aminoethanethiol, Sigma-Aldrich) stored overnight to allow a self-assembled monolayer (SAM) to form onto the gold surface.[3,6–8] After 12 h of incubation (as can be seen later on in Fig. 2, already

[a]Electronic mail: gregor.neuert@physik.uni-muenchen.de

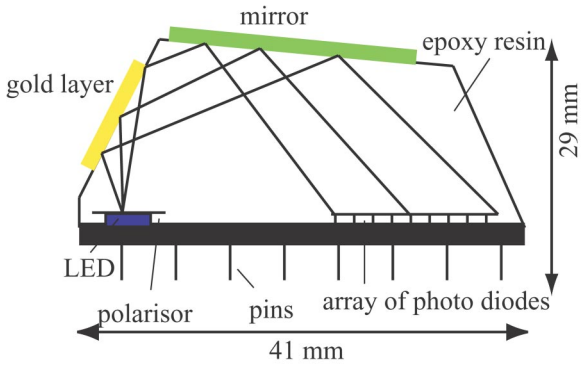

FIG. 1. (Color online) Schematics of the SPREETA sensor. A LED emits light at 840 nm, which passes a polarizer, illuminating the whole sensor surface. The reflected light is mirrored onto the array of photo diodes.

an incubation time of one hour would be sufficient), the SAM-coated cover slips were washed extensively with ddH_2O and placed into 1 M NaOH for 5 min to deprotonate the NH^{3+} groups of the SAM. Afterwards, the cover slips were washed with ddH_2O, dried in a stream of N_2 and processed immediately.

As a result of this procedure the gold-coated cover slips have a high density of NH_2 at the surface, which are used to couple carboxymethyl cellulose (CMC, Sigma).[3] A CMC solution was prepared and added to the solid form of 1-ethyl-3-(3-dimethylaminopropyl) carbodiimide hydrochlorid (EDC, Sigma)/N-hydroxysuccinimid (NHS, Sigma) to reach a final concentration of 5% CMC with 50 mM EDC/NHS in 10 mM hepes. 200 μl of this solution was pipette onto one cysteamine coated gold slide and covered by a second cysteamine coated gold slide in a sandwich like structure. Previous AFM studies had shown that a covalent attachment of the polymer to the gold surface is achieved this way.[9] These slips were then stored in an incubation chamber with a ddH_2O atmosphere at room temperature for 2 h. After the CMC coupling, the cover slips were washed extensively with ddH_2O and stored in ddH_2O for later use. Before use, the functionalized slips were well dried in a N_2 stream.

C. Fluid cell

The flow chambers were made from poly (dimethylsiloxane) (PDMS, Sylgard 184, Dow Corning) a fluid silicon

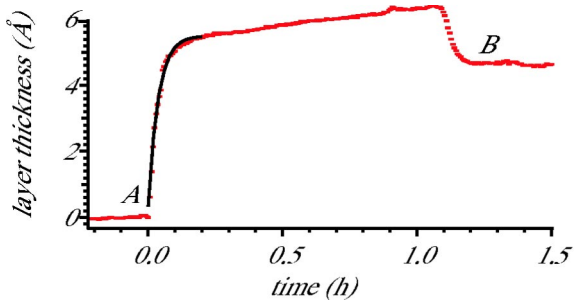

FIG. 2. (Color online) Binding kinetics of cysteamine layer on gold. (*A*) Start of the absorption. (*B*) Rinse with PBS. The thickness of $d=4.8$ Å is measured between points (*A*) and (*B*). The index of refraction of the cysteamine layer was assumed to be $n=1.525$. The black line is a guide for the eye.

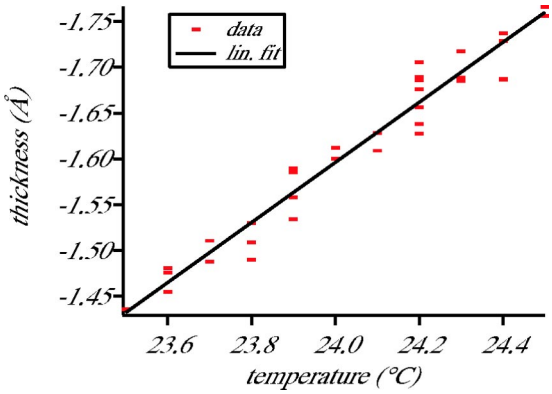

FIG. 3. (Color online) Linear drift of the surface plasmon plotted as thickness change ($n=1.5$ in water $n=1.33$) dependent on the temperature (°C) over a time period of 5.5 h. Linear least-squares line fit results in an average thickness error of 0.33 Å per °C. Red dots: measured data, black line: linear fit.

elastomer.[5] After mixing the elastomer with a catalyst, the mixture was degassed and cast into a special form. The silicon tubes, which later on allow the fluid exchange of the sample are already inserted and polymerized into the elastomer. The polymer was cured for 24 h at 60 °C. The approximately 2 mm thick fluid chambers were finished by cutting a 10 mm × 3 mm sample volume out of the PDMS. Before each measurement, the fluid chambers were cleaned with Helmanex, ddH_2O, ultra pure ethanol, and dried in a stream of N_2. The fluid chambers were then placed on top of the coated cover slip and sealed with a microscope slide. This assembly was fixed with a metal bar from the top.

To ensure a continuous flow of the buffer, the fluid cell was connected to a peristaltic pump. It is also possible to introduce sample liquid via a valve [Fig. 4(a)]. The flow was controlled down to values as low as 30 μl/min. This allows measurements of sample volume as small as 100 μl per channel in a stop flow manner. Before each measurement, the sensor was calibrated in air and buffer.

D. Cysteamine monolayer adsorption

The quantification of the online adsorption of cysteamine onto a freshly evaporated glass cover slip was the first proof of reliable operation of the instrument as shown in Fig. 2. The gold cover slip was prepared and placed into the instrument as described above. As a running buffer we used (PBS). After equilibration of the instrument, we switched to the sample liquid system that contained a 10 mM cysteamine solution dissolved in PBS and inject it into the fluid chamber. The thickness of the adsorbed layer in units of angstroms as a function of time in hours is plotted. The index of refraction n is set to $n=1.525$. The adsorption of the cysteamine starts at $t=0$ h (A) and rises rapidly, indicating the strong adsorption of the mercapto group to the gold surface. After 15 min. a plateau was reached which indicates a saturation of the gold surface with cysteamine. After one hour no significant increase of the signal was observed any longer, so that the adsorption of the cysteamine was stopped (B) by switching to the running buffer. The latter washed away unbound cysteamine, which resulted in a baseline shift of 4.8 Å,

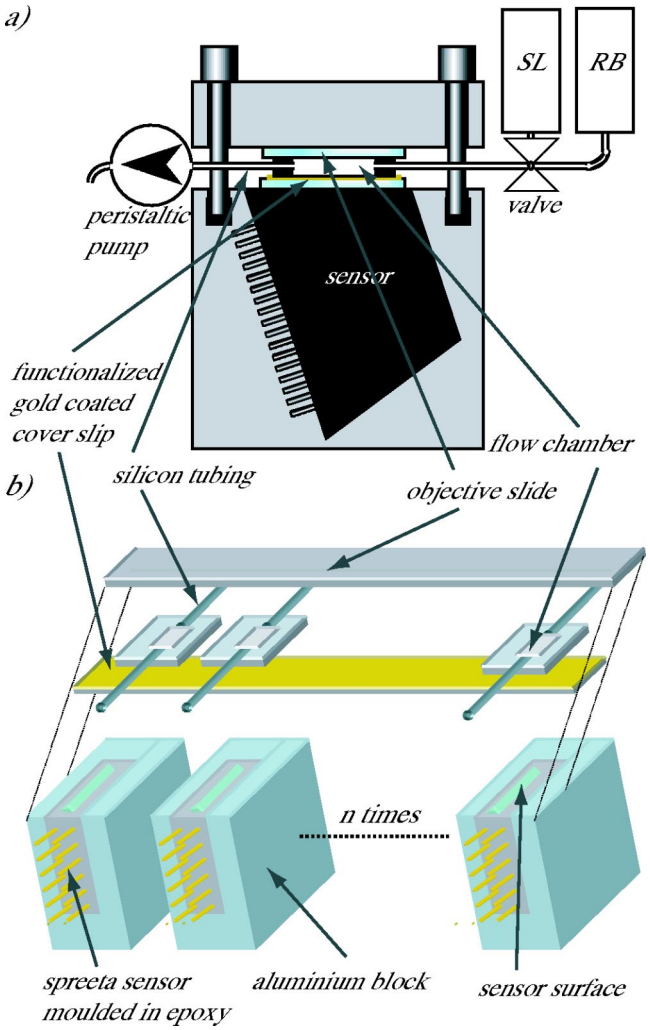

FIG. 4. (Color online) (a) Compiled setup contains the molded sensor with functionalized gold coated glass cover slip and fluid cell. The fluid cell is connected via a valve to the sample liquid (SL) or the running buffer (RB). To ensure a continuous flow of the buffer, the fluid cell was connected to a peristaltic pump. (b) The factory-made gold surface of the SPREETA sensors was removed with nitro hydrochloric acid. The bare sensor was molded with epoxy resin into an aluminium block. A cover slip, which was evaporated with 15 Å CrNi and 500 Å gold was optically coupled with index matching oil to the glass surface of the sensor. A flow chamber, made of PDMS, was placed onto the active sensing region of the sensor and sealed with a microscope slide.

which corresponds to a dense monolayer of cysteamine. This is in very good agreement with the theoretical value of 4.83 Å.

E. Temperature dependence of the sensor signal

Surface plasmons are very sensitive to temperature. Therefore we measured the temperature dependence of the plasmon resonance after encapsulation into the aluminium block (Fig. 3). The experiment was performed in ddH_2O. Plotted is the resonance angle in values of the thickness of a hypothetical film with a refractive index of $n=1.5$ in water ($n=1.33$) as a function of the temperature. This measurement was taken over 5.5 h and shows a linear thickness drift of 0.33 Å per °C.

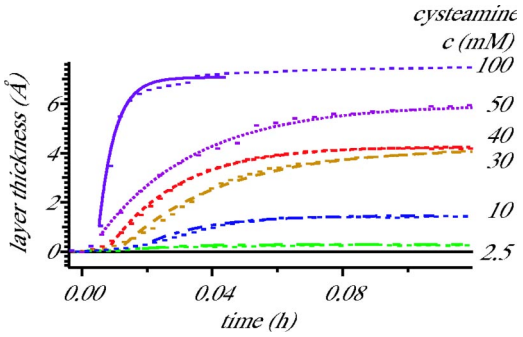

FIG. 5. (Color online) Simultaneous multichannel SPR measurements of the absorption of cysteamine onto the gold surface. Concentrations in PBS ranged between 100 and 2.5 mM. Thickness was measured based on an refractive index of $n=1.5$. Solid lines are first order exponential fits of the measured data.

III. MULTICHANNEL OPERATION

Because of this pronounced dependence of the surface plasmon resonance on the temperature we coupled several sensor units together to form a solid block [Figs. 4(a) and 4(b)]. This solid block connects all sensors thermally, ensuring the same temperature for each sensor. Having the same temperature at all sensors, it is therefore possible to use one sensor as a reference for the others. The temperature dependence can later be subtracted from the other sensor signals.

Another benefit of arranging single sensor units in parallel is the possibility to build a modular multichannel SPR device [Fig. 4(b)]. In our experimental setup it is possible to cover six SPR sensors at the same time with one gold slide. To demonstrate the ability of multichannel operation, we measured the absorption kinetic for cysteamine in a concentrations range between 2.5 and 100 mM.

In Fig. 5 the layer thickness is plotted as a function of absorption time in hours for six different channels in parallel. The cysteamine was solved and diluted in PBS. After the instrument was thermally equilibrated, we injected several solutions of cysteamine at different concentrations (2.5, 10, 30, 40, 50, and 100 mM) in the six flow channels. The measured concentration dependence in the absorption kinetic in the different channels is a convincing demonstration of the stable, reliable, and parallel operation of the instrument.

To explore the potential range of applications of this instrument in biophysical research we investigated the interaction of biotin with streptavedin as shown in Fig. 6. For this experiment we used a CMC surface as described before, which provides a carboxyl functionalized surface. All measurements in this experiment were performed in degassed 10 mM hepes buffer (Sigma) under a constant flow rate of 30 µl/min. After equilibration of the experiment 10 mM biotinhydrazid (Sigma–Aldrich) was mixed with an equal volume of 10 mM hepes with 100 mM EDC / NHS (channel 1,2). In channel 3 only biotinhydrazid without EDC/NHS was injected into the fluid system (*A*). The strong increase in signal is related to the large change of the refractive index related to EDC/NHS. By switching all three channels to hepes buffer after 32 min of incubation (*B*), we washed unbound biotinhydrazid and EDC/NHS away. This resulted in a strong decrease of the signal until a new baseline was reached. We

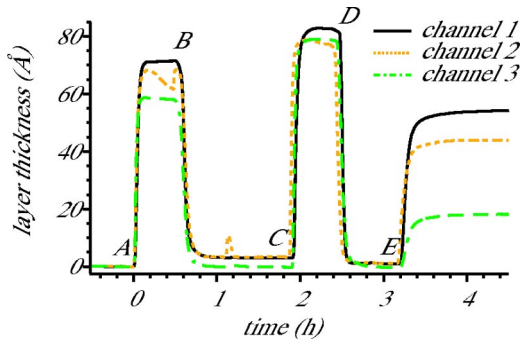

FIG. 6. (Color online) Competitive binding assay for streptavidin to biotinhydrazid. (*A*) Immobilization of biotinhydrazid with EDC/NHS (channel 1,2) and without EDC /NHS (channel 3); (*B*) rinse with 10 mM hepes; (*C*) deactivation of the remaining activated carboxyl groups with 1 M ethanolamine; (*D*) rinse with 10 mM hepes; (*E*) channel (1,3) streptavedin (0.1 mg/ml), channel 2: streptavedin 0.1 mg/ml preincubated with 1:25 biotinhydrazid.

then deactivated the surface by injecting a solution of 1 M ethanolamine (Sigma) (channel 1–3) (*C*) for 30 min. Since not all the EDC/NHS activated carboxyl groups have reacted with biotinhydrazid it is necessary to deactivate the remaining activated carboxyl groups with an excess of ethanolamine, so that no protein binds covalently to the surface, later on.

Afterward, we washed again with 10 mM hepes (*D*) until a stable baseline was reached. At point (*E*) we injected 0.1 mg/ml streptavedin in 10 mM hepes (channel 1,3). Preincubated streptavedin (0.1 mg/ml) with a 25-fold molar excess of biotinhydrazid was injected in channel 2 until saturation was reached. It can be clearly seen that the strongest interaction occurs between the biotin functionalized surface and streptavedin in channel 1. The coverage decreased for the preincubate streptavedin (channel 2). This was to be expected because the majority of the binding sites of streptavedin were blocked with free biotinhydrazid and binding of streptavedin to the surface is thus largely suppressed. For the surface that was not activated before (channel 3) the interaction of the streptavedin bound only non-specifically at much lower levels.

IV. DISCUSSION

Three major benefits helped this instrument to become a workhorse in our laboratory: multichannel operation, free access to the active gold surface with other techniques, and ease of operation. High end commercial instruments like the Biacore have a better thickness resolution but the accuracy of 1% of a protein monolayer, reached with our setup is more than sufficient for most applications. Also the option to design, test, and implement new surface functionalization protocols on the gold films with great ease and moderate costs has helped to standardize surface chemistry in our lab.

Having multiple channels running in parallel not only speeds up screening steps. Since all traces run on the same chip with the same history and chemistry, standard deviations between the traces came down drastically. Being able to design the fluid chamber, e.g., with an optical window to the upper side has allowed to combine SPR measurements with optical excitation and light induced chemistry. The integration of an AFM became possible and initiated a different set of experiments not reported here. The block design helped markedly to increase the temperature stability of the setup. An additional external thermostat, also controlling the sample fluids may help to improve this stability further if needed.

ACKNOWLEDGMENTS

The authors thank E. K. Sinner, Ch. Albrecht. K. Blank, T. Nickolaus, and E. Sackmann for helpful discussions. Financial support by the Deutsche Forschungs Gemeinschaft (SFB 486) is gratefully acknowledged.

[1] W. Knoll, Annu. Rev. Phys. Chem. **49**, 569 (1998); E. K. Sinner *et al.*, Anal. Biochem. **333**, 216 (2004); E. L. Florin and H. E. G. Gaub, Biophys. J. **64**, 375 (1993).
[2] W. M. Mullett, E. P. C. Lai, and J. M. Yeung, Methods **22**, 77 (2000).
[3] B. Johnson, S. Löfås, and G. Lindquist, Anal. Biochem. **198**, 268 (1991).
[4] J. Meléndez *et al.*, Sens. Actuators B **35–36**, 212 (1996).
[5] A. R. Wheeler *et al.*, Sens. Actuators B **98**, 208 (2004).
[6] C. D. Bain *et al.*, J. Am. Chem. Soc. **111**, 321 (1989).
[7] S. Löfås *et al.*, Sens. Actuators B **5**, 79 (1991).
[8] G. Brink *et al.*, Biochim. Biophys. Acta **1196** (2), 227 (1994).
[9] M. Grandbois *et al.*, Science **283**, 1727 (1999).

Lebenslauf

Name: Gregor Neuert

Geboren: 17. März 1974, Dillenburg

Ausbildung:

1980 - 1989	Hauptschule, Breitscheid
1989 - 1991	Berufsfachschule, Dillenburg
1991 - 1994	Berufliches Gymnasium, Dillenburg Allgemeine Hochschulreife
1994 - 1995	Wehrdienst
1995 - 1996	Studium der Elektrotechnik, TU-Ilmenau
1996 - 2001	Studium der Technischen Physik, TU-Ilmenau
2001	Diplom in Technische Physik, TU-Ilmenau, Prof. J. Schaefer
seit 2002	Promotion in Biophysik, LMU - München, Prof. H.E. Gaub

Auslandserfahrung:

1998 - 1999	Montana State University, Bozeman, Montana, USA und Pacific North West National Labs, Richland, Washington, USA

Forschungsschwerpunkte:

2001	Diplomarbeit: Growth of Palladium / Yttrium films and characterisation with Rutherford Backscattering Spectroscopy (RBS) and X-Ray Photoelectron Spectroscopy (XPS) sputter depth profiling
seit 2002	Promotion: Einzelmolekül-Kraftspektroskopie an molekularen Maschinen und Rezeptor-Ligand-Systemen

Danksagung

An dieser Stelle sei Dank gesagt an die vielen Leute, die mitgeholfen haben das diese Dissertation erfolgreich durchgeführt worden konnte.

Hier sei besonders folgenden Leuten gedankt:

Der gesamten Gambicrew für die tolle Atmosphäre.

Angelika Kardinal für das gute Management des Chemie-Labors.

Hermann Gump, Max Kessler, Christian Kirchner, Julia Schmitz, Ingo Schwaiger, Lars Sonneberg, und Elias Puchner für die anregenden Diskussionen rund um das AFM, die Chemie und der Hard- und Software.

Ferdinand Kühner, Michael Schlierf und Kay Gottschalk für Diskussionen rund um die AFM-Datenauswertung.

Eva Sinner und Birgit Wiltschi für die Diskussion rund um SPR, Antikörper und Biochemie.

Der Rief Group für allgemeine Diskussionen und Anregungen rund um AFM und Optische Falle.

Martin Benoit für die technischen Anregungen.

Herrn Aust und seiner Mannschaft für den Bau zahlreicher mechanischer Bauteile.

Herrn Wieser und Herrn Holopirek für die Realisierung verschiedenster elektronischer Schaltungen.

Julia Morfill für das Korrekturlesen und der anregenden Diskussionen

Stefan Kufer für die Zusammenarbeit beim SPR-Projekt.

Den Werkstudenten Ulrich Männl, Uwe Megerle, Evren Pamir, Carsten Rohr, Julian Schauseil und Julia Sedlmair für die sehr gute Zusammenarbeit.

Den Herrn Professoren Prof. E. Evans, Prof. H. Grubmüller, Prof. L. Moroder, Prof. D. Oesterhelt, Prof. M. Rief und Prof. E. Sackmann für hilfreiche Diskussionen.

Markus Seitz für viele konstruktive Vorschläge rund um die Chemie und die Azobenzole.

Thomas Nikolaus für sein großes praktisches Wissen zur Oberflachenchemie auf Glas und Gold.

Christian Albrecht für einen sehr guten Einstieg in die Oberflächenchemie, die Stempel Technologie und zahlreiche und wertvolle Diskussionen über Biochemie, Biologie und Kraftmessung.

Kerstin Blank für die Möglichkeit an ihren Wissen zu Proteinen und Antikörpern zu Partizipieren und für das Anregungen bezüglich dieser Dr. Arbeit.

Prof. Dr. Roland Netz für die Rechnungen zu den Azobenzolen, den guten Einstieg in Mathematica und die gute Zusammenarbeit.

Mein besonderer Dank gilt Thorsten Hugel, der mir einen schnellen Einstieg in die Einzelmolekül Kraftspektroskopie, die Azobenzole und sonstige Gebiete rund um die Biophysik ermöglichte. Weiterhin bin ich ihm sehr dankbar für diese besondere Einladung zum Ski fahren, die einiges in meinem Leben grundlegend verändert hat.

Prof. Dr. Hermann Gaub für die Möglichkeit in seiner Arbeitsgruppe zu Promovieren, für die tollen Projekte, die anregenden Diskussionen, die besonders gute Atmosphäre und das leckere Essen.

Meiner Familie für ihre Unterstützung während dieser Zeit.

Meiner Freundin, Shanshan Chen, die mir einen ganz neuen Horizont eröffnet hat, für das große Verständnis für meine Arbeit und die tolle Zeit zusammen.

Erklärung

Hiermit versichere ich, die vorliegende Arbeit selbstständig ausgeführt und keine weiteren Hilfsmittel als die im Text und im Literaturverzeichnus aufgeführten verwendet zu haben.

München, den 31. August 2005

_____

Gregor Neuert